# Instrumentation

# 4

**Learning Objectives**

- Separating ions by $m/z$ – basic principles
- Mass analyzers as designed from basic principles
- Types of mass analyzers and their modes of operation
- Guiding, collimating, and focusing ions along a path
- Hybrid instruments including ion mobility-mass spectrometry
- Detectors for mass-analyzed ions
- Vacuum generation for mass spectrometry
- Ability to judge fitness for purpose of commercial instruments

"A modern mass spectrometer is constructed from elements which approach the state-of-the-art in solid-state electronics, vacuum systems, magnet design, precision machining, and computerized data acquisition and processing" [1]. This statement published in 1979 has always been and still is absolutely true in the context of mass spectrometers.

Under the headline of instrumentation we shall mainly discuss the different types of mass analyzers in order to understand their basic principles of operation, their specific properties, and their performance characteristics. The order of treatment in this chapter neither reflects their ever-changing individual predominance in mass spectrometry nor does it follow a strictly historic time line. Rather, an attempt is made to follow a trail of easiest understanding. Of course, this is only one aspect of instrumentation; hence topics such as ion detection and vacuum generation will also be addressed in brief. As a matter of fact, sample introduction is more closely related to particular ionization methods than to the type of mass analyzer employed, and therefore, this issue is treated in the corresponding chapters on ionization methods.



J.H. Gross, *Mass Spectrometry*, DOI 10.1007/978-3-319-54398-7_4

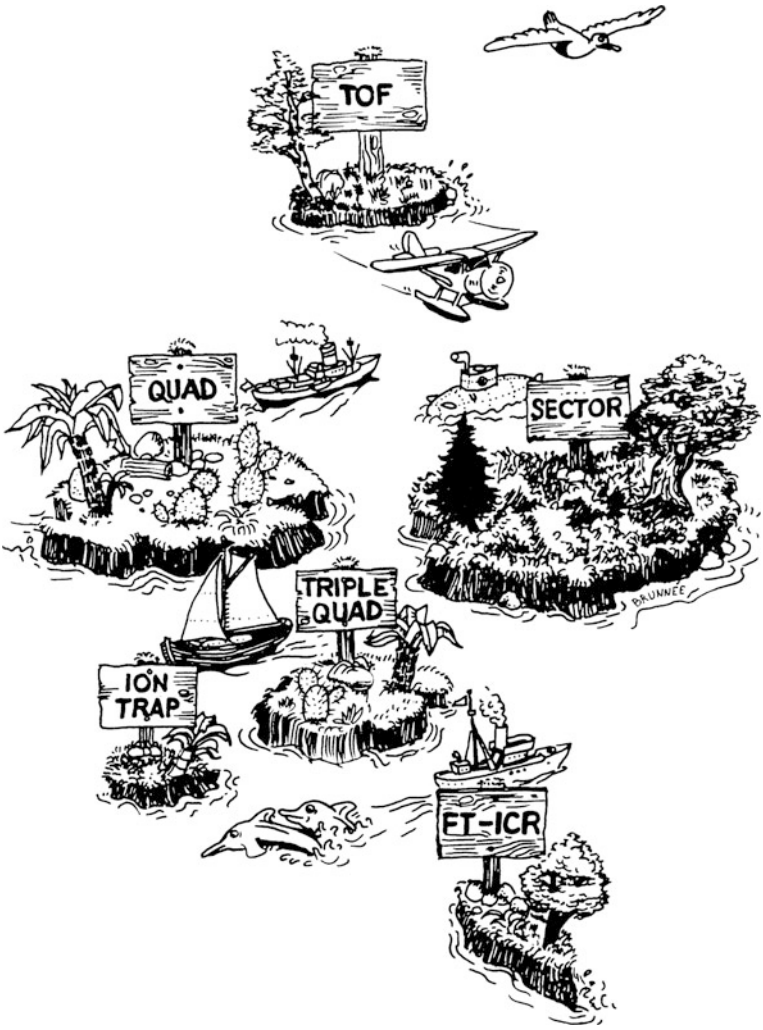


**Fig. 4.1** Mass spectrometer islands as presented in a cartoon by C. Brunnée in 1987. The actual situation is quite different, however: much of the cliffs of the sector and quad islands have vanished in the sea while all others have gained new land, and moreover, the Orbitrap island has been given birth in the south east (Reproduced from Ref. [2] with permission. © Elsevier Science, 1987)

From the very beginning to the present almost any physical principle ranging from time-of-flight to cyclotron motion has been employed to construct mass-analyzing devices (Fig. 4.1). Some were extremely successful at the time of their

**Table 4.1** Common mass analyzers

| Type | Acronym | Principle |
|---|---|---|
| Time-of-flight | TOF | Time dispersion of a pulsed ion beam; separation by time-of-flight |
| Magnetic sector | B | Deflection of a continuous ion beam; separation by momentum in magnetic field due to Lorentz force |
| Linear quadrupole | Q | Continuous ion beam in linear radio frequency quadrupole field; s due to instability of ion trajectories |
| Linear quadrupole ion trap | LIT | Continuous ion beam delivers ions for trapping; storage, and eventually separation in linear radio frequency quadrupole field by resonant excitation |
| Quadrupole ion trap | QIT | Trapped ions; separation in three-dimensional radio frequency quadrupole field by resonant excitation |
| Fourier transform-ion cyclotron resonance | FT-ICR | Trapped ions in magnetic field (Lorentz force); separation by cyclotron frequency, image current detection and Fourier transformation of a transient signal |
| Orbitrap | Orbitrap | Axial oscillation in inhomogeneous electric field; detection of frequency after Fourier transformation of a transient signal |

invention, for others it took decades until their potential had fully been recognized. The basic types of mass analyzers employed for analytical mass spectrometry are summarized in Table 4.1.

A comparison of Brunnée's cartoon with Table 4.1 reveals that linear ion traps and Orbitraps had not yet been invented at the time of his writing said review. An "updated version" of Brunnée's map was presented 2014 in Geneva at the International Mass Spectrometry Conference (IMSC) during the Brunnée Award lecture by Dimitris Papanastasiou (Fig. 4.2).

The properties of an ideal mass analyzer are well described [2], but despite the tremendous improvements made, still no mass analyzer is perfect. There is a wealth of articles and books that are highly recommended for those seeking a deeper look at the evolution of mass spectrometers [3–13]. In recent years, there has been a growing interest in employing miniature mass analyzers for *in situ* analysis [14, 15], for instance in environmental [16] and biochemical applications [17], for process monitoring, for detection of chemical warfare agents, and for space missions [18, 19]. The most recent completely new type of mass analyzer, the Orbitrap, was introduced in 2005 by Makarov [20].


**Fig. 4.2** The treasure islands of MS: The Brunnée map expanded to reflect latest advancements in mass analyzers like Orbitrap, ionization methods such as ESI, MALDI and discharge-based techniques, ion mobility spectrometry instrumentation, and the emerging role of intermediate pressure RF ion optics. Low-pressure gas dynamics (LPGD) provides a new tool for atmospheric pressure interface design. The expanded Brunnée map was presented at the IMSC 2014 Brunnée Award lecture by Dimitris Papanastasiou

## 4.1 How to Create a Beam of Ions

Consider an ion that is brought into or generated within an electric field between two oppositely charged plates of a capacitor. Such an ion will be accelerated towards the plate of opposite charge. If the attracting plate has a (round) orifice or a slit, an ion beam is produced by this simple ion source. Assuming the spread in ion kinetic energy to be small as compared to the total ion kinetic energy, i.e., $\Delta E_{\mathrm{kin}} << E_{\mathrm{kin}}$, the beam can be considered to be monoenergetic. The actual charge of an ion may be either positive or negative depending on the ionization method employed. Changing the polarity of the plates causes a switch from the extraction of positive ions to negative ions or vice versa. For practical reasons, the attracting electrode is usually grounded and the pushing plate is set to high voltage. Doing so allows to keep the entire mass analyzer grounded, thereby contributing substantially to safety of operation (Fig. 4.3). The extraction of ions and the shape of the ion beam can largely be improved if the acceleration voltage is applied in two [21] or

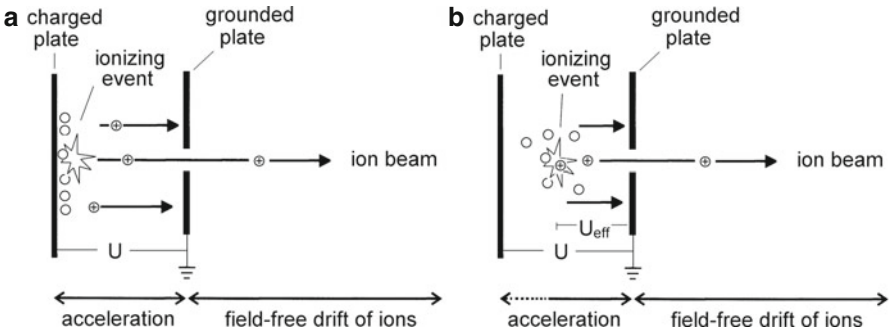


**Fig. 4.3** Simple single-stage ion sources. (**a**) Ionization from a surface or probe where the ionizing event is located on the charged plate; in reality ionizing events in a spatially confined volume above the surface have to be taken into account. (**b**) Gas phase ionization, where the effective accelerating voltage $U_{eff}$ depends on the actual position of the ion between the plates. After a neutral has been ionized (positive in this illustration), it is attracted by the opposite grounded plate. Those ions passing through a hole of the grounded electrode create an ion beam emerging into the field-free region behind. The ion beam produced by such a primitive ion source is not parallel, but has some angular spread

more successive stages instead of a single one and if ion optical lenses are part of the ion acceleration assembly.

**Keep it grounded**
Apart from a few exotic exceptions, all mass spectrometers are – and always have been – constructed in a way to ensure that most parts are electrically grounded. Voltage, especially because this often means high voltage, is only applied to comparatively small parts inside. This ensures safety of operation, and in addition, low capacitive load simplifies rapid DC voltage changes, enables high RF frequencies, and allows for quick polarity switching.

## 4.2 Time-of-Flight Instruments

### 4.2.1 Time-of-Flight: Basic Principles

The first *time-of-flight* (TOF) analyzer was constructed and published in 1946 by W. E. Stephens [22]. The principle of TOF is quite simple: ions of different $m/z$ are dispersed in time during their flight along a field-free drift path of known length. Provided all the ions start their journey at the same time or at least within a sufficiently short time interval, the lighter ones will arrive earlier at the detector than the heavier ones. This demands that they emerge from a pulsed ion source

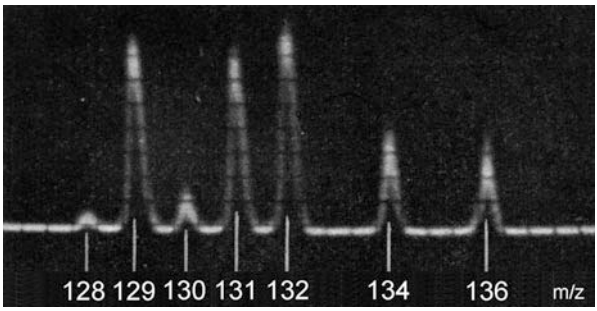


**Fig. 4.4** Oscilloscope output of the electron ionization TOF spectrum of xenon on a Bendix TOF-MS. The *dark horizontal lines* are a grid on the oscilloscopic screen. (For the isotopic pattern of Xe cf. Fig. 3.2.) (Adapted from Ref. [26] with permission. © Pergamon Press, 1959)

which can be realized either by pulsing ion packages out of a continuous beam or more conveniently by employing a true pulsed ionization method.

Soon, other groups embarked on Stephens' concept [23] and increasingly useful TOF instruments were designed and constructed [21, 24, 25] leading to their first commercialization by Bendix in the mid-1950s. These first-generation TOF instruments were designed for gas chromatography-mass spectrometry (GC-MS) coupling [26, 27]. Resolution-wise, their performance was poor as compared to modern TOF analyzers, but the specific advantage of TOFs over magnetic sector instruments was the rate of spectral acquisition, i.e., the number of spectra per second they provided (Fig. 4.4). In GC-MS the TOF analyzer soon became superseded by linear quadrupole analyzers and it was not until the late 1980s that development of TOF analyzers encountered a revival [28, 29] – the success of pulsed ionization methods, especially of matrix-assisted laser desorption/ionization (MALDI), made this possible (Chap. 11). Therefore, we will repeatedly refer to MALDI in our discussion of TOF analyzers.

MALDI generated a great demand for mass analyzers which are suitable to be used in conjunction with a naturally pulsed ion source and capable of transmitting ions of extremely high mass up to several $10^5$ u [30]. Since then, the performance of TOF instruments has tremendously increased [31, 32]. TOF analyzers have been adapted for use with other ionization methods and – together with Orbitraps and FT-ICR instruments – have superseded the established magnetic sector instruments in most applications [31, 33].

The main advantages of TOF instruments are:

- In principle, the *m*/*z* range of a TOF analyzer is unlimited [34, 35].
- Complete mass spectra are obtained of ions created during a short (nanoseconds) ionizing event, e.g., from a laser shot in LDI or MALDI.
- TOF analyzers offer high ion transmission and thus contribute to high sensitivity.
- The mass spectral acquisition rate of TOFs is very high, essentially $>10^3$ Hz.
- TOF instrument design and construction is comparatively straightforward.
- Modern TOF instruments allow for accurate mass measurements and tandem MS experiments [36].

### 4.2.2 TOF Instruments: Velocity of Ions and Time-of-Flight

Independent of the ionization method, the electric charge $q$ of an ion of mass $m_i$ is equal to an integer number $z$ of electron charges $e$, and thus $q = ez$. The energy uptake $E_{el}$ by moving through a voltage $U$ is given by

$$E_{el} = qU = ezU \tag{4.1}$$

Thereby, the former potential energy of a charged particle in an electric field is converted into kinetic energy $E_{kin}$, i.e., into translational motion

$$E_{el} = ezU = \frac{1}{2} m_i v^2 = E_{kin} \tag{4.2}$$

Assuming that the ion was initially at rest, which holds by first approximation, the velocity attained is calculated by rearranging Eq. (4.2) into

$$v = \sqrt{\frac{2ezU}{m_i}} \tag{4.3}$$

i.e., $v$ is inversely proportional to the square root of mass.

**A racing soccer ball** The velocity of the [60]fullerene molecular ion, $C_{60}^{+\bullet}$, after acceleration by 19.5 kV is obtained from Eq. (4.3) as

$$v = \sqrt{\frac{2 \cdot 1.6022 \times 10^{-19}\text{C} \times 19,500\text{V}}{1.1956 \times 10^{-24}\text{kg}}} = 72,294\,\text{m s}^{-1}$$

An ion velocity of 72,294 m $s^{-1}$ appears rather high, but merely is 0.0024% of the speed of light. The acceleration voltages and thus, the ion velocities are the highest in TOF-MS, although magnetic sector instruments are operated with kilo-electron-volt ion beams, too (Sect. 4.3). The other types of mass analyzers require ions to enter at much lower kinetic energies.

**Valid for any mass analyzer**
Equation (4.3) describes the velocity of any ion after acceleration in an electric field, and therefore it is valid not only for TOF-MS, but for any part of a mass spectrometer handling beams of ions.

One now can quite easily imagine measuring the time for an ion of unknown $m/z$ in traveling a distance $s$ after being accelerated by a voltage $U$. The relationship between velocity and time $t$ needed for traveling the distance $s$ is

$$t = \frac{s}{v} \tag{4.4}$$

which upon substitution of $v$ by Eq. (4.3) becomes

$$t = \frac{s}{\sqrt{\frac{2ezU}{m_i}}} \tag{4.5}$$

Equation (4.5) yields the time needed for the ion to travel the distance $s$ at constant velocity, i.e., in a *field-free* environment after the process of acceleration has been completed. Rearrangement of Eq. (4.5) reveals the relationship between the instrumental parameters $s$ and $U$, the experimental value of $t$ and the ratio $m_i/z$

$$\frac{m_i}{z} = \frac{2\,e\,U\,t^2}{s^2} \tag{4.6}$$

It is also obvious from Eq. (4.5) that the time to drift through a fixed length of field-free space is proportional to the square root of $m_i/z$

$$t = \frac{s}{\sqrt{2eU}} \sqrt{\frac{m_i}{z}} \tag{4.7}$$

and thus, the time interval $\Delta t$ between the arrival times of ions of different $m/z$ is proportional to $s \times ((m_i/z_1)^{½} - (m_i/z_2)^{½})$.

**Mass, not *m/z***
Here, the ratio $m_i/z$ denotes ion mass [kg] per number of electron charges. The index i at the mass symbol is used to avoid confusion with the *mass-to-charge ratio*, $m/z$, as used to specify the position of a peak on the abscissa of a mass spectrum (Sect. 1.4.3).

**Small differences in time-of-flight** According to Eq. (4.7) the $C_{60}^{+\bullet}$ ion, $m/z$ 720, dealt with in the preceding example will travel through a field-free flight path of 2.0 m in 27.665 µs, while it takes slightly longer for its isotopolog $^{13}C^{12}C_{59}^{+\bullet}$, $m/z$ 721. The proportionality to the square root of $m/z$ gives (use of $m_i/z$ values yields identical results as the dimension is cancelled):

$$\frac{t_{721}}{t_{720}} = \frac{\sqrt{721}}{\sqrt{720}} = 1.000694$$

Thus, $t_{721} = 27.684$ µs. This corresponds to a difference in time-of-flight of 19 ns under these conditions (cf. Fig. 4.9).

The proportionality of time-of-flight to the square root of $m/z$ causes $\Delta t$ for a given $\Delta(m/z)$ to decrease with increasing $m/z$: under otherwise the same conditions $\Delta t$ per 1 u is calculated as 114 ns at $m/z$ 20, 36 ns at $m/z$ 200, and just 11 ns at $m/z$ 2000. Therefore, the realization of a time-of-flight mass analyzer depends on the ability to measure short time intervals with sufficient accuracy [37–39]. At this point it becomes clear that the performance of the early TOF analyzers – among other reasons – suffered from the low-efficiency electronics of their time. It took until the mid-1990s to overcome this barrier [32].

**"Compressed" isotopic patterns of multiply charged ions** The time-of-flight of multiply charged ions ($z > 1$) explains the position and appearance of signals caused by ions of higher charge states (Sect. 3.8). As $z$ increases to 2, 3 etc., the numerical value of $m/z$ is reduced by a factor of 2, 3 etc., i.e., the ion will be detected at lower $m/z$ than the corresponding singly charged ion of the same mass. According to Eq. (4.7), the time-of-flight is reduced by a factor of 1.414 (the square root of 2) for doubly charged ions which is the same time-of-flight as for a singly-charged ion of half of its mass. Accordingly, the time-of-flight is reduced by a factor of 1.732 (the square root of 3), for triply charged ions corresponding to a single-charged ion of one third of its mass, and so on for higher charge states.

**Inferring the charge state**
For multiply charged ions, the $m/z$ scale is compressed by a factor of $z$ equal to the charge state of the ion. Isotopic patterns remain unaffected as far as the relative intensities are concerned. As $\Delta(m/z)$ between isotopic peaks is reduced inversely proportional to $z$, the charge state can readily be assigned, e.g., doubly charged ions cause isotopic peaks at $\Delta(m/z) = 0.5$, triply charged ions cause them at $\Delta(m/z) = 0.333$, and so on.

### 4.2.3 Linear Time-of-Flight Analyzer

Restricting its use to laser desorption/ionization (LDI) and matrix-assisted laser desorption/ionization (MALDI, Chap. 11), a simple TOF instrument can be set up as follows (Fig. 4.5): The analyte is supplied as a thin layer on a *sample holder* or *target* upon which a pulsed laser is focused. The acceleration voltage $U$ is applied between this target and a grounded counter electrode. Ions formed and desorbed during the laser pulse are continuously extracted and accelerated as they emerge from the target into the gas phase. When leaving the acceleration region $s_0$ the ions should possess equal kinetic energies. They drift down a field-free flight path $s$ in the order of 1–2 m and finally hit the detector. Typically, *microchannel plate* (MCP) detectors are employed to compensate for the angular spread of the ion beam (Sect. 4.12). A fast *analog-to-digital converter* (8 bit or 10 bit ADC)

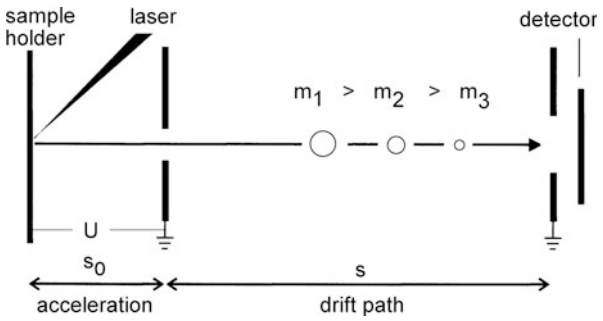


**Fig. 4.5** Scheme of a linear TOF instrument designed for use in combination with a laser desorption ion source. Once created during a laser pulse onto the sample layer, ions are continuously accelerated by a voltage $U$. While drifting along the field-free drift path $s$, they are dispersed in time. Lighter ions reach the detector first

transforms the analog output of the detector for computer-based data storage and data processing. Such an instrumental setup where the ions are traveling on a straight line from the point of their creation to the detector is called *linear TOF*.

In principle, any other ionization method can be combined with a TOF analyzer even if it is not an intrinsically pulsed technique, provided there are means to extract ions in a pulsed manner from such an ion source (Sect. 4.2.6).

The drift time $t_d$ as calculated by means of Eq. (4.7) is not fully identical to the total time-of-flight. Obviously, the time needed for acceleration of the ions $t_a$ has to be added. Furthermore, a short period of time $t_0$ may be attributed to the laser pulse width and the process of desorption/ionization, which is typically in the order of a few nanoseconds. Thus, the total time-of-flight $t_{total}$ is given by

$$t_{total} = t_0 + t_a + t_d \tag{4.8}$$

A rigorous mathematical treatment of the TOF analyzers as needed for the construction of such instruments of course has to include all contributions to the total time-of-flight [32, 36–38, 40–42].

The transmittance of a linear TOF analyzer approaches 90% because ion losses are solely caused by collisional scattering due to residual gas or by poor spatial focusing of the ion source. With a sufficiently large detector surface located at a short distance from the ion source exit, a very high fraction of the ions will be collected by the detector.

Even metastable decompositions during the flight do not reduce the intensity of a molecular ion signal, because the fragments formed conserve the velocity of the fragmenting ion and are therefore detected simultaneously with their intact precursors. In such a case, the ionic *and* the neutral fragment cause a response at the detector. These properties make the linear TOF analyzer the ideal device for analyzing easily fragmenting and/or high-mass analytes [43].

**Detection of neutrals**
In linear TOF analyzers, neutrals formed by metastable fragmentation also give rise to a signal. This is because they impinge on the detector after having travelled down the flight tube side-by-side with the ionic product of ion dissociation. As a result, nonfragmenting intact precursor ions plus both ionic and neutral products of the metastable dissociation of precursor ions will hit the detector simultaneously. Therefore, linear TOF analyzers are best suited for the analysis of large and labile molecules, e.g., oligonucleotides (Sect. 11.5). This presents a rare case where neutrals contribute to a useful signal in mass spectrometry.

The example in Sect. 4.2.2 demonstrates that the differences in time-of-flight of ions differing by 1 u in mass are in the order of about 10 ns at about $m/z$ 1000. The time elapsing during desorption/ionization is roughly 10–50 ns in case of standard UV lasers, but can be longer with IR lasers. Consequently, the variation in starting times for ions of the same $m/z$ value is often larger than the difference in time-of-flight of neighboring $m/z$ values, thereby limiting the resolution.

### 4.2.4 Better Vacuum Improves Resolving Power

The mass resolution of a TOF analyzer is directly proportional to its total flight path length [44]. Improved vacuum conditions result in an elongated mean free path for the ions and thus reduce the risk of collisions in transit through the analyzer. The resolving power of a TOF analyzer clearly depends on the background pressure [45]. Despite improvements of resolving power in the order of a factor of two can be realized (Fig. 4.6), enhanced pumping systems alone are not able to effect a breakthrough in resolving power.

**Only QITs use buffer gas**
The quadrupole ion trap (Sect. 4.5) is the only type of mass analyzer that uses buffer gas to damp ion trajectories. All other mass analyzers require the highest possible vacuum for optimum performance.

### 4.2.5 Energy Spread of Laser-Desorbed Ions

Laser-desorbed ions possess comparatively large initial kinetic energies of some 10 eV that are superimposed on the kinetic energy provided by the acceleration voltage, which is typically in the order of 10–30 kV. Obviously, higher acceleration

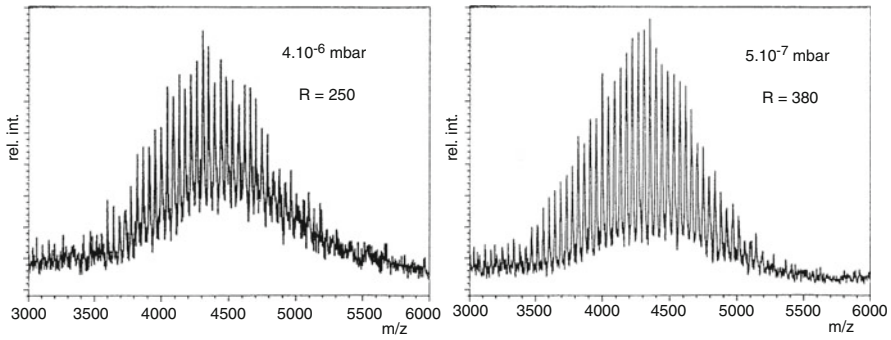


**Fig. 4.6** Dependence of resolution on analyzer pressure: linear MALDI-TOF spectra of polyethylene glycol 4000 recorded at a pressure of $4 \times 10^{-4}$ Pa (*left*) and $5 \times 10^{-5}$ Pa (*right*) (Adapted from Ref. [45] with permission. © John Wiley & Sons, 1994)

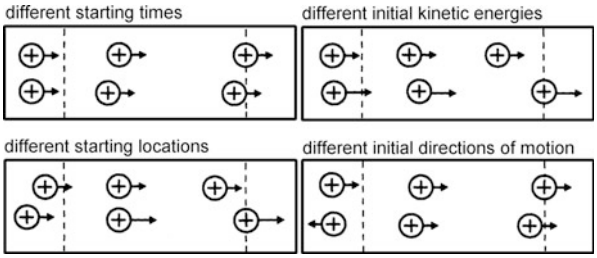


**Fig. 4.7** Effects of initial time, space, and kinetic energy distributions on mass resolution in TOF-MS (Adapted from Ref. [39] with permission. © American Chemical Society, 1992)

voltages are advantageous in that they diminish the relative contribution of the energy distribution caused by the ionization process. Figure 4.7 illustrates the possible effects of deviations from the assumption that ions initially are at rest on an equipotential surface [39]. All these effects together limit resolution to $R \approx 500$ for continuous extraction linear TOF analyzers.

**Bothersome energy spread**

The spread in ion kinetic energies from thermal energy as well as from inhomogeneous acceleration presents a general problem in the construction of mass analyzers. Accordingly, there are numerous approaches to narrow down the kinetic energy distributions of ions or to compensate for their effects.

### 4.2.6 Reflector Time-of-Flight Analyzer

The *reflector* or *reflectron* was devised by Mamyrin in 1994 [46]. In the reflector TOF analyzer – often abbreviated *ReTOF* – the reflector acts as an ion mirror that focuses ions of different kinetic energies in time. Its performance is improved by using two-stage or even multistage reflector designs.

Commonly, reflector instruments are also equipped with a detector behind the reflector allowing linear mode operation simply by switching off the reflector voltage. A complete mathematical treatment of single-stage and two-stage reflectors is found in the literature [36–38, 42]. Here, we will restrict ourselves to a qualitative explanation of the reflector.

A simple reflector consist of a retarding electric field located behind the field-free drift region opposed to the ion source. In practice, a reflector is comprised of a series of ring-shaped electrodes at increasing potential. The reflection voltage $U_r$ is set to about 1.05–1.10 times the acceleration voltage $U$ in order to ensure that all ions are reflected within the homogeneous portion of the electric field of the device

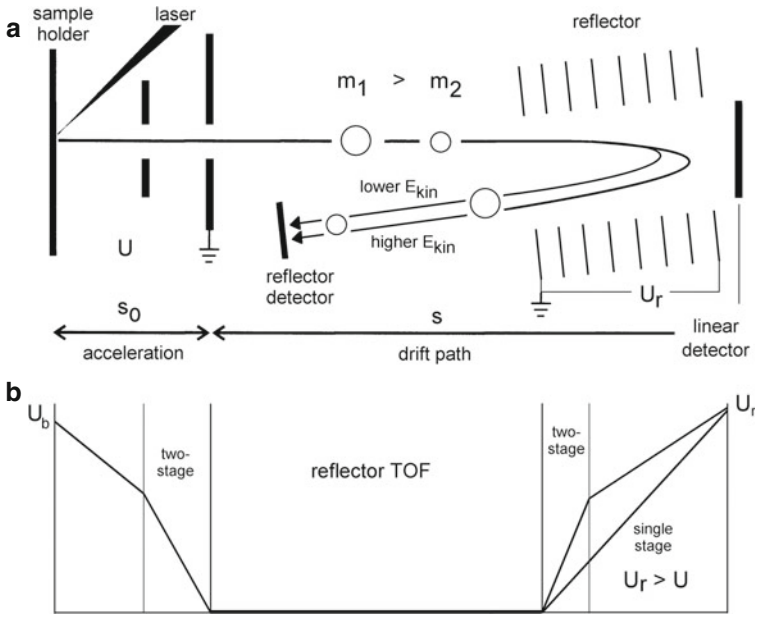


**Fig. 4.8** ReTOF analyzer. (**a**) Principle of operation, (**b**) potentials along the instrument. Ions of different kinetic energy penetrate the reflector to different depths before they come to a halt and get ejected into the opposite direction. Faster ions have to travel a longer path than slower ones, and thus, time focus is achieved at some point on the return path. There, the detector receives ions of the same mass at (about) the same time. A small angle between the axis of the flight path and the reflector allows the detector to be placed beside the ion source

(Fig. 4.8). The ions penetrate the reflectron until they reach zero kinetic energy and are then expelled from the reflector in opposite direction. The kinetic energy of the leaving ions remains unaffected, however their flight paths vary according to their differences in kinetic energy. Ions carrying more kinetic energy will fly deeper into the decelerating field, and thus spend more time within the reflector than less energetic ions. Thereby, the reflector achieves a correction in time-of-flight that substantially improves the resolving power of the TOF analyzer [32, 37–39]. In addition, the reflector provides (imperfect) focusing with respect to angular spread of the ions leaving the source and it corrects for their spatial distribution [37, 46]. Adjusting the reflector at a small angle with respect to the ions exiting from the source allows the reflector–detector to be placed adjacent to the ion source (Mamyrin design). Alternatively, a detector with a central hole to transmit the ions leaving the ion source has to be used in *coaxial reflectrons* (cf. Sect. 9.5).

Although the reflector elongates the flight path and hence the dispersion in time-of-flight, this effect is of lower importance than its capability to compensate for initial energy spread. Simple elongation of the flight path can also be achieved with longer flight tubes in linear instruments. However, too long flight paths may even decrease the overall performance of TOF analyzers due to loss of ions by angular spread of the ion beam and scattering of ions after collisions with residual gas.

Nonetheless, the remarkable improvements of resolving power delivered by TOF analyzers with their very long flight paths have more recently led to the development of TOF analyzers with folded ion paths and sophisticated ion optics (Sect. 4.2.11).

The ability of the ReTOF to compensate for the initial energy spread of ions largely increases the resolving power of TOF instruments. While a typical continuous extraction TOF instrument in linear mode cannot resolve isotopic patterns of analytes above about $m/z$ 500, it will do when operated in reflector mode (Fig. 4.9). At substantially higher $m/z$, the ReTOF still fails to resolve isotopic patterns, even though its resolution is still better than that of a linear TOF analyzer.

**Metastable ions in a ReTOF**

In case of metastable fragmentations, ReTOF analyzers behave differently from linear TOF analyzers. If fragmentation occurs between ion source and reflector, the ions will be lost by the reflector due to their change in kinetic energy. Transmission occurs only for fragments still having kinetic energies close to that of the precursor due to the energy tolerance of the reflector, as, for instance, $[M + H–NH_3]^+$ in case of a peptide of about $m/z$ 2000. However, such ions are not detected at correct $m/z$, thereby giving rise to a "tailing" of the signal. Ions fragmenting in transit from reflector to detector are treated the same way as ions in the linear TOF. Thus, the elongated flight path of the ReTOF analyzer also allows more time for fragmentation. This can complicate the detection of very labile analytes in reflector mode.

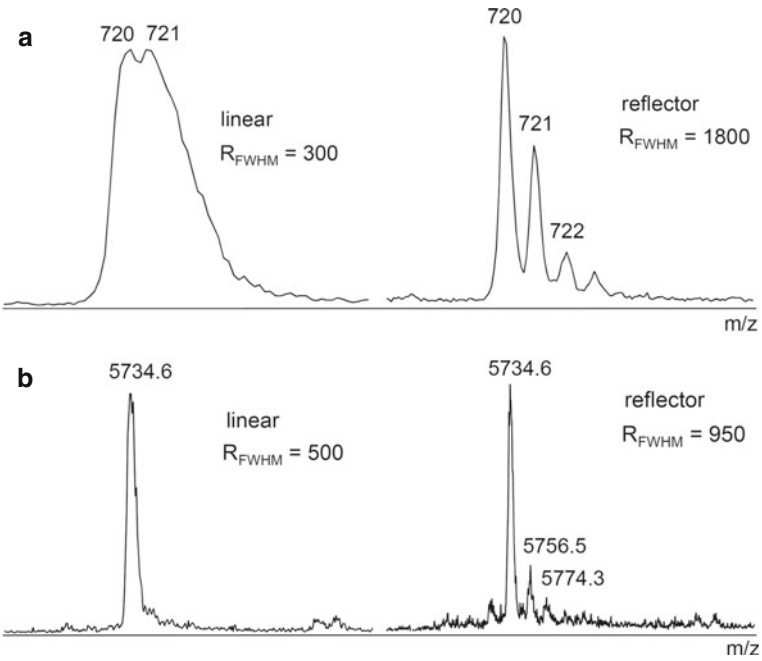


**Fig. 4.9** $C_{60}$ molecular ion signal of at *m/z* 720 (**a**) and the $[M + H]^+$ ion signal of bovine insulin, *m/z* 5734.6 (**b**), as obtained on a TOF instrument in linear mode (*left*) and reflector mode (*right*). All other experimental parameters remained unchanged

### 4.2.7 Delay Before Extraction to Improve Resolving Power

In MALDI-TOF-MS, the energy spread of the emerging ions is of significant magnitude as a result of the MALDI process, which in addition, creates a temporal distribution of ion formation. The most successful approach of handling such conditions is presented by ion sources allowing a delay between generation and extraction/acceleration of the ions. *Time-lag focusing* dates back to 1955 [21] and since then has been adapted to the needs of MALDI-TOF-MS by several groups [47–50].

The advantage of pulsed acceleration is its capability to focus the ions in time thereby reducing the effect of initial position and initial velocity on resolution. In addition, the delay permits the plume generated upon laser irradiation to disperse while still in a field-free region prior to acceleration. This avoids collisions of energetic ions with neutrals in the initially dense plume that could broaden the translational energy distribution and cause fragmentation due to CID (Sect. 9.3). Continuous extraction MALDI ion sources had to be operated with laser fluences

close to the threshold for ion formation in order not to sacrifice the limited resolution any further. With pulsed acceleration, this effect is greatly reduced.

After allowing the ions to separate in space according to their different initial velocities during a delay of some hundreds of nanoseconds the acceleration voltage is switched on with a fast pulse. This procedure also ensures that laser-induced reactions have terminated before ion acceleration begins. A delay of about 200 ns was empirically found to be required to realize the desired effect [36, 42].

Longer delays allow to achieve very high resolving power at the focused mass, but outside the optimized $m/z$ range resolution remains limited. More recently, the so-called *panoramic pulsed ion extraction* (PAN) was introduced (Bruker Daltonik) that makes use of a time-modulated extraction pulse to stretch the optimum resolution over a wide $m/z$ range.

**Many names**
Unfortunately, establishing patents and trademarks has caused redundant names for almost the same thing: *time lag focusing* (TLF, Micromass); *delayed extraction* (DE, Applied Biosystems); *pulsed ion extraction* (PIE), and more recently *panoramic pulsed ion extraction* (PAN, Bruker Daltonik).

Using a two-stage acceleration ion source allows the electric field between target (repeller) and extraction plate $P_1$ to be varied. The remaining fraction of the acceleration voltage is applied in the second stage. At the onset of extraction, ions with high initial velocities have traveled farther than slower ones, and therefore experience only a fraction of the extraction voltage d$V$ between target and extraction plate $P_1$. The voltage of the second stage is the same for all ions. As a result, the fastest ions receive less energy from the accelerating field than the slowest. Thereby, such ion sources compensate for the initial energy distribution [50].

The optimum settings of the delay time and of the ratio of pulsed to fixed voltage ($V_1/V_2$) depend on $m/z$ with a tendency towards longer delays and/or a larger $V_1/V_2$ ratio for heavier ions. In practice, the variation of potentials in pulsed ion extraction with time can be handled as follows (Fig. 4.10): target and extraction plate $P_1$ are maintained at the same potential during the delay time, thereby creating a field-free region $d_1$. After the delay has passed, $P_1$ switches from $V_1$ by a variable value d$V$ to $V_2$ causing extraction of the ions.

**Impressive gain in resolving power** Regardless of the manufacturer of the hardware, the effect of a time lag on resolution is quite dramatic. The resolving power of linear instruments is improved by a factor of 3–4 and reflector instruments become better by a factor of about 2–3 [50]. The advantages are obvious by comparison of MALDI-TOF spectra of substance P, a low mass peptide, as obtained in continuous extraction mode and after PIE upgrade of the same instrument (Fig. 4.11). Modern mid-class MALDI-TOF instruments easily deliver twice that resolution.

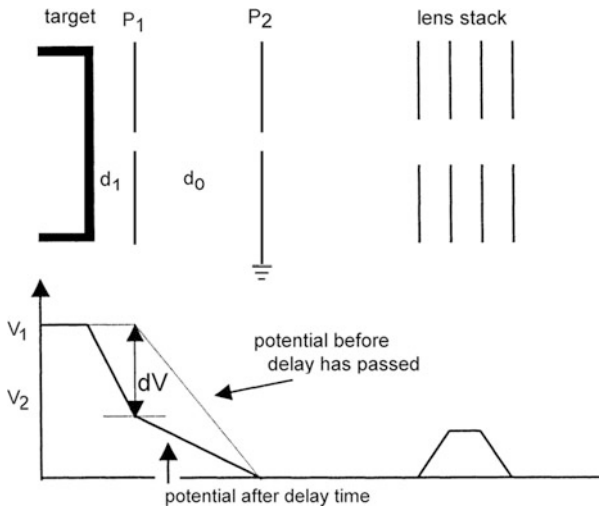


**Fig. 4.10** Variation of potentials in pulsed ion extraction with time. The lens stack acts as angular focusing device for the ion beam (By courtesy of Bruker Daltonik, Bremen)

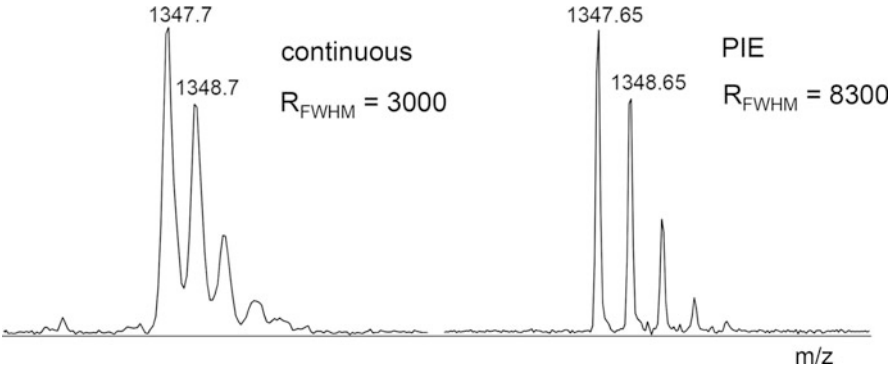


**Fig. 4.11** MALDI-TOF spectra of substance P, a low-mass peptide, as obtained from a Bruker Biflex ReTOF in continuous extraction reflector mode (in 1995, *left*) and after PIE upgrade of this instrument (in 2001, *right*)

### 4.2.8 Orthogonal Acceleration TOF Analyzers

Up to here, the TOF analyzer has been under consideration bearing MALDI-TOF equipment in mind, just because MALDI as a pulsed ionization method delivers ions to a TOF analyzer in an ideal manner. In fact, MALDI initiated such tremendous improvements of TOF analyzers that it became attractive to combine these compact but powerful analyzers with other, inherently nonpulsed, ionization methods. The major breakthrough for generalized use of TOF analyzers arose from the design of the *orthogonal acceleration* TOF analyzer (oaTOF). In an

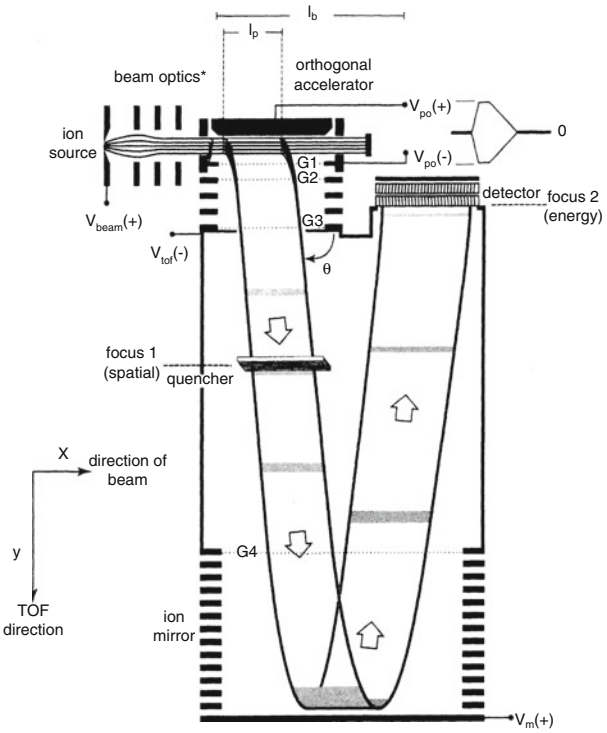


**Fig. 4.12** An orthogonal acceleration reflector TOF instrument. See text for discussion (Reproduced from Ref. [55] by permission. © John Wiley & Sons, 2000)

oaTOF analyzer, pulses of ions are extracted orthogonally from a continuous ion beam (Fig. 4.12) [51, 52]. The oaTOF analyzer can be of linear or ReTOF type. Although different problems have to be overcome for each ionization method, the oaTOF analyzer is in principle suited for any of them [29, 53–55].

The main advantages of oaTOF analyzers are:

- High sensitivity due to good duty cycle and high transmission of TOF analyzers.
- High spectral acquisition rate (spectra per second) even after pre-averaging.
- High mass-resolving power.
- Mass accuracies as good as 1 ppm for formula determination.
- Compact design and small footprint.

Therefore, it is not astonishing that oaTOF instruments are currently widespread in use for numerous kinds of applications. Electrospray ionization (ESI) oaTOF instruments with accurate mass capabilities represent the majority of these systems [56–58], but gas chromatography–mass spectrometry (GC-MS) instruments are

also available. In particular for *fast GC* applications [59, 60] and for HR-GC-MS [61] oaTOF systems are advantageous. Today, a large portion of the instruments incorporating oaTOF analyzers are hybrids mostly of the quadrupole-oaTOF type. We will therefore deal with them in the section on hybrid instruments.

### 4.2.9 Operation of the oaTOF Analyzer

Ions leaving the ion source are focused to form an almost parallel ion beam, i.e., to minimize ion motion orthogonal to the ion beam axis. Then, the ion beam enters the orthogonal accelerator ($x$-axis) [29, 53, 55]. The ion kinetic energy in this beam is only in the range of 10–20 eV. A package of ions of length $l_p$ is pushed out orthogonally from its initial direction by a sharp pulse, and is thus accelerated into the TOF analyzer ($y$-axis) by a voltage of 5–10 kV. From the TOF analyzer's point of view the orthogonal acceleration unit can be regarded as the ion source. Usually, ions are accelerated through a two-stage setup analogous to the Wiley-McLaren ion source [21].

The design of the TOF analyzer itself is similar to those discussed before, but its diameter is much wider because the velocity of the ions in $x$-direction, $v_{beam}$, is not affected by the orthogonal push-out process. Therefore, the detector needs to be comparatively wide in $x$-direction to enable ions extracted anywhere from the whole path $l_p$ to hit its surface. In practice, the detector needs to be several centimeters in length. The angle $\theta$ between the $x$-direction and the flight axis into the TOF analyzer is given by

$$\theta = \tan^{-1}\sqrt{\frac{-V_{tof}}{V_{beam}}} = \tan^{-1}\left(\frac{v_{tof}}{v_{beam}}\right) \tag{4.9}$$

where $V_{tof}$ and $V_{beam}$ are the acceleration voltages for ion beam and orthogonal accelerator, respectively, and $v_{tof}$ and $v_{beam}$ are the corresponding ion velocities.

While one ion package travels through the TOF analyzer and is being dispersed in time, the accelerator is refilled with new ions from the ion source (the time-of-flight to cover an $m/z$ range up to about 5000 by the oaTOF is about 100 µs). During the drift time of an ion through the oaTOF, it travels a distance $l_b$. The ratio of the length of the orthogonal accelerator $l_p$ to $l_b$, determines the efficiency of the mass analyzer in terms of the ratio of ions used to ions created. This efficiency is known as the *duty cycle* of an instrument (next paragraph). The duty cycle of an oaTOF instrument is at an optimum if the time-of-flight to pass the TOF analyzer is slightly longer than the time needed for the continuous ion beam to refill the orthogonal accelerator. As soon as the heaviest ions have reached the detector, the next package is pulsed into the analyzer, giving rise to 10,000 complete mass spectra per second. In order to reduce the amount of data and to improve the signal-to-noise

ratio, summation of several single spectra is done by an acquisition processing unit before the spectra are passed to a computer for data storage and post-processing.

### 4.2.10 Duty Cycle

In mass spectrometry the term *duty cycle* is used to specify the fraction of time of an ion current as continuously delivered from an ion source that is finally used for mass analysis. The duty cycle of scanning instruments is intrinsically low as only ions of one $m/z$ value hit the detector at a time while all others are discarded by the analyzer, e.g., at $R = 1000$ only a fraction of $10^{-3}$ of the $m/z$ range reaches the detector corresponding to a duty cycle of just $10^{-3}$. Linear and ReTOF analyzers, on the other side, are capable of using almost all ions that are created from a pulsed ionizing event, and thus, these allow duty cycles in the order of 0.9. Although the oaTOF analyzer is by far better than scanning devices, it has to deal with a batch operation of the ion pulser. Fast (low-mass) ions traverse the orthogonal accelerator in a shorter time span than slow (high-mass) ions, thereby causing discrimination of low-mass ions. This behavior poses limitations on the mass range that can be simultaneously pulsed into the TOF analyzer. Depending on the axial velocity distribution of the ions and on the $m/z$ range to be analyzed, the duty cycle of oaTOF analyzers is in the 3–30% range.

**Determination of the duty cycle** In oaTOF operation, the frequency between acceleration pulses is selected as to avoid spectral overlap due to mixing of subsequent ion packages traveling along the TOF analyzer. The slowest ions arrive at the detector at a time that is determined by the ratio of the length of the ion entrance window, $l_p$, to the distance between the midpoints of this window and the detector, $l_b$. The duty cycle ($Du$) for the heaviest ion at $m/z_{max}$ is therefore given by $Du = l_p / l_b$. (Fig. 4.12) [62]. Furthermore, as the velocity of ions is proportional $(m/z)^{-2}$ (Eq. 4.3) the duty cycle for low-mass ions at $m/z_{low}$ is given by

$$Du = \frac{l_p}{l_b}\sqrt{\frac{m/z_{low}}{m/z_{max}}} \tag{4.10}$$

In practice, the ratio $l_p$ / $l_b$. is about 0.25, and thus, for $m/z_{low} = 100$ and $m/z_{max} = 2000$ we obtain $Du = 0.056$ for the low-mass ion.

Nonetheless, it is not the duty cycle alone that defines the transmission of oaTOF analyzers. Actually, the overall sensitivity of instruments is also influenced by ion losses during entrance into the orthogonal accelerator, divergence of ions prior to pulsing, eventual grids in the flight path, etc.

### 4.2.11 TOF Analyzers with a Folded Eight-Shaped Flight Path

It should have become clear that elongated flight paths could provide an effective means of increasing the resolving power of a TOF analyzer if it were not for the ion losses due to spreading of the beam by Coulombic repulsion and by scattering of ions upon collision with residual gas. Apart from these considerations, a flight tube of say 10 m in length would be impracticable for any commercial instrument. On the next few pages we will therefore take a – hopefully instructive – view of some extraordinary TOF analyzer designs to get a perspective on what can be done.

Folding the flight path into compact dimensions presents an elegant concept to build a TOF analyzer featuring a very long flight path. An approach by M. Toyoda makes use of four electrostatic sectors that enable eight-shaped ion optical geometries for multi-turn and multi-passage ion paths [44]. While electrostatic sectors enable curved ion paths, they still cannot provide angular focusing of the ion beam to a level required for multiple passages through the analyzer. Therefore, additional ion optical elements such as electrostatic lenses and/or DC quadrupoles are incorporated, leading to a rather complex ion optical system. Additionally, ion injection from an external ion source into this "race track" has to be incorporated into the design if the final instrument is intended to be of practical use.

One representative of this TOF geometry is the MULTUM Linear plus instrument [44, 63], which consists of four cylindrical electrostatic sectors and 28 DC quadrupole lenses. The setup of this TOF analyzer is shown in Fig. 4.13 and the corresponding ion trajectories as visualized by a computer simulation are depicted in Fig. 4.14. The ions are injected at moderate kinetic energy of 1.5 keV and one cycle, a "full eight", corresponds to 1.284 m. Thus, the analyzer fits into a suitcase-sized housing (60 × 70 × 20 cm).

**Outstanding resolving power** The mass resolving power of the MULTUM Linear plus instrument increases as more repetitive cycles are employed. This has been demonstrated for the doublet of $CO^{+\bullet}$ and $N_2^{+\bullet}$ ions at $m/z$ 28 (Fig. 4.15). It is remarkable that the time interval to the neighboring peak increases while the peak width in the spectra corresponding to 25.5, 101.5, 301.5, and 501.5 cycles or about 33, 130, 387, and 644 m path length, respectively, remains almost constant at 8 ± 1 ns. Finally, a mass resolution of $R_{FWHM} = 350{,}000$ is achieved after 501.5 cycles equaling a flight path of 644 m and a flight time of 6.3 ms.

It is an inherent weakness of this design that the next injection of ions has to wait until the preceding ion package has completed its journey through the TOF analyzer. Otherwise, fast ions of the following ion injection could overtake the slower ones of the previous one. The design does, however, not permit to distinguish this sort of interference, and thus, suffers from very low duty cycle as it takes several milliseconds to complete a single run. The $m/z$ range per analysis is also limited due

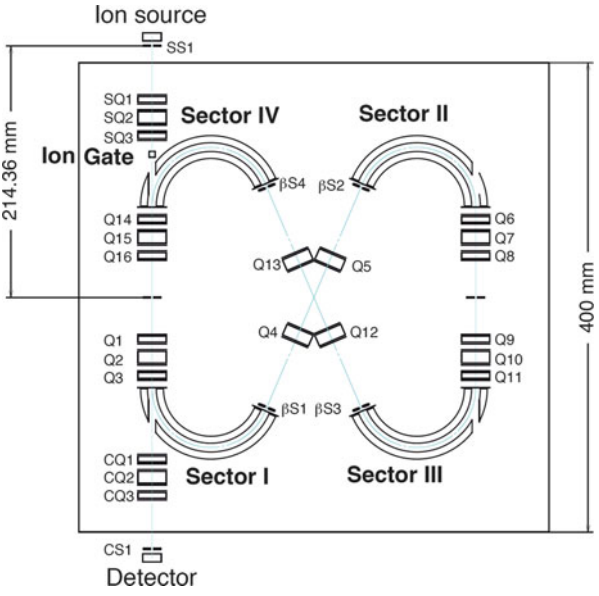


**Fig. 4.13** Complex but compact ion optical design of the MULTUM Linear plus TOF analyzer. The eight-shaped path is realized by electrostatic sectors and numerous DC quadrupole lenses (*SQ*, *Q*, and *CQ*) (Reproduced from Ref. [63] by permission. © IM Publications, 2010)

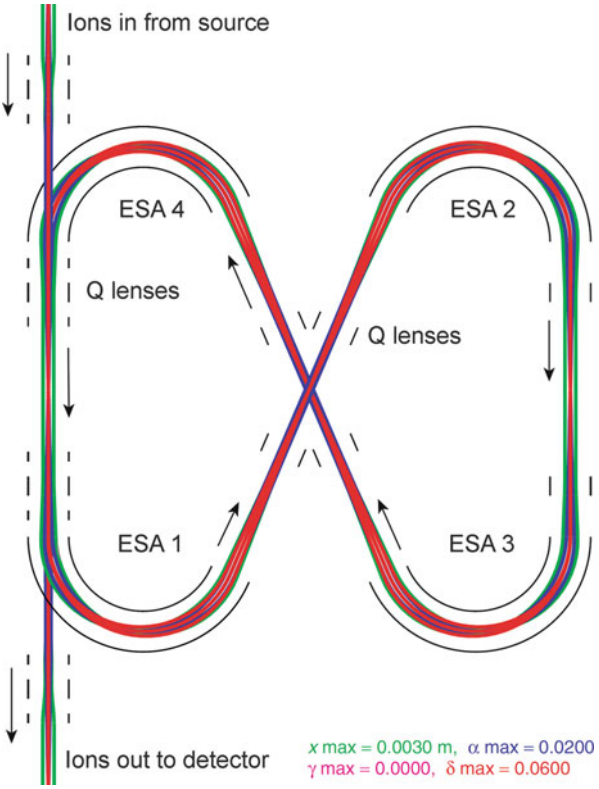


**Fig. 4.14** Simulated ion trajectories in the MULTUM Linear plus (cf. Fig. 4.13). The *arrows* indicate the direction of ion motion (Adapted from Ref. [44] by permission. © John Wiley & Sons, 2003)

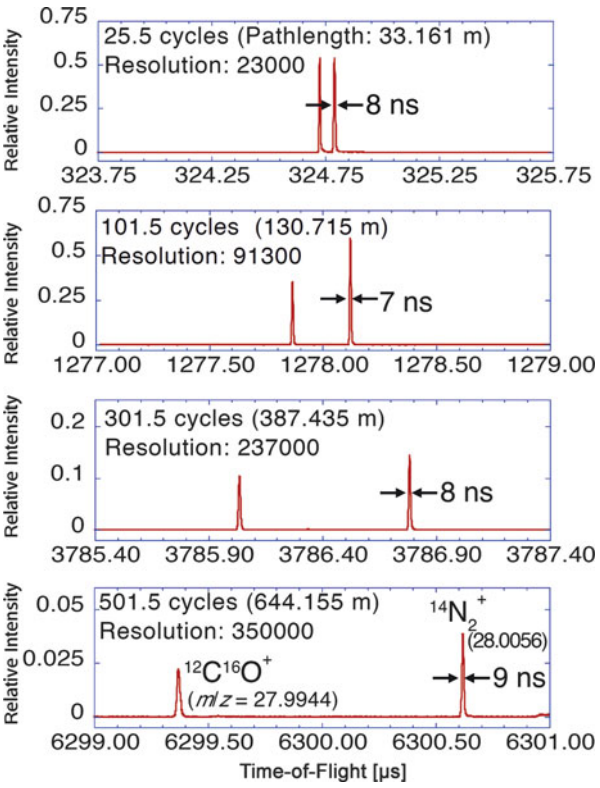


**Fig. 4.15** Gain of resolution upon increasing ion flight path through the MULTUM Linear plus as demonstrated for the doublet of $CO^{+\bullet}$ and $N_2^{+\bullet}$ at *m*/*z* 28. From *top* to *bottom* the spectra correspond to 25.5, 101.5, 301.5, and 501.5 cycles or about 33, 130, 387, and 644 m path length, respectively (Reproduced from Ref. [63] by permission. © IM Publications, 2010)

to this phenomenon: lighter ions would overtake the heavier ones after some cycles. In other words, only ions traveling the same number of cycles can be reliably analyzed.

**Space mission** From the commercial point of view, this unconventional yet impressive design still possesses some prototype character. Nonetheless, it has seen an application on the ROSETTA space mission. In fact, the lander Philae carried a miniature instrument of this design for the COSAC project [64, 65]. The lander was dropped on the surface of the comet 67P/Churyumov-Gerasimenko on November 12, 2014 after a 10-year journey of some seven billion kilometers. After some difficulties due to an unlucky touch down, it finally managed to acquire a mass spectrum on the comet's surface [66].

The problems of indistinguishable ion packages and of overtaking lighter ions can be resolved by tilting the axis of ion injection out of the x,y plane to introduce a translational motion in z direction. This way, ions are moving through a stack of eight-shaped paths. While the number of cycles is then defined by the analyzer hardware, the design allows to cover a large *m*/*z* range as required in analytical mass spectrometry [67–69].

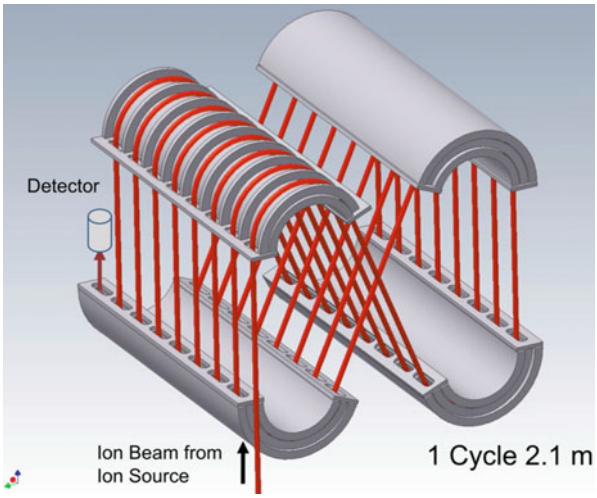


**Fig. 4.16** SpiralTOF analyzer using four arrays of electrostatic analyzers (*gray*). The outer electrode of the top left ESA has been omitted. The ion flight path is visualized as a *red line* (Reproduced with permission from Ref. [71] © Mass Spectrometry Society of Japan, 2014)

JEOL has developed a MALDI-TOF instrument incorporating the so-called "SpiralTOF" analyzer. The geometry comprises eight loops of 2.1 m each resulting in a total flight path of about 17 m (Fig. 4.16). While not actually flat, the entire analyzer fits into a compact almost cubic housing. As the ion source uses delayed extraction (Sect. 4.2.7) to minimize the translational energy spread of the ions prior to entering the SpiralTOF assembly, this instrument can deliver 80,000 resolving power [70–72]. An application of this instrument to MALDI analysis of a synthetic polymer is shown in Sect. 11.5.

### 4.2.12 Multi-reflecting TOFs

Alternatively, TOF analyzers can be compacted by folding the flight path via multiple reflection of the ions. The concept of multi-pass and multi-reflecting TOF analyzers has been explored by H. Wollnik [73, 74]. Following the line of thought that leads from the MULTUM design to the SpiralTOF, it appears logical to employ an array of reflectors and some tilt of the direction of motion to avoid overtaking of lighter ions. Rather than using the same pair of reflectors to oscillate ion packages back and forth as many times as possible, such a multi-reflector design with a defined number of cycles offers free selection of the $m/z$ range to be covered. The setup that has finally been commercialized employs an array of multi-stage reflectors that are aligned in a way as to effect a "zig-zag" or "jig-saw" ion path [75]. To avoid ion loss by scattering, a set of electrostatic lenses is positioned halfway between the opposed reflectors. It requires carefully tuned spatial focusing of both reflector stages and lenses to keep ions on track along such a flight path.

Ions leaving the source are injected into the first reflector at an angle and then pass a switchable deflector electrode. With the deflector electrode switched on, ions are sent into the second reflector stage and leave from there to hit the detector after

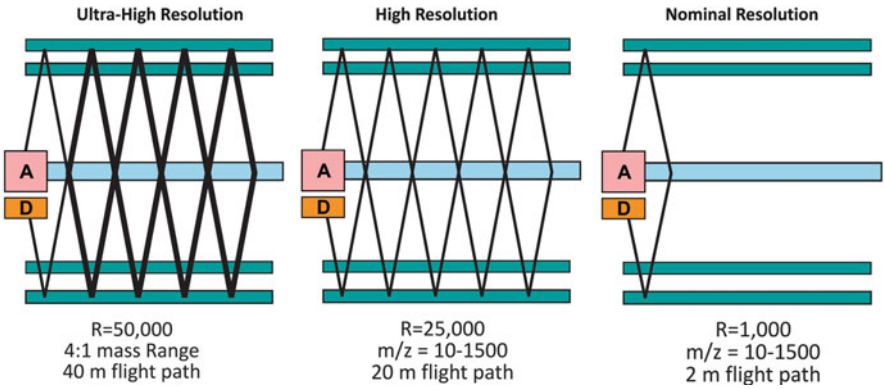


**Fig. 4.17** Scheme of multi-reflecting TOF operational modes (*A* ion source, *D* detector). By using a switchable deflector ions can either be passed through one double reflection to deliver $R = 1000$, to five double reflection to achieve $R = 25{,}000$, or even to have a second full passage enabling $R = 50{,}000$ (Courtesy of LECO, Germany)

having gone through a rhombic flight path of just 2 m (Fig. 4.17). In this mode, the instrument can deliver $R = 1000$. When no potential is applied to the deflector, ions move on to start their zig-zag journey until they are reflected at the end of the array to send them back on a path leading to the detector. Providing a flight path of 20 m, this mode delivers $R = 25{,}000$. By using the deflector to send ions back, the ions are going for second passage through the mass analyzer to enable $R = 50{,}000$ after 40 m of flight. The latter mode limits the $m/z$ range to a ratio of 1:4, e.g., $m/z$ 200–800, because ions of the first and second passage are simultaneously traveling on the track.

A better idea of the dimensions of this compact analyzer and of the penetration depth of the multi-stage reflectors is conveyed by Fig. 4.18. This multi-reflecting TOF analyzer is commercialized by LECO as Pegasus HRT series of instruments [76, 77].

**Multi-reflecting TOF at CERN** At CERN, the online precision mass spectrometer ISOLTRAP uses a dedicated multi-reflecting TOF analyzer between the linear RF ion trap and two Penning traps for precision mass measurement of exotic nuclei [78]. The MR-TOF analyzer comprises two ion-optical mirrors between which oscillating ions are separated according to their different mass-to-charge ratios. By the multiple reflections, the analyzer of less than 1 m in length allows for total ion flight paths of several hundreds of meters. Tests of an offline version of this device delivered a resolving power of up to $R = 80{,}000$ [79]. As part of the highly specialized setup of ISOLTRAP at CERN, the MR-TOF serves for purification of contaminated ion beams. Furthermore, the MR-TOF can be operated as a mass spectrometer on its own, in particular for precision mass measurements of nuclides that are shorter-lived or that have lower yields than those accessible for Penning trap mass spectrometry [78–80].

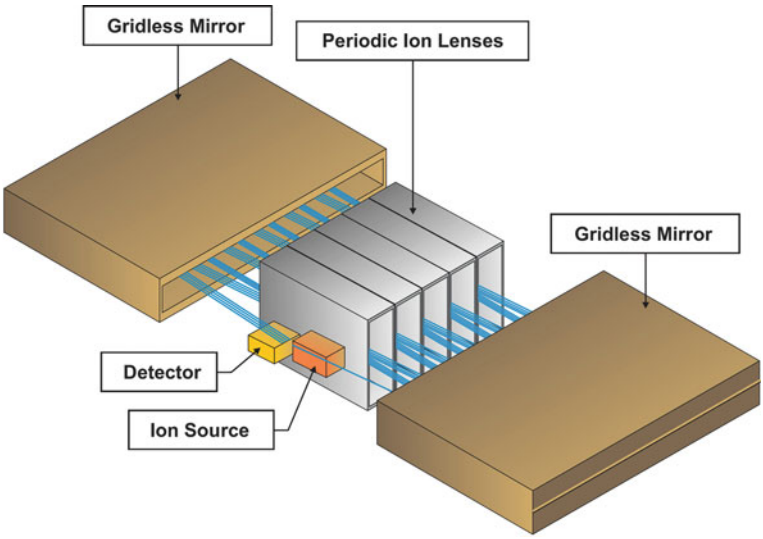


**Fig. 4.18** Schematic of the multi-reflecting TOF analyzer. During the most part of their journey, ions are traveling either within reflectors or are passing electrostatic lenses (Courtesy of LECO, Germany)

### 4.2.13 Essence of TOF Instruments

**Principle of Operation**

Ions of equal kinetic energy but different in mass are moving at different velocities. When such ions are traveling down a field-free drift path of given length, their flight times depend on mass, more precisely on the square root of $m/z$. Measuring the time-of-flight (TOF) allows to calculate the ionic mass. The mass resolving power of a TOF analyzer is proportional to its length.

**TOF Configurations**

The simplest form of a TOF analyzer is presented by the linear TOF with continuous ion extraction from the source. The reflector TOF (ReTOF) design offers 2–4-fold improved resolving power that can be further boosted by implementation of a delay between ion creation and onset of ion acceleration. Typically, such TOF analyzers, generally of reflector design, are attached on-axis to MALDI sources featuring some sort of pulsed ion extraction.

Continuous ion sources can be used in combination with orthogonal-acceleration (oaTOF) analyzers. For $m/z$ analysis in oaTOFs, ions are deflected from an ion beam orthogonal to its direction. Commonly, the TOF analyzer of these instruments is also of reflector design. Furthermore, oaTOFs are well-suited for combination with other mass-analyzing devices.

**Performance Characteristics**
The performance of TOF analyzers in terms of mass range, resolving power, and mass accuracy varies widely in accordance with their design (on-axis TOF versus oaTOF), mode of operation (linear or reflector mode), and intended use (MALDI versus ESI, APCI versus EI, CI) of the instrument. Thus, TOFs may cover ranges of up to *m*/*z* 1000 (GC-MS), to *m*/*z* 5000 (ESI, APCI sources), and even to far beyond *m*/*z* 100,000 (MALDI). TOFs can deliver resolving power of $R = 1000$ (GC-MS, GC × GC-MS) to $R > 30{,}000$. Accordingly, mass accuracies range from just 0.2 u to 0.001 u.

**TOF Analyzers in the Laboratory**
TOF analyzers are widely used in modern instrumentation. Their success is based on a balance between performance in terms of resolving power, mass accuracy, mass range, speed, and sensitivity on the one side and of reasonable investment on the other. Their compact footprint in the laboratory and moderate power consumption also contribute to their success. On-axis TOF and oaTOF analyzers make up the majority of today's TOF instrumentation, while the more complex folded ion path layouts are less common.

## 4.3 Magnetic Sector Instruments

### 4.3.1 Evolution of Magnetic Sector Instruments

*Magnetic sector instruments* paved the road to organic mass spectrometry. "Whereas mass spectrometry was still very an art rather than a science in 1940, the picture changed drastically during the war years. Vacuum and electronic techniques had matured" [81]. It took until the 1950s for magnetic sector instruments to become commercially available [7, 8]. These pioneering instruments were fairly bulky and not very easy to use [81–83]. Nevertheless, they provided analytical information of a kind that chemists had long been seeking for. They continuously became faster, more accurate, with higher resolving power [3, 5, 9, 84]. The first instruments used a single magnetic sector (symbol B) to effect separation of the ions. Later, the introduction of *double-focusing instruments* which in addition were equipped with an *electrostatic sector* or *electrostatic analyzer* (ESA, symbol E) in addition defined a standard which is still valid. With few exceptions, magnetic sector instruments are comparatively large devices capable of high resolution and accurate mass determination, and suited for a wide variety of ionization methods.

**Trends in instrumentation**
Two decades ago, double-focusing sector instruments were commonly used with a large chemical diversity of samples. Within the last decade, however, there has been a strong tendency to replace sector instruments with TOF, Orbitrap, or FT-ICR instruments, and moreover, to even substitute classical ionization methods such as EI, CI, or FAB with APCI or ESI just to redirect the stream of samples to those preferable modern mass analyzers. Recently, manufacturers have "rediscovered" the utility of EI and CI and started to offer TOF and Orbitrap analyzers adapted to these ionization methods. These instruments often are dedicated to gas chromatography-mass spectrometry (GC-MS), but direct insertion probes are also having a renaissance (Sect. 5.2).

### 4.3.2 Principle of the Magnetic Sector

The *Lorentz Force Law* can be used to describe the effects exerted onto a charged particle entering a constant magnetic field. The Lorentz force $F_L$ depends on the velocity $v$, the magnetic field $B$, and the charge $q$ of an ion. In the simplest form the force is given by the scalar equation [3, 4, 85, 86]

$$F_L = qvB \tag{4.11}$$

which is valid if $v$ and $B$ (both are vectors) are perpendicular to each other. Otherwise, the relationship becomes

$$F_L = qvB(\sin\alpha) \tag{4.11a}$$

where α is the angle between $v$ and $B$. Figure 4.19 demonstrates the relationship between the direction of the magnetic field, the direction of the ionic motion, and the direction of the resulting Lorentz force. Each of them is at right angles to the others. An ion of mass $m$ and charge $q$ traveling at a velocity $v$ in a direction perpendicular to an homogeneous magnetic field will follow a circular path of radius $r_m$ that fulfills the condition of equilibrium of $F_L$ and centripetal force $F_c$

$$F_L = qvB = \frac{m_i v^2}{r_m} = F_c \tag{4.12}$$

Upon rearrangement we obtain the radius $r_m$ of this circular motion

$$r_m = \frac{m_i v}{qB} \tag{4.13}$$

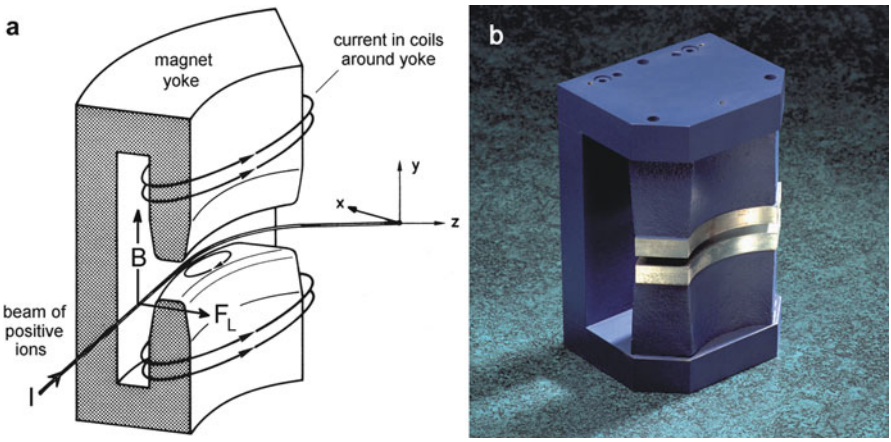


**Fig. 4.19** The Right Hand Rule (*I* thumb, *B* index finger, $F_L$ middle finger) to determine the direction of the Lorentz force (**a**), where the current corresponds to the direction where positive charges move, i.e., the figure directly applies for positive ions. (**b**) A real magnet yoke without coils and flight tube. With kind permission of Thermo Electron (Bremen) GmbH, (*left*) and Waters Corporation, MS Technologies, Manchester, UK (*right*)

This shows the working principle of a magnetic sector where the radius $r_m$ depends on the momentum $mv$ of an ion, which itself depends on $m/z$.

**Momentum analyzer**
The magnetic sector does not directly separate ions by mass. Rather it effects ion separation by their momentum and this feature can be used as a measure of mass provided all ions possess equal kinetic energy.

Finally, dispersion in momentum causes a dependence of $r_m$ on the square root of mass becoming obvious by substitution of $v$ from Eq. (4.3) and $q = ez$

$$r_m = \frac{m_i}{ezB}\sqrt{\frac{2ezU}{m_i}} = \frac{1}{B}\sqrt{\frac{2m_iU}{ez}} \tag{4.13a}$$

Alternatively, the ratio $m_i/q$ can be expressed by rearranging Eq. (4.13)

$$\frac{m_i}{q} = \frac{r_m B}{v} \tag{4.14}$$

which upon substitution of $v$ as performed above becomes

$$\frac{m_\mathrm{i}}{q} = \frac{r_\mathrm{m} B}{\sqrt{\frac{2qU}{m_\mathrm{i}}}} \quad \Rightarrow \quad \frac{m_\mathrm{i}}{q} = \frac{{r_\mathrm{m}}^2 B^2}{2U} \tag{4.14a}$$

For singly charged ions ($z = 1$, $q = e$) we obtain the more widespread form

$$\frac{m_\mathrm{i}}{e} = \frac{{r_\mathrm{m}}^2 B^2}{2U} \tag{4.14b}$$

**Basic equation of MS**
Equation (4.14b) has become known as the *basic equation of mass spectrometry*. Nowadays, there is no more justification for a single basic equation of mass spectrometry because of the large variety of mass analyzers employed.

### 4.3.3 Focusing Action of the Magnetic Field

The focusing action of an homogeneous magnetic field on a beam of ions having the same $m/z$ and the same kinetic energy can best be illustrated by a 180° sector (Fig. 4.20). If the beam is divergent by a half-angle α, the collector slit must be $\alpha^2 r_\mathrm{m}$ wide to pass all ions after suffering 180° deflection. This is because the ions come to a first order, i.e., imperfect, focus as they all traverse the magnetic field at the same radius but not all of them entered the field at right angles. Ions of different $m/z$ fly at a different radius, e.g., the lighter ions of $m/z_1$ hit the wall while ions of $m/z_2$ reach the collector slit. To allow for detection of various masses, such an analyzer could either be equipped with a photographic plate in the focal plane to become a so-called *mass spectrograph*, or it could be designed with variable magnetic field to detect different masses at the same point by bringing them subsequently to the collector slit. Indeed, such a 180° geometry with *scanning* magnetic field has been used by Dempster [87]. Later, the term *mass spectrometer* was coined for this type of instruments [83].

Among other complications, the 180° design requires large and heavy magnetic sectors. It is by far more elegant to employ magnetic sectors of smaller angles (Fig. 4.21). An optimized magnetic sector alone can provide a resolving power of $R = 2000$–$5000$ depending on its radius. The limitation arises from the fact that ions emerging from the ion source are not really monoenergetic. This way, ions of different $m/z$ can have equal momentum and thus cause overlap of adjacent ion beams at the detector.

**Energy spread limits resolving power** Equation (4.13a) describes the radius $r_\mathrm{m}$ in the magnetic field. Obviously, the value $r_\mathrm{m}$ remains constant as long as $m_\mathrm{i}U = const.$ If the instrument is set to pass an ion of say $m/z$ 500 and 3000 eV kinetic energy, it

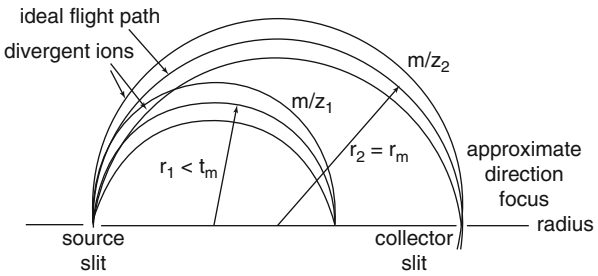


**Fig. 4.20** Direction focusing properties of a 180° magnetic sector on a diverging beam of ions of the same *m*/*z* and the same kinetic energy and effect on ions of different *m*/*z*. In this illustration, *B* has to come out of the plane towards the reader for positive ions

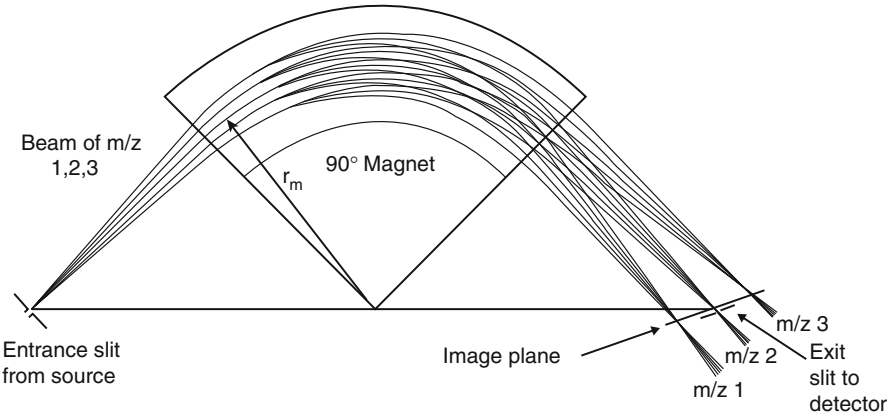


**Fig. 4.21** Ion separation and direction focusing in a plane by a 90° magnetic sector. A divergent beam of ions of *m*/*z* 1, 2, 3 is separated into three beams and focused to a point on the image plane (divergence shown exaggerated). Only ions of *m*/*z* 2 are passing the exit slit and eventually hit the detector (Adapted from Ref. [88] with permission. © Wiley-VCH, 1999–2014)

will simultaneously allow the passage for ions of *m*/*z* 501 having 2994 eV or of *m*/*z* 499 having 3006 eV of kinetic energy. This is why high resolving power demands narrow kinetic energy distributions.

### 4.3.4 Double-Focusing Sector Instruments

The *electrostatic sector* or *electrostatic analyzer* (ESA) produces a radial electric field between two oppositely charged plates extending over the ESA angle ϕ (Fig. 4.23). An ion passes the ESA midway on a circular path if

$$F_e = qE = \frac{m_i v^2}{r_e} = F_c \tag{4.15}$$

where $F_e$ represents the electric force, $E$ the electric field strength, and $r_e$ the radius of the ESA. Rearrangement of Eq. (4.15) demonstrates that the ESA acts as an energy dispersive device

$$r_e = \frac{m_i v^2}{qE} = \frac{m_i v^2}{ezE} \tag{4.16}$$

**Energy filter**
The ESA effects energy dispersion. Thus, the kinetic energy distribution of an ion beam can be reduced. The ESA does not allow for mass separation among monoenergetic ions.

Upon substitution of Eq. (4.3) for $v$ one obtains the simple relationship

$$r_e = \frac{2U}{E} \tag{4.17}$$

to describe the radius of the ESA. As with the magnetic sector before, the ESA has direction-focusing properties in one plane (Fig. 4.22). Ions entering the ESA in the middle and at right angles to the field boundaries pass through on a path of equipotential, whereas ions with a velocity component towards one of the capacitor

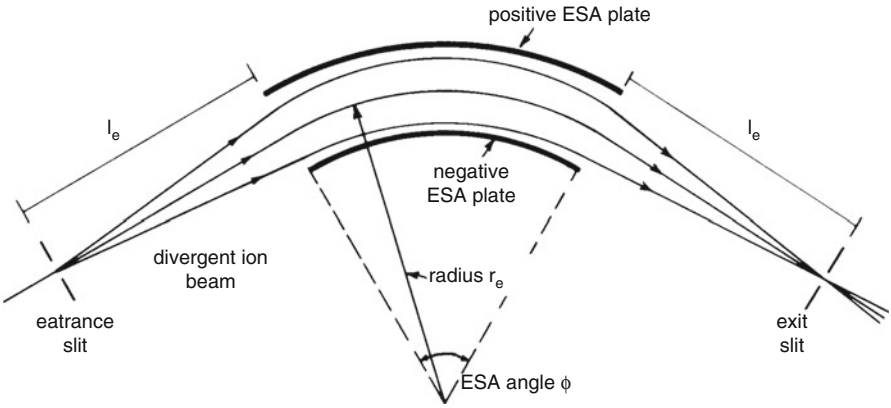


**Fig. 4.22** Direction focusing of a radial electric field. Ions of appropriate kinetic energy are focused at the exit slit. Divergent ions pass the ESA close to either plate. Here, the electric potentials are set to transmit positive ions. The image distance $l_e$ depends on the ESA angle

plates are brought into focus at the focal length $l_e$. To understand this, imagine an ion drifting towards the outer plate having the same charge sign as the ion. As it approaches the plate it is decelerated by the opposed electric field and finally reflected towards the center of the beam. With its radial component of $v$ inverted it crosses the ideal path at $l_e$. In an analogous fashion an ion approaching the inner plate becomes accelerated by the attractive force. The resulting higher velocity causes an increase in centripetal force, and thereby effects a correction of the flight path in the appropriate sense.

Energy focusing is achieved by combining a magnetic sector and an electric sector in a way that the energy dispersion of the magnetic field is just compensated by the energy dispersion of the electric field. Additional direction focusing is obtained if the radii and angles of these fields and their mutual alignment does not diminish the focusing properties of each of them. Then, an ion optical system is obtained that is able to focus ions onto a single image point, although these were emerging from the ion source in (slightly) different directions and with (slightly) different kinetic energies. This is called *double focusing*. Double focusing can improve the resolving power of a magnetic sector instrument more than ten times.

### 4.3.5 Geometries of Double-Focusing Sector Instruments

The following passages present examples of particular double-focusing geometries that either have been milestones in instrument design [3, 5] or still are incorporated in modern mass spectrometers.

The EB design by Mattauch and Herzog combines a 31° 50′ ESA with a 90° magnetic sector producing an image plane that allows for simultaneous photographic detection of a comparatively large $m/z$ range [89]. This mass spectrograph attains double-focusing over the total image plane resulting in resolving powers of $R > 10{,}000$. Thus, it became the basis for numerous commercial instruments (Fig. 4.23). The *Mattauch-Herzog geometry* has survived until today in dedicated instruments for spark source (SS)-MS and isotope ration (IR)-MS (Sect. 15.2) [90].

An EB design effecting an image plane of 140 mm in length with a linear mass scale for detection on a photographic plate has been published by Bainbridge and Jordan (*Bainbridge-Jordan geometry*) [92]. Their paper is especially recommended as it also nicely illustrates the use of photographic plates in those days.

The third famous type of EB arrangement has become known as *Nier-Johnson geometry* (Fig. 4.24) [93]. Here, the ion beam first passes through the electrostatic analyzer producing energy-resolved beams without mass dispersion in the plane of an intermediate slit located at the focal point of the ESA. It then passes through a magnetic analyzer to achieve mass dispersion of the ions. Different from the Mattauch-Herzog *mass spectrograph*, the Nier-Johnson *mass spectrometer* was constructed to be used in conjunction with a *scanning magnet* to focus one specific $m/z$ after the other onto a point detector. This presented a major advantage for the use of UV recorders or electronic data acquisition as well as for the achievement of better ion optics.

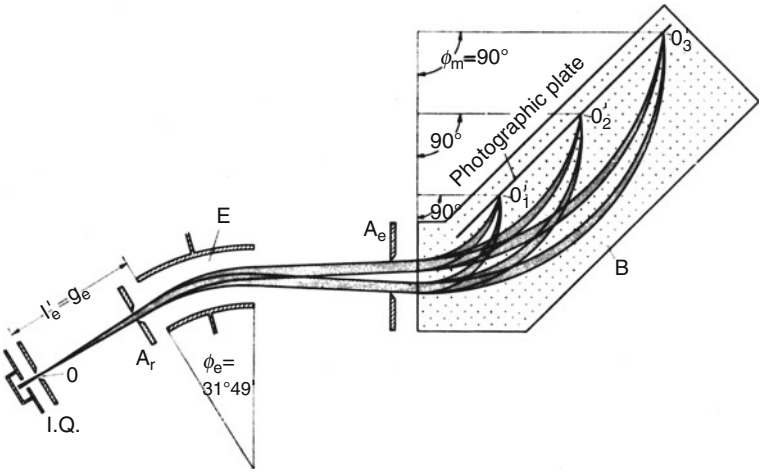


**Fig. 4.23** Mattauch-Herzog double-focusing mass spectrograph providing direction and momentum focusing of ions on a plane [89]. The ESA precedes the magnet. Placing a photographic plate in the image plane allows simultaneous recording of a *m*/*z* range (Reproduced from Ref. [91] with kind permission of Curt Brunnée)

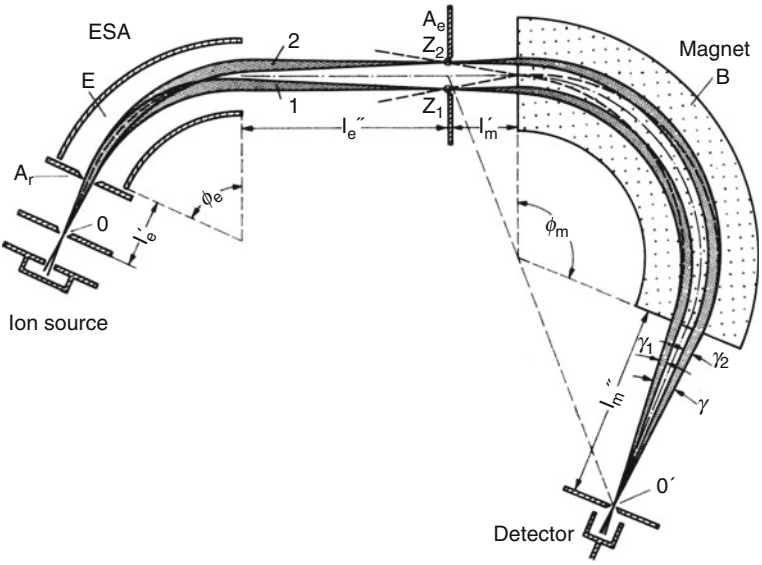


**Fig. 4.24** Double-focusing mass spectrometer of EB geometry, basically a Nier–Johnson type instrument. Direction and velocity focusing are shown exaggerated. After exiting the ESA, the energy-resolved beam passes through a wide intermediate slit into the magnetic sector. The large aperture ensures good overall transmission (Reproduced from Ref. [91] with kind permission of Curt Brunnée)

**Scan**
Typically, on magnetic sector mass spectrometers a spectrum is produced by varying the strength of the magnetic field to successively pass through ions of different $m/z$. This is termed *magnetic field scan* [94]. For scans *linear in time*, the *scan rate* is given in units of $m/z$ $s^{-1}$, e.g., 500 $m/z$ $s^{-1}$. For scans *exponential in time*, the *scan rate* is reported in units of s per decade, e.g., 10 s/decade means 10 s from $m/z$ 30 to 300 or from $m/z$ 100 to 1000.

Some later EB instrument models were constructed to be used in combination with an (optional) array detector, e.g., the JEOL HX-110 (EB), the Thermo Finnigan MAT 900 (EB), and the Micromass Autospec (EBE) instruments could be equipped in that way. The array detector was located at the focus plane of the magnet.

Successful constructions of *reversed geometry*, i.e., BE instead of *forward* EB design, have been presented in the form of the MAT 311 in the mid-1970s and shortly after by the VG Analytical ZAB-2F instrument [95] based on a proposal by Hintenberger and König [96].

More recent BE geometry instruments are presented by the Thermo Finnigan MAT 90 and 95 series (Fig. 4.25), the JEOL JMS-700, and although not strictly due to its EBE geometry [97], the Micromass Autospec. However, the only instrument of this millennium incorporating a redesigned BE geometry has been the Thermo Scientific DSF introduced in 2005. In contrast to organic and biomedical MS, double-focusing designs are still highly relevant in inorganic MS (Chap. 15) [90].

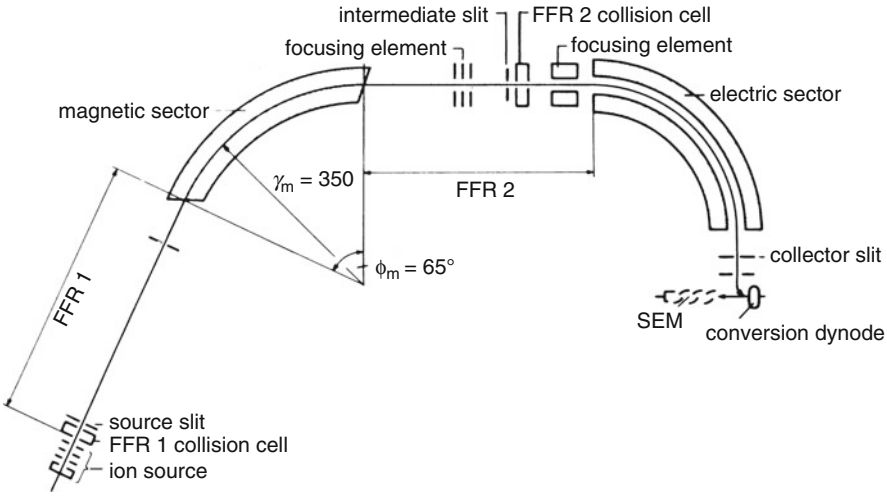


**Fig. 4.25** The Finnigan MAT 90 double-focusing mass spectrometer with rotated pole faces of the magnetic sector (Reproduced from Ref. [2] with permission. © Elsevier Science, 1987)

### 4.3.6 Adjusting the Resolving Power of a Sector Instrument

The ion optics of a sector instrument are the analog to a cylindrical lens in light optics. Accordingly, the reduction of an aperture can be used to obtain a sharper image, i.e., to increase resolving power (Sect. 3.4). Slits are used instead of circular apertures to comply with the cylindrical properties of the ion optical system. Most important are the settings of the *object slit* (*source slit*, *entrance slit*) and the *image slit* (*collector slit*, *exit slit*, *detector slit*). Intermediate slits may be used in addition. Unfortunately, closing slits also means cutting off ions from the beam, and thus reduction of the transmission of the mass analyzer. In the ideal case, the improvement of resolution by a factor of 10 goes along with a reduction in transmission to 10%, in reality the effect is often worse.

**Setting the slits** The influence of relative slit width on peak shape and resolution is demonstrated on the second isotopic peak of toluene molecular ion, $^{13}C_2{}^{12}C_5H_8^{+\bullet}$, *m*/*z* 94 (Fig. 4.26). With the entrance slit at 50 µm and the exit slit at 500 µm the peak is flat-topped (*left*), because a narrow beam from the entrance sweeps over the wide open detector slit keeping the intensity constant as the scan proceeds until the beam passes over the other edge of the slit. Closing the exit slit to 100 µm increases resolution to 2000 without affecting the peak height (*center*), but reduces the peak area by a factor of 4 in accordance with an increase in resolution by the same factor. Further reduction of the exit slit width to 30 µm improves resolution at the cost of peak height (*right*). (Any sector instrument must behave alike, otherwise, cleaning or other maintenance are required.)

**Operate to fit your needs**
The ultimate resolution of a magnetic sector mass spectrometer is reached when the slits are closed to a width of a few micrometers. Often, the slit height is also reduced, e.g., from 5 to 1 mm. In daily work, the resolution will be set to fit the actual task, e.g., $R = 1000–2000$ for low-resolution work, $R = 3000–5000$ if accurate mass determination at high scan rates is needed (GC-MS, Chap. 14) or isotopic patterns of high mass analytes have to be resolved, or $R = 7000–15{,}000$ in slow-scanning accurate mass measurements.

### 4.3.7 Optimization of Sector Instruments

To improve the performance of sector instruments in terms of scan speed, resolving power, transmission, and mass range, the construction, in particular that of the magnet, needs some additional refining.

The rapid change of a magnetic field suffers from hysteresis, i.e., the magnetic flux does not exactly follow the change of the electric current through the coils in

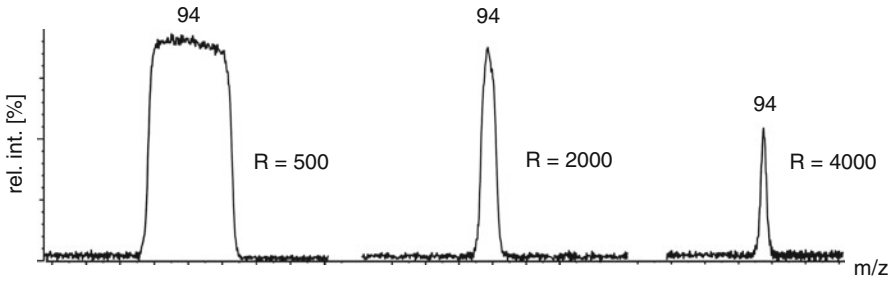


**Fig. 4.26** The influence of relative slit width settings on peak shape and resolution on a magnetic sector instrument. The peak shape first changes from flat-topped (*left*) to Gaussian (*center*) and finally resolution improves at cost of peak height (*right*)

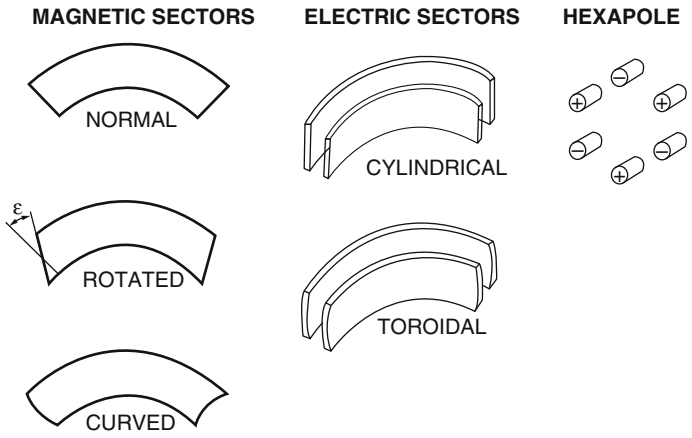


**Fig. 4.27** Types and shapes of ion optical elements used in magnetic sector instrument design (By courtesy of Thermo Fisher Scientific, Bremen)

time, but lags behind due to the induction of eddy currents. On one side, this causes problems in creating a scan perfectly linear in time, on the other this prevents high scan rates as required for GC-MS. Lamination of the yoke substantially reduces these problems [98] and is employed in all modern sector instruments.

In order to extend the mass range one either has to increase the field strength or the radius of the magnet. However, there are limitations of the field strength with non-superconducting magnets at about 2.4 T. Instead of simply enlarging the radius, the pole faces of the magnet can be rotated to preserve a compact design by reduction of its focal length (Figs. 4.27, 4.28, and 4.29) [2].

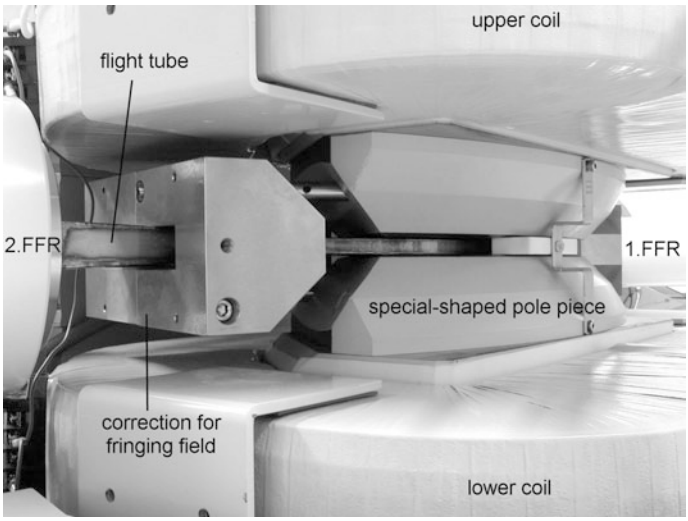


**Fig. 4.28** Flight tube passing through the gap of the magnetic sector of a JEOL JMS-700 instrument seen from the ESA side. The shapes of the pole pieces of the yoke and the additional blocks around the tube are designed to minimize fringing fields. In addition the pole faces are rotated to increase the mass range

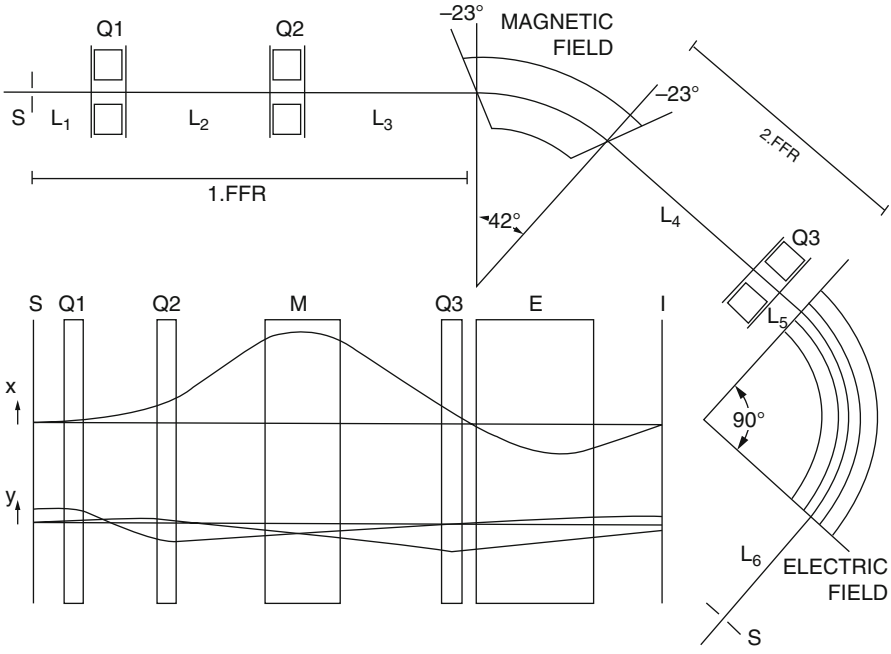


**Fig. 4.29** Layout of the JEOL JMS-700. Three DC quadrupole lenses are used to improve the transmission of the magnetic sector. The inset shows horizontal ($x$) and vertical ($y$) trajectories where the height of the beam ($y$) is clearly reduced to pass through a narrow gap between the pole shoes of the magnet (Adapted from Ref. [99] with permission. © Elsevier Science, 1985)

Another problem is due to fringing fields. To reduce these defocusing effects at the entrance and exit of the field, the pole pieces of the yoke of the electromagnet generally have specially shaped edges.

Furthermore, pure EB and BE designs are somewhat limited concerning the transmittance through a narrow magnet gap as compared to instrument designs using some DC quadrupole (q) or DC hexapole (h) lenses to form the ion beam (Fig. 4.29) [99, 100]. However, quadrupole and hexapole lenses do not alter the effective instrument geometry, i.e., such an analyzer behaves like a pure BE analyzer in any mode of operation.

### 4.3.8 Summary of Magnetic Sector Instruments

**Ion Separation**
Ions moving perpendicular to a magnetic field are forced on a circular path by action of the Lorentz force. The radius of that motion is determined by a counterbalance of Lorentz force and centripetal force. Ions of equal kinetic energy but different in mass therefore travel on individual radii, and thus, a separation by momentum is effected. The radius of ion motion or the magnetic field strength to achieve a defined radius to hit the detector is then used to derive $m/z$ values of the ions.

**Configurations**
Magnetic sector instruments can be built relying on magnetic (B) separation alone. Such single-focusing instruments are limited in resolving power. At least one order of magnitude higher resolving power is achieved when the kinetic energy spread of ions is compensated or filtered by means of an electrostatic sector (E). Designs employing B and E are termed double-focusing. E and B can be combined in numerous ways thereby giving rise to EB, BE, EBE, BEBE, and other designs.

**Performance Characteristics**
Double-focusing magnetic sector instruments, either in BE or EB configuration, typically can achieve resolving powers in excess of $R = 60{,}000$. However, this requires extremely slow scanning and comes at the expense of very low transmission, as the slits need to be closed down. High transmission at wide-open slits results in $R = 1000$–$2000$ and allows faster scanning. Accurate mass measurements are typically performed at moderate scan rates and $R = 5000$–$10{,}000$ and require internal mass calibration.

**Magnetic Sector Instruments in the Laboratory**
In organic and biomedical MS, magnetic sector instruments were most popular in the 1960s to early 2000s. More recently, most have been replaced by TOF, FT-ICR, or Orbitrap mass analyzers. In inorganic MS, in particular for isotope ratio determinations and spark-source MS, magnetic sector instruments are still of high

relevance as they can deal with large energy dispersion and allow for multi-collector setups in the image plane of the magnet.

## 4.4 Linear Quadrupole Instruments

### 4.4.1 Introduction

Since the Nobel Prize-awarded discovery of the mass-analyzing and ion-trapping properties of two- and three-dimensional electric quadrupole fields [101, 102] and the concomitant construction of a *quadrupole* (Q) *mass spectrometer* [103, 104], this type of instrument has steadily gained importance. Chiefly starting from GC-MS that demanded for rapid scanning analyzers, quadrupole instruments made their way into the MS laboratories [105–108], although those early systems offered poor resolving power and low mass range, e.g., $m/z$ 1–200. Modern quadrupole instruments cover up to $m/z$ 2000 or even higher with good resolving power and represent some kind of routine device in LC-MS. The advantages of linear quadrupoles are:

- Linear quadrupoles offer high transmission.
- Quadrupoles are light-weight, very compact, and comparatively low-priced.
- Quadrupoles require low ion acceleration voltages.
- Quadrupoles allow high scan speeds since scanning is realized by solely sweeping electric potentials.

**Terminology**
Linear quadrupoles were the first to be incorporated in commercial instruments. Thus, these instruments are simply referred to as quadrupole mass spectrometers and the attribute "linear" is often omitted. As we will see later (Sects. 4.5 and 4.6) other electrode shapes are also possible but are forming electric RF quadrupole fields of other geometries. These designs are also available in commercial mass spectrometers.

### 4.4.2 The Linear Quadrupole

A linear quadrupole mass analyzer consists of four hyperbolically or cylindrically shaped rod electrodes extending in the $z$-direction and mounted in a square configuration ($xy$-plane, Figs. 4.30 and 4.31). The pairs of opposite rods are each held at the same potential which is composed of a DC and an AC component.

As an ion enters the quadrupole assembly in the $z$-direction, an attractive force is exerted on it by one of the rods with its charge actually opposite to the ionic charge. If the voltage applied to the rods is periodic, attraction and repulsion in both the $x$-

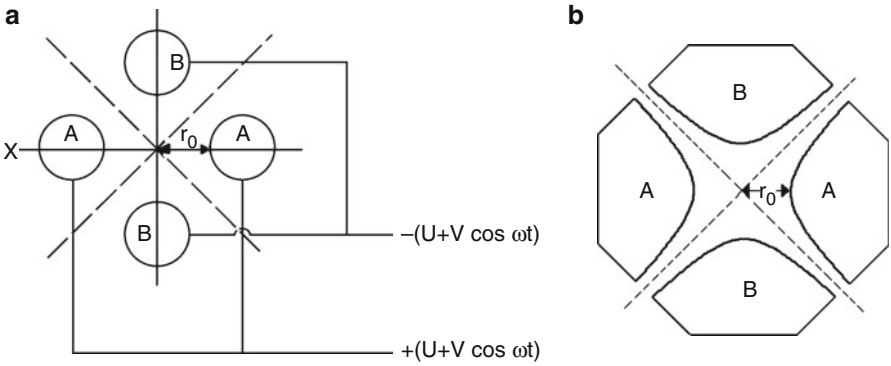


**Fig. 4.30** Cross section of a quadrupole (**a**) for the cylindrical approximation and (**b**) for the hyperbolic profile of the rods. The electric field is zero along the *dotted lines*, i.e., along the asymptotes in (**b**) ((**a**) Courtesy of Waters Corp., MS Technologies, Manchester, UK)

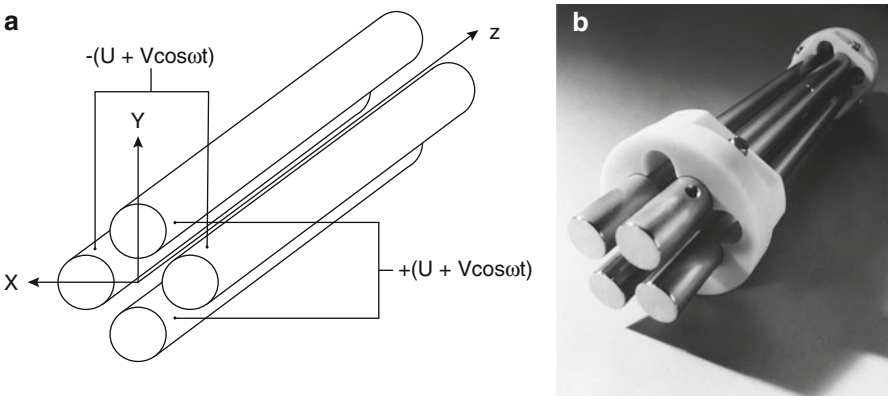


**Fig. 4.31** Linear quadrupole mass analyzer: schematic (**a**) and photograph (**b**) (By courtesy of (**a**) JEOL, Tokyo and (**b**) Waters Corp., MS Technologies, Manchester, UK)

and *y*-directions will alternate in time, because the sign of the electric force also changes periodically in time. If the applied voltage is composed of a DC voltage $U$ and a radiofrequency (RF) voltage $V$ with the frequency ω the total potential $\Phi_0$ is given by

$$\Phi_0 = U + V\cos\omega t \tag{4.18}$$

Thus, the equations of motion are

$$\begin{aligned} \frac{d^2x}{dt^2} + \frac{ez}{m_i {r_0}^2}\ (U + V\cos\omega t)x = 0 \\ \frac{d^2y}{dt^2} - \frac{ez}{m_i {r_0}^2}\ (U + V\cos\omega t)y = 0 \end{aligned} \tag{4.19}$$

Remember that $m_i$ denotes ion mass [kg] and charge is $q = ez$, where $e$ is the electron charge [C] and $z$ the charge number. In case of an inhomogeneous periodic field such as the above quadrupole field, there is a small average force which is always in the direction of the lower field. The electric field is zero along the dotted lines in Fig. 4.30, i.e., along the asymptotes in case of the hyperbolic electrodes. It is therefore possible that an ion may traverse the quadrupole without hitting the rods, provided its motion around the $z$-axis is stable with limited amplitudes in the $xy$-plane. Such conditions can be derived from the theory of the *Mathieu equations*.

**Mathieu equations**
The Mathieu functions were originally derived in 1868 by Émile Léonard Mathieu, a French mathematician, to describe the vibrations of elliptical drumheads. It turned out that they are also useful to treat quadrupole mass filters and several other physical phenomena.

Now, writing Eq. (4.19) in dimensionless form yields

$$\begin{aligned} \frac{d^2x}{d\tau^2} + (a_x + 2q_x\cos 2\tau)x = 0 \\ \frac{d^2y}{d\tau^2} + \left(a_y + 2q_y\cos 2\tau\right)y = 0 \end{aligned} \tag{4.20}$$

The parameters $a$ and $q$ can now be obtained by comparing with Eq. (4.19)

$$a_x = -a_y = \frac{4qU}{m_i {r_0}^2\omega^2}, \quad q_x = -q_y = \frac{2qV}{m_i {r_0}^2\omega^2}, \quad \tau = \frac{\omega t}{2} \tag{4.21}$$

For a given set of $U$, $V$, and ω the overall ion motion can result in a stable trajectory causing ions of a certain $m/z$ value or $m/z$ range to pass the quadrupole. Ions oscillating within the distance $2r_0$ between the electrodes will have stable trajectories. These are transmitted through the quadrupole and detected thereafter. The path stability of a particular ion is defined by the magnitude of the RF voltage $V$ and by the ratio $U/V$.

By plotting the parameter $a$ (ordinate, time invariant field) vs. $q$ (abscissa, time variant field) we obtain the stability diagram of the two-dimensional quadrupole field. This reveals the existence of regions where (*i*) both $x$- and $y$-trajectories are stable, (*ii*) either $x$- or $y$-trajectories are stable, and (*iii*) no stable ion motion occurs

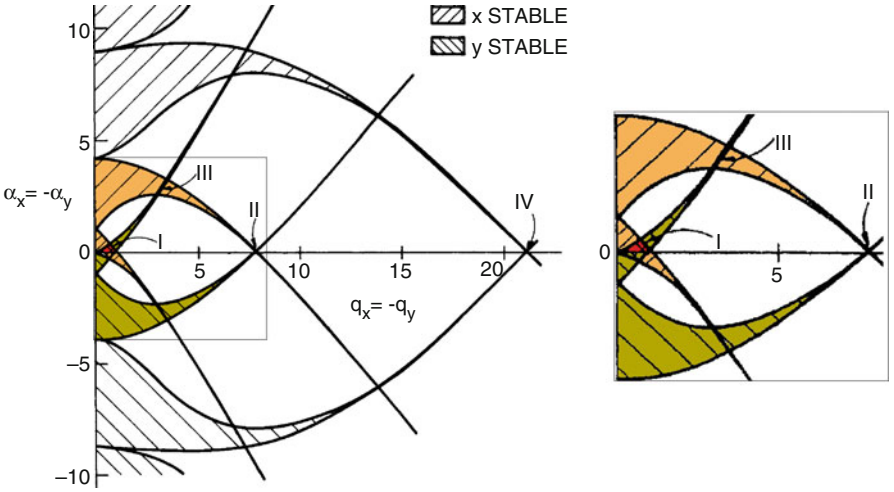


**Fig. 4.32** Stability diagram for a linear quadrupole analyzer showing four stability regions (I–IV) for *x*- and *y*-motion. The portion within the *square frame* is zoomed to double size on the *right*. Stability region I only covers the small *red region* in the center (Adapted from Ref. [107] with permission. © John Wiley & Sons Inc., 1986)

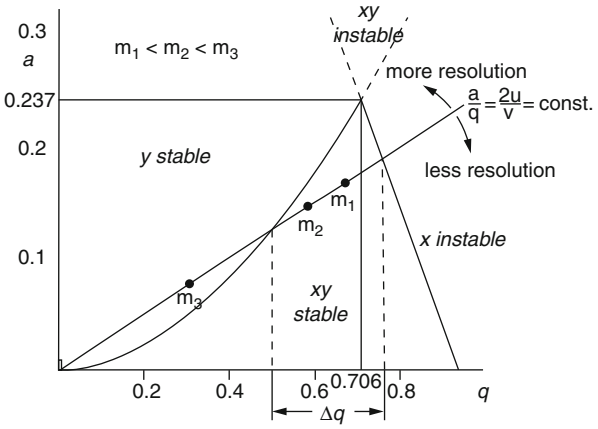


**Fig. 4.33** Detail of the upper half of region I of the stability diagram for a linear quadrupole analyzer (Reproduced from Ref. [102] with permission. © World Scientific Publishing, 1993)

(Fig. 4.32) [107]. Among the four stability regions of the first category, the tiny central region I is of special interest for the normal mass-separating operation of the linear quadrupole. Zooming in to region I (*x*- and *y*-trajectories stable) yields what is commonly referred to as the *stability diagram of the linear quadrupole* (Fig. 4.33) [101, 102].

If the ratio $a/q$ is chosen so that $2\,U/V = 0.237/0.706 = 0.336$, the *xy*-stability region shrinks to one point, the apex, of the diagram (cf. Eq. 4.21, Fig. 4.33).

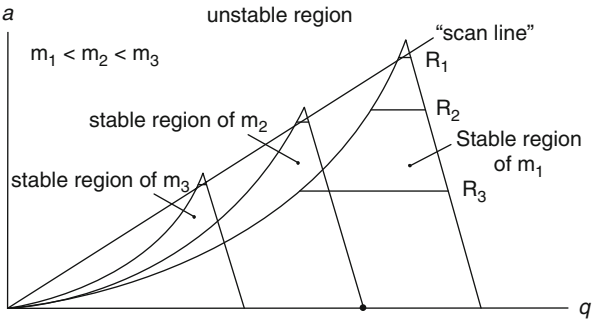


**Fig. 4.34** Scanning of linear quadrupoles means performing a $U/V = constant$ linked scan. Resolution is adjusted by variation of the $a/q$ ratio: higher $a/q$ ratio means higher resolving power and is represented by a steeper "scan line"; $R_1 > R_2 > R_3$

By reducing $a$ at constant $q$, i.e., reducing $U$ relative to $V$, an increasingly wider $m/z$ range can be transmitted simultaneously. Sufficient resolving power is achieved as long as only a small $m/z$ range remains stable, e.g., one specific $m/z \pm 0.5$ for *unit resolution* (Sect. 4.4.3). Thus, the width ($\Delta q$) of the stable region determines the resolving power (Fig. 4.34). By varying the magnitude of $U$ and $V$ at constant $U/V$ ratio an $U/V = constant$ linked scan is obtained allowing ions of increasingly higher $m/z$ to pass the quadrupole.

Overall, the quadrupole analyzer rather acts as a mass filter than as a momentum (B sector) or energy (ESA) spectrometer; hence the widespread use of the term *quadrupole mass filter*.

**Scanning a quadrupole**

Scanning of any linear quadrupole means shifting the whole stability diagram along a "scan line", because each $m/z$ value has a stability diagram of its own (Figs. 4.33 and 4.34). The representation of a scan by a "scan line" would only be correct in case of infinite resolving power, i.e., if the apices were connected. Any real resolving power is represented by a horizontal line across the stability region, where only ions falling in the region above that line are transmitted.

Ion trajectory simulations allow for the visualization of the ion motions while traveling through a quadrupole mass analyzer (Fig. 4.35). Furthermore, the optimum number of oscillations to achieve a certain level of performance can be determined. It turns out that best performance is obtained when ions of about 10 eV kinetic energy undergo approximately a hundred oscillations (Fig. 4.36) [109].

**Typical quadrupoles**

Standard quadrupole analyzers have rods of 10–20 mm in diameter and 15–25 cm in length. The radiofrequency is in the order of 1–4 MHz, and the DC and RF voltages are in the range of some $10^2$–$10^3$ V. Thus, ions of about 10 eV kinetic energy undergo about 100 oscillations during their passage.

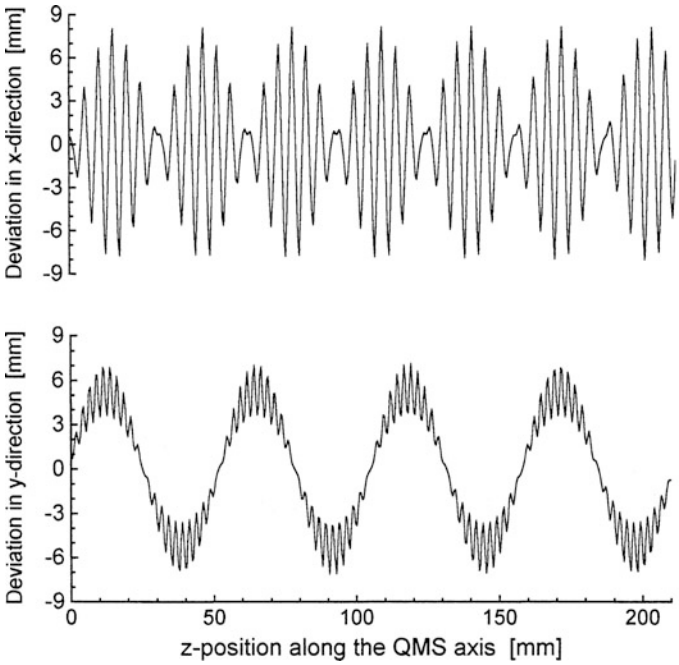


**Fig. 4.35** Projection of a 3D trajectory simulation of a stable ion onto the *x*- and *y*-coordinates (Reproduced from Ref. [109] with permission. © Elsevier Science, 1998)

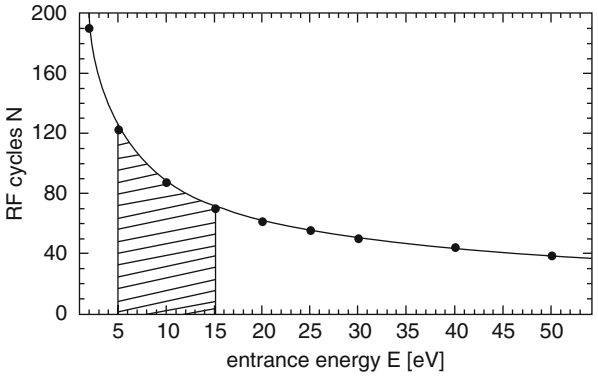


**Fig. 4.36** Relation of RF cycles experienced by the ions as a function of entrance energy. The *shaded area* marks the region of optimized performance (Reproduced from Ref. [109] with permission. © Elsevier Science, 1998)

### 4.4.3 Resolving Power of Linear Quadrupoles

Quadrupole analyzers generally are operated at so-called *unit resolution*, normally restricting their use to typical low resolution (LR) applications [110, 111]. At unit resolution adjacent peaks are just separated from each other over the entire $m/z$ range, i.e., $R = 20$ at $m/z$ 20, $R = 200$ at $m/z$ 200, and $R = 2000$ at $m/z$ 2000. An example of unit resolution is presented in Sect. 4.5.3.

The resolution as adjusted by the $U/V$ ratio cannot arbitrarily be increased, but is ultimately limited by the mechanical accuracy with which the rods are constructed and supported ($\pm 10$ µm) [110]. Above an $m/z$ value characteristic of each quadrupole assembly, any further improvement of resolution can only be achieved at the cost of significantly reduced transmission. Nonetheless, high-performance quadrupoles allowing for about tenfold unit resolution can be built [111].

Theoretically, the electrodes of a quadrupole mass filter should have a hyperbolic cross section for optimized geometry of the resulting quadrupole field, and thus for optimized performance (Fig. 4.37) [101, 102]. However, for ease of manufacture, cylindrical rods are often employed instead. By adjusting the radius of the rods carefully ($r = 1.1468 \times r_0$), a hyperbolic field may be approximated [112]. However, even slight distortions of the ideal quadrupole field either from interference with external fields or due to low mechanical precision or inadequate shape of the device cause severe losses of transmission and resolution [113]. The expected advantages of hyperbolic rods [114] have been demonstrated by ion trajectory calculations [109, 115]: circular rods cause a reduction in macromotion frequency because of an increased residence time of the ions in close vicinity to the rods (Fig. 4.38); this in turn means reduced resolution.

Besides optimization of mechanical accuracy, the resolving power of quadrupoles can be improved by innovative modes of operation. The operation as a multiple pass system with ion reflection at either end extends the flight path and

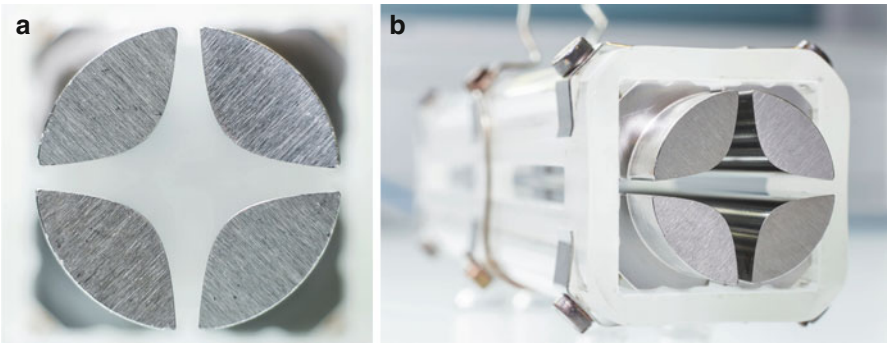


**Fig. 4.37** Linear quadrupole with hyperbolic rods. (**a**) Head on view showing the cross section of the rods and (**b**) whole device partially revealing the polished inner surfaces. The rods are mounted in a precision-machined quartz frame. This particular quadrupole once belonged to a Finnigan TSQ 700 instrument

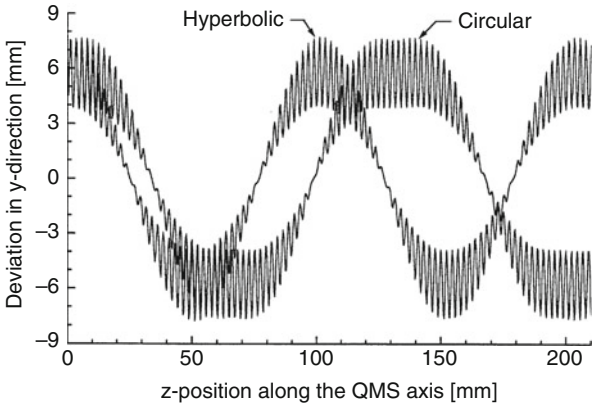


**Fig. 4.38** Motion in the *y*-coordinate of ions traveling along a quadrupole with circular rods compared to ions in a quadrupole with ideal hyperbolic field. Circular rods cause a reduced macromotional frequency and longer residence time in the close vicinity to the (non-ideal) rod surfaces (Reproduced from Ref. [109] with permission. © Elsevier Science, 1998)

thus the number of RF cycles. The same effect can be obtained from increased radiofrequency and for ions traveling slower through the device [110]. Alternatively, the quadrupole may be operated in stability regions other than the first, e.g., in the second or fourth [110, 116]; doing so requires higher ion kinetic energies of about 750 eV.

### 4.4.4 RF-Only Quadrupoles, Hexapoles, and Octopoles

Setting the DC voltage $U$ to zero transforms the quadrupole into a wide band pass for ions. In the stability diagram this mode of operation is represented by an operation line equivalent to the $q$-axis (Figs. 4.33 and 4.34). Such devices are commonly known as *RF-only quadrupoles* (q). *RF-only hexapoles* (h) and *RF-only octopoles* (o) are used analogously. Generally, higher-order RF 2 $N$–multipoles differ from quadrupoles in that they do not exhibit a sharp $m/z$ cutoff in transmission, because $x$ and $y$ motions are strongly coupled, which causes the boundaries of ion stability to become rather diffuse. For low trapping voltages, the ion trajectories in an RF 2 $N$–multipole are approximated by an effective mechanical potential, $U_{\mathrm{eff(r)}}$, given by [108, 117]:

$$U_{\mathrm{eff(r)}} = \frac{N^2}{4} \frac{(ze)^2}{m_i \Omega^2} \frac{V^2}{r_0^2} \left(\frac{r}{r_0}\right)^{2N-2} \tag{4.22}$$

where $N$ is the order of the multipole, e.g., $N = 3$ for a hexapole. According to Eq. (4.22), higher-order multipoles exhibit increasingly steeper potential wells, offer better ion-guiding capabilities and better wide-band pass characteristics, i.e., wider $m/z$ range acceptance (Fig. 4.39). This property led to the widespread application of RF quadrupoles, RF hexapoles, and RF octopoles as *ion guides* and *collision cells* [118].

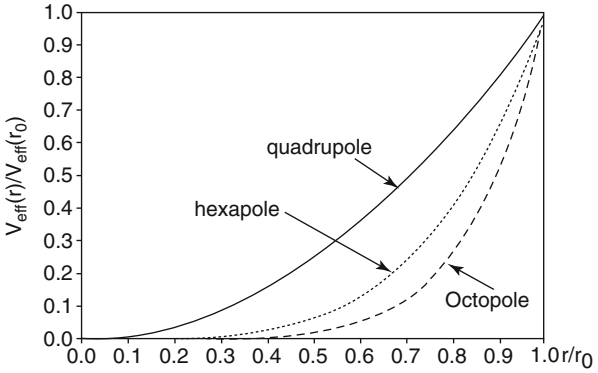


**Fig. 4.39** Comparison of effective potentials for quadrupole ($r^2$), hexapole ($r^4$) and octopole fields ($r^6$) (Reproduced from Ref. [117] with permission. © Wiley Periodicals, Inc., 2005)

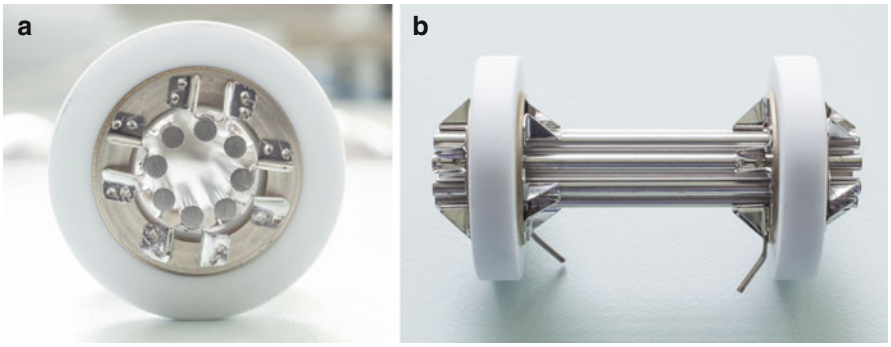


**Fig. 4.40** RF octopole ion guide used to bridge a differential pumping stage of an ESI interface in a Finnigan LCQ instrument. (**a**) Head-on view to show the octopole alignment and (**b**) side view. Each of the two pins pointing down is connected to supply the RF voltage to four of the rods in alternation. The round rods are ca. 3 mm in diameter and the length of this device is about 7 cm

RF ion guides are employed in many ways to transfer ions of low kinetic energy, typically of 1–50 eV, from one functional unit to another without substantial losses [117, 119]. Ion guides are used to adapt atmospheric pressure ion sources to mass analyzers, e.g., for APCI, ESI, and ambient MS (Fig. 4.40; Chaps. 7, 8, 12, and 13). From the viewpoint of the ions, they act like a hose or pipe while being fully permeable for neutrals. Thus, the RF ion guide allows residual gas to effuse through the gaps between the rods into the vacuum pumps, whereas ions are escorted into the mass analyzer. Examples for RF ion guide usage will be given in the instrument schemes to follow later in this chapter.

In contrast to expectations based on scattering by collisions with residual gas, RF-only multipoles deliver even improved transmission at moderate vacuum conditions in the range of $10^{-3}$–$10^{-2}$ mbar. This is due to a reduction in ion kinetic energy and concomitant collisional damping of ion motion toward the central axis of the device, so-called *collisional cooling* [108, 120–122]. It has been shown that

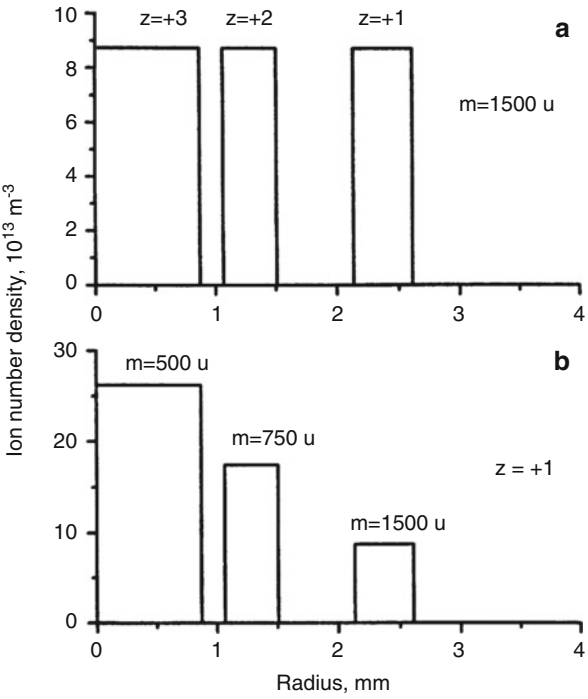


**Fig. 4.41** Calculated number density distributions of ions stored in a collisional cooling RF-only quadrupole ion guide having an inner radius of 4 mm and being operated at 1 MHz. (**a**) Radial positions of ions of 1500 u bearing 1, 2, and 3 positive charges. (**b**) Radial position of ion clouds of singly charged ions of *m*/*z* 500, 1000, and 1500 (Reproduced from Ref. [121] with permission. © John Wiley & Sons, Ltd., 2000)

ions of 25 eV kinetic energy are slowed down to 0–2 eV upon passing through a 15-cm-long RF-only quadrupole ion guide at $8 \times 10^{-3}$ mbar [120, 123]. Ions of higher mass (not higher *m*/*z*) are more prone to this effect, e.g., a sevenfold increase was found for ions of about 200 u, whereas ions of about 17,000 u showed 80-fold improvement in transmission [120]. Here, collisional cooling causes a confinement of the ion beam towards the central axis of the quadrupole which in turn increases the transmission efficiency through an exit aperture. This phenomenon is known as *collisional focusing* (cf. Fig. 4.43 in Sect. 4.5.1) [108, 122, 124].

It is even more interesting that the cooled ion cloud forms concentric cylindrical layers inside the RF-only multipole, each of those layers being composed of ions of the same *m*/*z* value with higher *m*/*z* ions gathering in more outward radial layers. This behavior is due to more effective RF focusing for ions of lower *m*/*z* that pushes these ions closer towards the center. Multiply charged ions form more distinct radial boundaries of the layers as compared to singly charged ion clouds of the same *m*/*z* and charge density (Fig. 4.41). The gaps of low ion population between the layers result from space charge repulsion [121]. Formation of such *m*/*z*-stratified structures requires sufficiently high charge density and effective collisional damping. Both RF-only collision multipoles and linear quadrupole ion traps as employed for external ion accumulation fulfill those criteria. When the linear ion density increases, the maximum ion cloud radius also increases. Overfilling of the multipole capacity results in a strong discrimination against high *m*/*z* ions, because the ion clouds expand to larger radii causing outer layers (high-*m*/*z* ions) to hit the multipole rods [121].

**Conditions for thermalization**
From the work by Douglas [120] a rule of thumb can be derived to judge whether thermalization occurs. This $p \times d$ *rule* demands the product of pressure ($p$ in Torr) times path length ($l$ in mm) to be larger than 0.2 mTorr. For example, at $2 \times 10^{-3}$ Torr a RF-only device of 100 mm length is just sufficient for effective ion cooling as we have $2 \times 10^{-3}$ Torr $\times$ 100 mm = 0.2 mTorr.

RF-only *quadrupole*, *hexapole*, or *octopole collision cells* [117, 125, 126] are part of so-called *triple quadrupole mass spectrometers*, which essentially represent QqQ, QhQ, or QoQ instruments, respectively, depending on the type of RF-only collision cell actually in place. They are efficient tools for tandem mass spectrometry (Chap. 9).

Different from magnetic sector or TOF instruments having collimated beams of energetic ions, the ions are exiting from quadrupoles in almost any direction on the *xy*-plane. Thus, real field-free regions as employed in sector or TOF instruments have to be replaced by ion-guiding collision cells to allow CID of ions of 5–100 eV kinetic energy. RF-only collision cells need not to be straight: starting from the Finnigan TSQ700 bent geometries were introduced, and 90° cells or 180° cells are nowadays common. Besides a reduced footprint of the instrument, the bent geometries have other beneficial effects such as the elongation of the flight path through the collision region for improved fragmentation efficiency and the exclusion of neutrals or photons from hitting the detector, and thus, reduced noise levels.

**Ions can even stop**
The initial kinetic energy of slow ions can be lost upon several collisions. At $5 \times 10^{-3}$ mbar (0.5 Pa) fragment ion kinetic energies are reduced to about 1 eV [123]. The ions may even stop their motion along the cell [121, 124]. Under such conditions, the continuous ion current into the cell is the only impetus to push the ions through as a result of space-charge effects. The resulting dwell time of about 10 ms allows up to about 5000 (reactive) collisions to take place at about $5 \times 10^{-2}$ mbar (5 Pa) collision gas (or reagent gas) pressure in an octopole collision cell [127].

Within the last decade, RF quadrupole ion guides with square or at least rectangular rod cross sections have also been used. Most of this development has been done by instrument manufacturers and few has been published on this topic. However, it appears that these square-rod quadrupoles offer the same level of performance as round-rod higher-order RF ion guides at reduced cost of

manufacture. We will get back to square rods in the context of linear quadrupole ion traps in the next section.

**Postponed summary** A summary of RF quadrupole devices will be given in Sect. 4.6.12. As we will see during the next two sections dealing with linear quadrupole ions traps and ion traps with three-dimensional quadrupole fields these devices have much in common, suggesting to summarize and compare them together later.

## 4.5 Linear Quadrupole Ion Traps

### 4.5.1 Linear RF-Only Multipole Ion Traps

As we have just learned, collisional cooling may bring translational ion motion along the axis of an RF-only multipole almost to a halt, thereby transforming such an RF-only multipole ion guide into an ion storage device [121]. To prevent ions inside the multipole from escaping via either open end, one creates a trapping potential well by placing electrodes of slightly higher potential adjacent to the front and rear ends of the multipole [128]. Such devices are known as *linear* (*quadrupole*) *ion traps* (LIT).

**Only quadrupoles are mass-selective**
Quadrupoles are the only devices capable of mass-selective operation, whereas higher-order RF ion guides or higher-order LITs can only guide, accumulate, store, and finally release ions for subsequent $m/z$ analysis.

While the entrance plate of the LIT is held at low potential, ions may enter the radially ion-confining RF field. The time span for ion accumulation is limited by

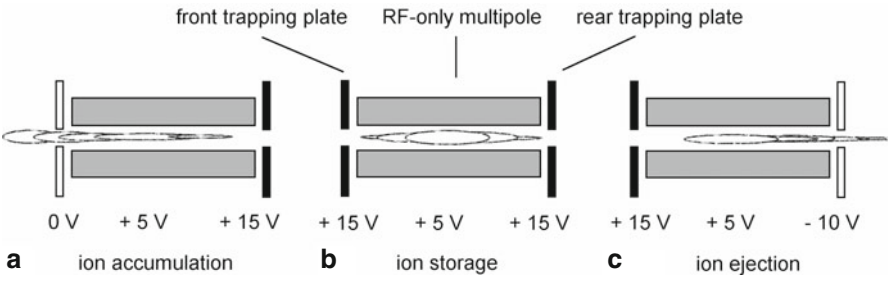


**Fig. 4.42** Operation of a linear RF multipole ion trap illustrated using typical DC voltage offsets for positive ions. (**a**) Ion accumulation with backside potential wall up, (**b**) storage of ions with both trapping potentials up, and (**c**) axial ejection of ions from trap using an attractive exit plate potential. The trapping RF multipole section is held at constant DC offset of +5 V in this example

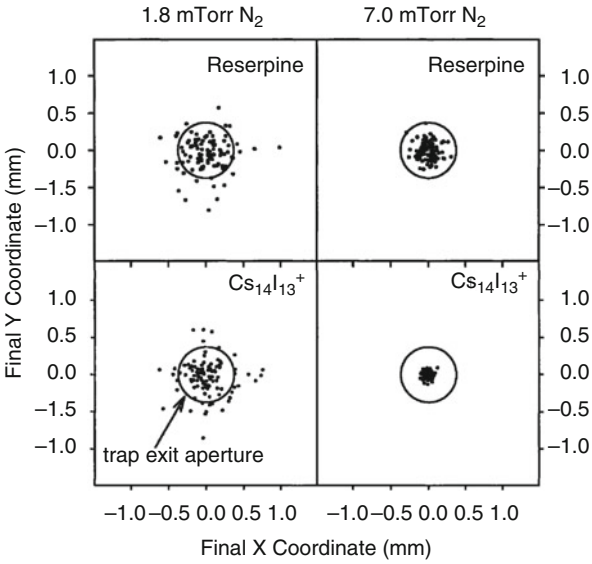


**Fig. 4.43** Radial distribution of 100 ion trajectories at the LIT exit aperture (*circle* indicates 0.7 mm aperture hole) for ions of reserpine and $Cs_{14}I_{13}^+$ cluster ions. Collisional focusing is well improved when raising the LIT pressure from 1.8 mTorr ($2.4 \times 10^{-3}$ mbar) to 7.0 mTorr ($9.3 \times 10^{-3}$ mbar) (Adapted from Ref. [122] with permission. © John Wiley & Sons, Ltd., 2001)

reflection of the fast ions at the backside potential wall affording that the entrance gate has to be closed before the lightest ions to be stored can exit the trap via the entrance (Fig. 4.42). Storage of ions in the presence of some buffer gas, e.g., argon or nitrogen at $10^{-3}$–$10^{-2}$ mbar, then allows for their thermalization and collisional focusing towards the LIT axis (Fig. 4.43). Both actual ion kinetic energy of the entering ion beam and the degree of thermalization directly influence the potential required to stop axial ion motion [122]. Vice versa, the trapping efficiency of an LIT for faster ions improves with rising pressure (Fig. 4.44) [129]. Finally, the ions can be axially ejected at any convenient point in time. Alternatively, the RF multipole may be segmented, typically into a longer middle and two shorter ends, which are operated at the same RF drive frequency and amplitude but at a DC offset voltage to create the switchable trapping potential well analogous to the trapping plates [130].

LITs present a rapidly expanding field of instrumentation; they have been established to collect ions externally before injecting them in bunches into an FT-ICR [131] or oaTOF analyzer [122, 128]. LITs capable of scanning by either axial or radial excitation of the ions and even capable of precursor ion selection for MS/MS experiments [129, 130, 132] and have been incorporated in commercial mass spectrometers [117, 133–135]. LITs can be built to store ions of very high $m/z$, e.g., singly charged ions of bovine serum albumine, $m/z$ 66.000, or even charged particulate matter [136].

This tells us that LITs are highly versatile devices:

- LITs may thermalize ions during their passage to provide narrow kinetic energy distributions before the next step of ion manipulation.

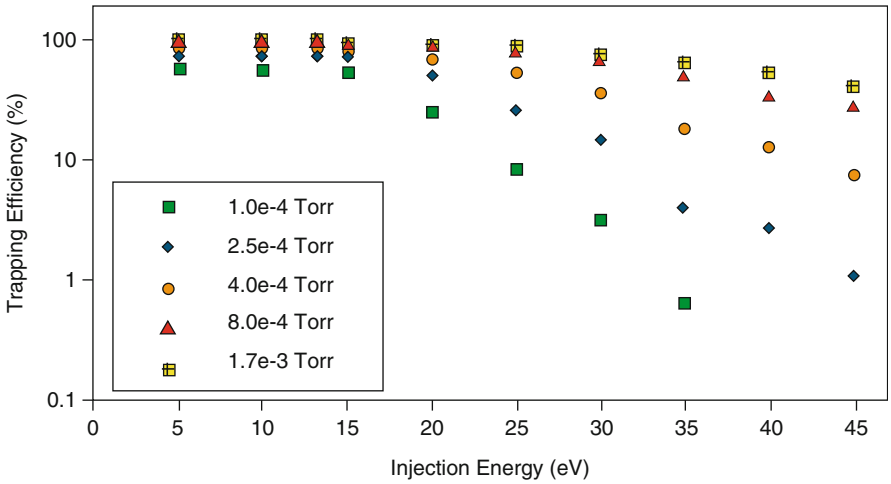


**Fig. 4.44** Dependence of the trapping efficiency of an LIT on ion injection energy (reserpine $[M + H]^+$ ions, $m/z$ 609) for varying LIT pressures (from the top $1.3 \times 10^{-4}$ mbar, $3.3 \times 10^{-4}$ mbar, $5.3 \times 10^{-4}$ mbar, $1.1 \times 10^{-3}$ mbar, $2.3 \times 10^{-3}$ mbar) (Adapted from Ref. [129] with permission. © John Wiley & Sons, Ltd., 2002)

- LITs can accumulate ions until a population suitable for the respective next step of mass analysis is reached.
- LITs can deliver packages of ions for a mass analyzer operating in batch mode.
- LITs themselves are capable of mass-selective operation and scanning to serve as mass analyzers on their own (Sect. 4.5.2).
- LITs are even capable of precursor ion selection and subsequent ion fragmentation by collisions with buffer gas for MS/MS experiments.

**A new time scale**
With RF multipoles and even more so with LITs, we have definitely gone beyond the domain of the classical mass spectrometric time scale (Sect. 2.6.2). In ion trapping devices, ions are stored for milliseconds to seconds, i.e., $10^3$–$10^6$ times longer than their lifetimes in beam instruments.

### 4.5.2 Mass-Analyzing Linear Quadrupole Ion Trap with Axial Ejection

Linear ion traps provide high capacities as far as the number of trapped ions is concerned, because the ion cloud can expand along the entire device. It is thus desirable to operate such an LIT not only for ion thermalization and ion accumulation but also as a mass analyzer. In principle, there are two modes possible: one employs excitation of the ions to achieve mass-selective ejection in radial direction

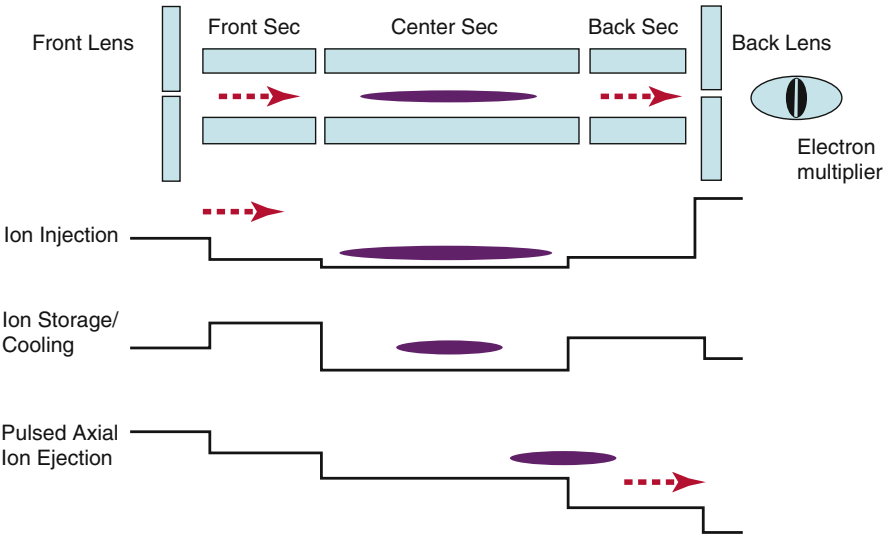


**Fig. 4.45** Sequence of DC voltages applied of the lenses and sections of a segmented linear ion trap to achieve mass-selective isolation and axial pulse-out of trapped ions from the mass analyzer. The reasons for segmenting of the LIT are explained in Sect. 4.5.3 and Fig. 4.49 (Reproduced from Ref. [140] with permission. © American Chemical Society, 2004)

[137], the other uses mass-selective axial ejection by application of an auxiliary AC field to the rods of the LIT [129]. The latter mode makes use of the fact that near the exit of the LIT radial ion motion (RF-controlled) and axial ion motion (trapping potential-controlled) are coupled via the fringing fields. When the ion radial secular frequency (governed by the stability parameters and the drive RF) matches that of the auxiliary AC field, ion excitation is effected in a way that also enhances its axial kinetic energy, and thus, leads to ejection from the LIT (Fig. 4.45) [138] and Chap. 5 in [139]).

An instrument incorporating a LIT with mass-selective axial ejection has been developed by Hager by replacing either the RF-only collision quadrupole or the second mass-analyzing quadrupole of a QqQ instrument with a LIT. The attained configurations are Q-LIT-Q (Fig. 4.46) and QqLIT, respectively [129, 134, 135]. The QqLIT offers enhanced sensitivity as compared to its QqQ precursor model and offers new modes of operation [134] and Chap. 3 in [141]). The QqLIT has been commercialized by AB Sciex as their Q-Trap series.

As with the linear quadrupole before, the potential $\Phi_{(x,y,z,t)}$ in the two-dimensional quadrupole field of the LIT is expressed by a DC voltage $U$ and an RF drive voltage $V$ with the frequency $\Omega$ [129, 138] and Chap. 5 in [139])

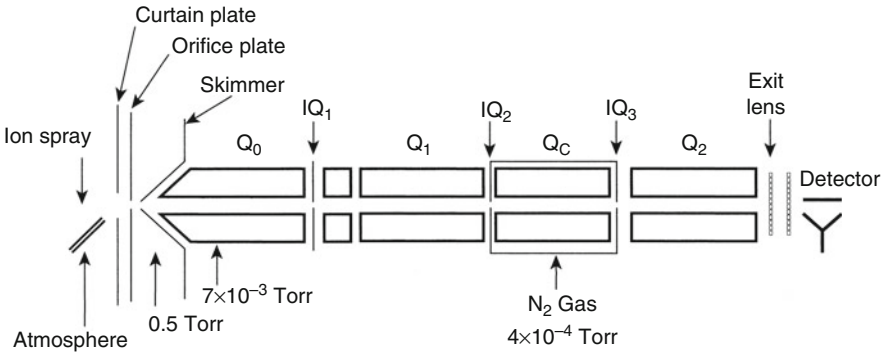


**Fig. 4.46** A quadrupole-LIT hybrid instrument. In this scheme, the RF-only collision quadrupole has been replaced by the LIT. The other option, replacement of Q2 by a LIT, is finally in commercial use (Adapted from Ref. [129] with permission. © John Wiley & Sons, Ltd., 2002)

$$\Phi_{(x,y,z,t)} = (U - V\cos\Omega t)\frac{(x^2 - y^2)}{r_0^2} \tag{4.23}$$

from which the equations of motion can be derived. Assuming singly charged ions, i.e., $q = e$, we have

$$\begin{aligned} &\frac{d^2x}{dt^2} + \frac{e}{m_i {r_0}^2}\ (U - V\cos\Omega t)x = 0 \\ &\frac{d^2y}{dt^2} - \frac{e}{m_i {r_0}^2}\ (U - V\cos\Omega t)y = 0 \\ &\frac{d^2z}{dt^2} = 0 \end{aligned} \tag{4.24}$$

where $m_i$ is the mass of the ion, $r_o$ is the distance between the central axis of the LIT and the surface of the rod. At least, these relationships hold valid as long as ions are sufficiently distant to the fringing fields at the end of the rods.

In practice, there is no DC component, and thus, only the Mathieu parameter $q$ is required, which is obtained by solving the above equations

$$q_x = \frac{4eV}{m_i {r_0}^2 \Omega^2} \tag{4.25}$$

The voltage $V$ is the zero-to-peak amplitude of the RF drive voltage. For an ion inside the quadrupole field the fundamental resonant frequency $\omega_n$ is obtained as

$$\omega_n = (2n + \beta)\left(\frac{\Omega}{2}\right) \tag{4.26}$$

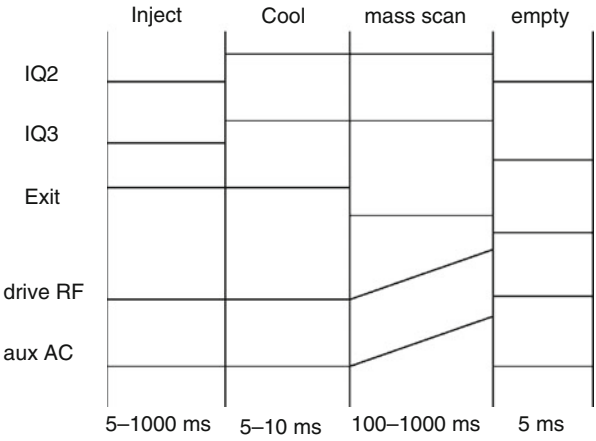


**Fig. 4.47** Scan function as used in the QqLIT instrument. IQ2, IQ3, and Exit belong to the trapping plates and the exit lens. Vertical displacements of lines indicate changes of the respective voltages. Note that the time slices are not to scale and that the duration of ion accumulation and mass scan may vary substantially (Adapted from Ref. [129] with permission. © John Wiley & Sons, Ltd., 2002)

For $n = 0$ Eq. (4.26) simplifies to become

$$\omega = \frac{\beta\Omega}{2} \tag{4.26a}$$

which for $q_x < 0.4$ can be approximated by the relationship

$$\omega \approx \frac{q_x}{\sqrt{8}}\Omega \tag{4.27}$$

The stability diagram for the LIT is analogous to that of the linear quadrupole (Figs. 4.32 and 4.33). While a description of the scanning of the LIT to achieve mass-selective axial ejection requires complex mathematics [138] far beyond the scope of this book, the practical application of LIT can easier be understood.

The scan function of such an instrument can be displayed in four time slices comprising:

1. ion injection until enough ions are accumulated,
2. trapping and thermalization,
3. mass scan by linear alteration of RF drive and auxiliary AC voltage,
4. a short blanking pulse to reset the LIT prior to the next scan cycle (Fig. 4.47).

**Combination of two analyzer concepts**

The QqLIT setup combines into one single instrument different types of mass analyzers, a scanning linear quadrupole, and a scanning linear quadrupole ion trap all connected via an RF-only ion guide. Instruments combining different types of mass analyzers are termed *hybrid instruments*. Most modern mass spectrometers are assembled from different elements to achieve optimum capabilities in the sense of creating instruments uniting the best of two worlds [133]. An overview of hybrids is presented at the end of the analyzer section.

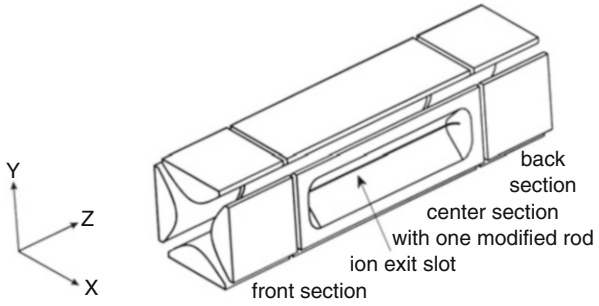


**Fig. 4.48** A segmented linear quadrupole ion trap with mass-selective radial ejection capability. Applying higher potential to the front and back sections creates an axial trapping potential for ions in the center section. Radial trapping is again provided by the RF quadrupolar field. Ions are exiting through the slot in one of the four rods. The commercial design offers doubled sensitivity by using two detectors at opposite rods (Adapted from Ref. [130] by permission. © Elsevier Science, 2002)

### 4.5.3 Mass-Analyzing Linear Ion Trap with Radial Ejection

A scanning LIT [130] can alternatively be realized using a mass-selective radial ejection mode of operation. Such a LIT can either serve as a stand-alone mass analyzer (Thermo Scientific LTQ™ series) or can be combined into a hybrid LIT-FT-ICR instrument (Thermo Scientific LTQ-FT™ series). In the LTQ-FT instruments, the LIT shields the ultrahigh vacuum of the FT-ICR from collision gas and decomposition products in order to operate under optimum conditions. More importantly from the analytical point of view, the LIT can accumulate, mass-select and fragment selected ions prior to the next FT-ICR cycle while the ICR cell is still busy with the previous ion package (FT-ICR cf. Sect. 4.7). By using an Orbitrap analyzer (Sect. 4.8) in place of the FT-ICR cell, the same company offers the Thermo Scientific LTQ-Orbitrap™ series as an economical nonetheless powerful alternative to their LTQ-FT.

The LIT is composed of a quadrupole with hyperbolic rods that is cut into three segments of 12 mm in length for both trapping sections and 37 mm in length for the ion storage compartment (Fig. 4.48) [130]. The segmented design avoids fringing fields from the trapping plates as obvious from the electric field calculations using the SIMION software package (Fig. 4.49) [142, 143]. Although necessary for the axial ejection scan mode discussed in the preceding section, the radial excitation scanning requires the absence of fringing fields in the trapping zone. One pair of opposite storage compartment rods has cut a slit of 0.25 mm width and 30 mm length to allow for radial ejection of ions onto a conversion dynode. The conversion dynode is held at −15 kV (for positive-ion operation), and upon ion impact it delivers secondary electrons to an electron multiplier. In the commercial variant of the instrument, two detectors are in use to double the sensitivity of the device. The field inhomogeneity introduced by cutting slits into the rods is counterbalanced by

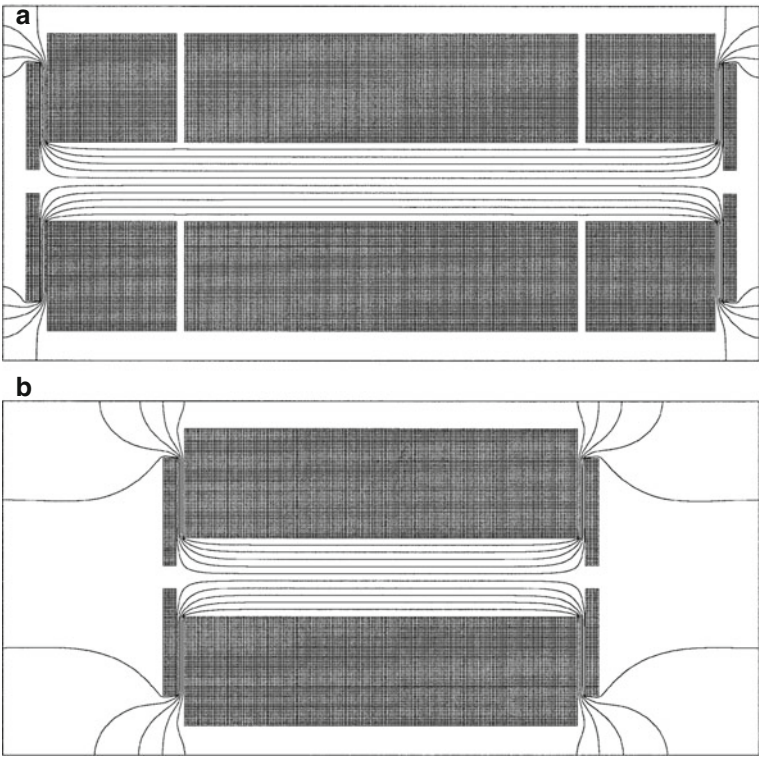


**Fig. 4.49** SIMION simulation of the resonance excitation field comparing (**a**) a three-section ion trap and (**b**) a single-section device with end plates for trapping. In (**a**) the field inside the trapping compartment remains unperturbed from fringing fields (Adapted with permission from Ref. [130]. © Elsevier Science Publishers, 2002)

aligning them slightly outward from their theoretical $x$-position [130]. To operate as an $m/z$ analyzer, the assembly of rods needs (*i*) a DC voltage supply to create the axial trapping field ($z$-coordinate), (*ii*) an RF voltage supply (1 MHz, $\pm$ 5 kV rod to ground) to deliver the radial quadrupolar trapping field ($x$,$y$-plane), and (*iii*) two phases of supplemental AC voltage (5–500 kHz, $\pm$ 80 V) that is applied across the $x$-rods for ion isolation, activation, and mass-selective ejection.

### 4.5.4 Constructing an Instrument Around the LIT

It takes more than just a nicely working $m/z$ analyzer to put together an instrument suitable for real-world use and commercial success. Thus, the elaboration in this

short paragraph presents an example of what is relevant for any type of mass spectrometer.

To build a useful mass spectrometer, the above LIT is connected to an electrospray ionization (ESI, Chap. 12) source using RF-only ion guides to bridge the distance from the source orifice to the entrance of the LIT. As the ESI process starts at atmospheric pressure, the incipient ions need to be continuously transferred from outside the mass spectrometer into the high vacuum of the $m/z$ analyzer. This can be achieved by so-called *differential pumping* (Sect. 4.13). Differential pumping makes use of the fact that macroscopic flow is only sustained as long as the mean free path of a molecule is shorter than the average dimension of the aperture it has to pass or of the vessel where it is contained. In practice, a powerful rotary pump (30 $m^3$ $h^{-1}$) maintains a pressure in the order of 1 mbar behind a 0.4–0.5 mm orifice. The next stages of the differentially pumped system are usually pumped by turbomolecular pumps. In modern instruments one split-flow turbomolecular pump often serves for both ports. In case of the LIT instrument the intermediate region is thus evacuated to about $2 \times 10^{-3}$ mbar and the LIT itself to $2.6 \times 10^{-5}$ mbar (Fig. 4.50).

The resulting mass spectrometer is able to deliver unit resolution over an $m/z$ 150–2000 range at about 3 scans per second (Fig. 4.51) and even to provide higher resolution at lower scan rates ([130, 144] and Chap. 5 in [139]).

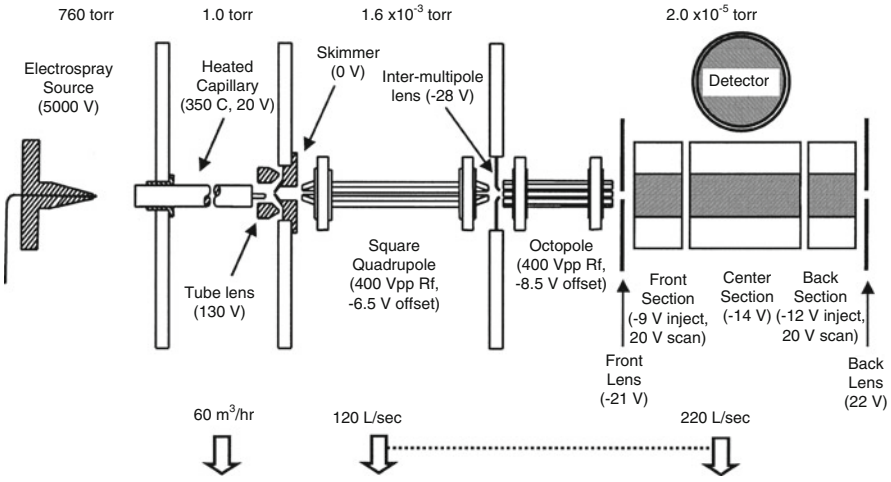


**Fig. 4.50** Radial ejection LIT mass spectrometer with ESI source, more precisely the Thermo Fisher LTQ as of 2002. A square RF quadrupole is used to bridge the second pumping stage while an RF octopole like the one shown in Fig. 4.40 is used in the third pumping state. Typical operating voltages and pressures are given (Reprinted with permission from Ref. [130]. © Elsevier Science Publishers, 2002)

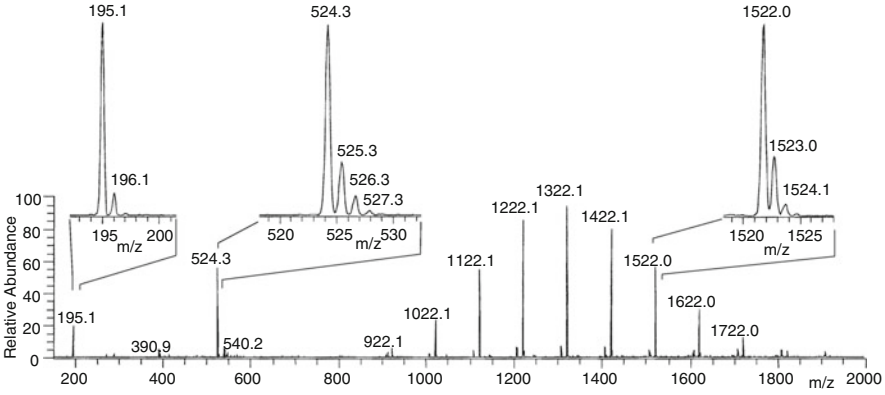


**Fig. 4.51** Full scan mass spectrum of a calibration mixture containing caffeine, $[M + H]^+$ at $m/z$ 195, the peptide MRFA, $[M + H]^+$ at $m/z$ 524, and Ultramark 1621 yielding a series of ions from $m/z$ 922 to 1722. The expanded views of selected signals show unit resolution, i.e., uniform resolution over the whole range (Adapted with permission from Ref. [130]. © Elsevier Science Publishers, 2002)

**Just a reminder** As already pointed out at the end of the linear quadrupole section, a summary of all RF quadrupole devices will be given in Sect. 4.6.12.

## 4.6 Ion Trap with Three-Dimensional Quadrupole Field

### 4.6.1 Introduction

In contrast to the linear two-dimensional quadrupole field of the LIT, the *quadrupole ion trap* (QIT) originally developed by Wolfgang Paul creates a three-dimensional RF quadrupole field of rotational symmetry to store ions within defined boundaries. The invention of the QIT goes back to 1953 [101–103]; however, it took until the mid-1980s to access the full analytical potential of quadrupole ion traps [139, 145–149].

**Naming**
Wolfgang Paul himself preferred to call the device *"Ionenkäfig"* (ion cage) because it does not actively act to catch ions from the outside. The acronym QUISTOR derived from *quadrupole ion store* was also in use for a while. To be precise, we would have to call it *ion trap with three-dimensional quadrupole field*, as used in the title of this section. Rather than insisting on this lengthy term we will be using the commonly accepted term *quadrupole ion trap* (QIT).

The first commercial quadrupole ion traps were incorporated in GC-MS benchtop instruments in the late 1980s (Finnigan MAT ITD and ITMS). Electron ionization was effected inside the trap by admitting the GC effluent and a beam of electrons directly into the storage volume of the trap. Later, external ion sources became available, and soon a large number of ionization methods could be fitted to the QIT analyzer [150–152]. Modern QITs cover ranges up to about $m/z$ 3000 with fast scanning at unit resolution, and in addition, offer *"zoom scans"* over smaller $m/z$ ranges at higher resolution; instruments delivering resolving power up to 5-fold unit resolution are commercially available. Accurate mass measurements with QITs were expected [148] but not realized so far. The tandem-in-time capabilities of QITs can be employed to conveniently perform $MS^n$ experiments [146, 147], and their compact size is ideal for field applications [16].

**Historical versus didactical**
Historically, both the linear quadrupole analyzer and the quadrupole ion trap originate from the early 1950s (even from the same inventor), whereas the scanning linear ion trap is a design of the 1990s. A detailed timeline of the development of quadrupole ion traps can be found in the comprehensive monographs by March and Todd [139, 145]. However, from a teaching perspective, it appears advisable to align the explanations in the logical order as presented here. Once the concepts of trapping and mass-selective release from a quadrupole ion trap have been understood, the step from linear to rotational symmetry should be comparatively easy.

### 4.6.2 Principle of the Quadrupole Ion Trap

The *quadrupole ion trap* (QIT) consists of two hyperbolic electrodes serving as end caps along with a ring electrode that replaces two of the linear quadrupole rods, i.e., it could theoretically be obtained by rotating the axial cross section of a linear quadrupole with hyperbolic rods by 360° around an axis that traverses the apices of two opposed rods (Figs. 4.52 and 4.53). Thus, a section through the $rz$-plane of the QIT closely resembles that of the entrance of a linear quadrupole with hyperbolic rods (cf. Figs. 4.30 and 4.37) [105, 150]. However, the angle between the asymptotes enclosing the ring electrode is 70.5° ($2 \times \arctan(1/\sqrt{2})$) instead of 90°. The end caps are electrically connected and the DC and RF potentials are applied between them and the ring electrode. The working principle of the QIT is based on creating stable trajectories for ions of a certain $m/z$ or $m/z$ range while removing unwanted ions by letting them collide with the walls or by axial ejection from the trap due to their unstable trajectories [139, 145, 149].

For the QIT, the electric field has to be considered in three dimensions. Let the potential $\Phi_0$ be applied to the ring electrode while the hyperbolic end caps are grounded. The axial coordinate of the trap is designated as the $z$-axis, the value $z_0$

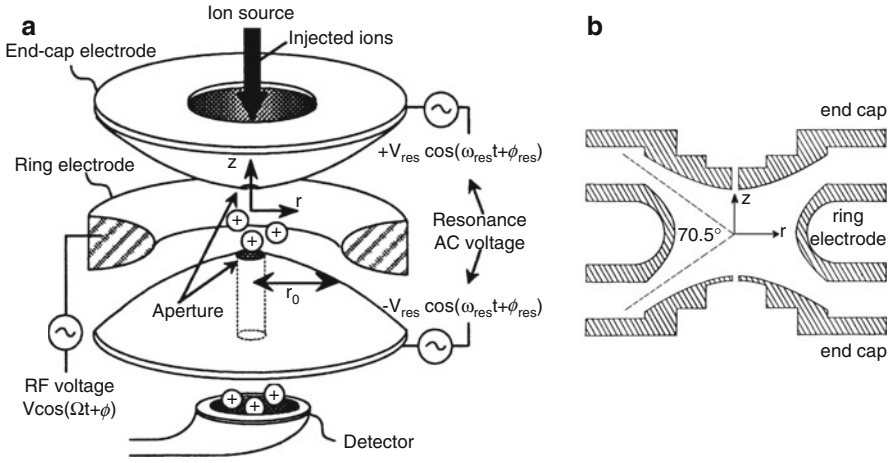


**Fig. 4.52** A quadrupole ion trap. (**a**) QIT with external ion source (illustration stretched in *z*-direction) and (**b**) section in the *rz*-plane (in scale). (**a**) (Reproduced from Ref. [153] by permission. © John Wiley & Sons, 2000)

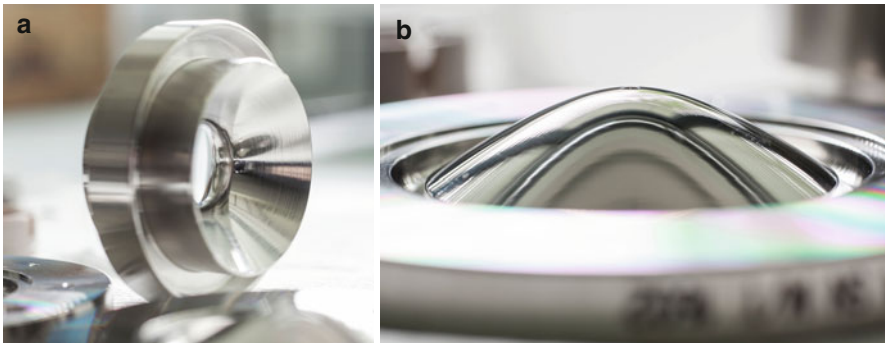


**Fig. 4.53** Electrodes of the Finnigan LCQ quadrupole ion trap analyzer. (**a**) Ring electrode with symmetrical hyperbolic cross section of the inner walls of the ring. (**b**) One of the pair of hyperbolic end cap electrodes

defines the physical dimension of the trap (center to cap), and $z$ presents the actual position of an ion with respect to the $z$-axis. The $x,y$-plane is resolved into the cell radius $r_0$ where $r$ analogously defines the actual radial position of an ion. With the pair of end caps grounded the potential inside the trap is given as

$$\Phi_0 = U + V \cos \Omega t \tag{4.28}$$

Then, the field can be described in cylindrical coordinates (using the standard transformations $x = r \cos \theta$, $y = r \sin \theta$, *and* $z = z$) by the expression [145, 150]

$$\Phi_{x,y,z} = \frac{\Phi_0}{{r_0}^2}\left(r^2\cos^2\theta + r^2\sin^2\theta - 2z^2\right) \tag{4.29}$$

Because of $\cos^2 + \sin^2 = 1$ this reduces to

$$\Phi_{r,z} = \frac{\Phi_0}{{r_0}^2}\left(r^2 - 2z^2\right) \tag{4.30}$$

The equations of motion of a singly charged ion of $q = e$ in such a field are

$$\begin{aligned} \frac{d^2z}{dt^2} - \frac{4e}{m_i\left(r_0^2 + 2z_0^2\right)}\ (U - V\cos\Omega t)z = 0 \\ \frac{d^2r}{dt^2} + \frac{2e}{m_i\left(r_0^2 + 2z_0^2\right)}\ (U - V\cos\Omega t)r = 0 \end{aligned} \tag{4.31}$$

Solving these differential equations which are again of the Mathieu type, finally yields the parameters $a_z$ and $q_z$

$$\begin{aligned} a_z &= -2a_r = -\frac{16eU}{m_i\left(r_0^2 + 2z_0^2\right)\ \Omega^2} \\ q_z &= -2q_r = \frac{8eV}{m_i\left(r_0^2 + 2z_0^2\right)\ \Omega^2} \end{aligned} \tag{4.32}$$

where $\Omega = 2\pi f$ and $f$ is the fundamental RF frequency of the trap ($\approx$1 MHz). To remain stored in the QIT, an ion has to be simultaneously stable in the $r$ and $z$ directions. The occurrence of stable ion trajectories is determined by the stability parameters $\beta_r$ and $\beta_z$ which depend on the parameters $a$ and $q$. The borders of the first stability region are defined by $0 < \beta_r, \beta_z < 1$ [154].

A stability diagram can be drawn where the stability region closest to its origin is of greatest importance for the operation of the QIT (Fig. 4.54). At a given $U/V$ ratio, ions of different $m/z$ are located along a straight line crossing the stability region; ions of higher $m/z$ are nearer to the origin than lighter ones. The regions of stability as plotted in the $a/q$ plane are represented as envelopes of characteristic shape. Ions with their $m/z$ value inside the boundaries are stored in the QIT. The low-mass limit of the trapped $m/z$ range is strictly defined by $q_z = 0.908$.

Collisional cooling (Sect. 4.4.4) by several tens of soft collisions during the dwell time of the ions inside the QIT significantly enhances its resolving power and sensitivity [155, 156]. The light buffer gas, normally helium at 0.1 Pa, serves to dampen the ion motion towards the center of the trap, and thus, keeps them away from the electrode surfaces and from field inhomogeneities as induced by the entrance and exit holes of the QIT [157].

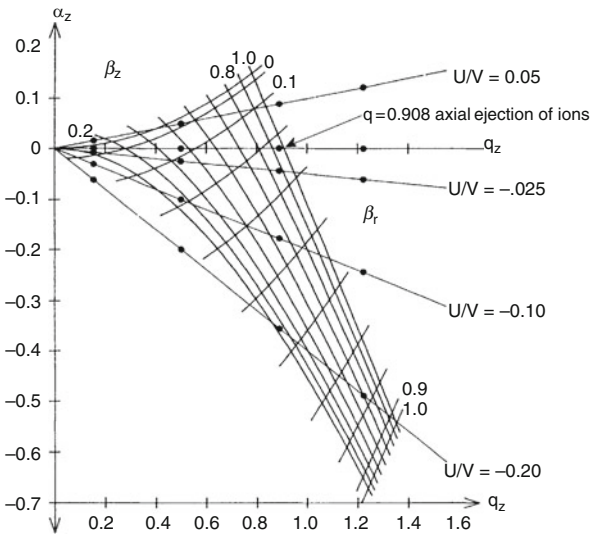


**Fig. 4.54** Stability diagram for the quadrupole ion trap. The points collected on a common line mark the *a*/*q* values of a set of ions. Each line results from different settings of the *U*/*V* ratio (Reproduced from Ref. [145] by permission. © John Wiley and Sons, 1989)

### 4.6.3 Visualization of Ion Motion in the Ion Trap

The way the three-dimensional quadrupole field acts to keep ions within a certain volume, i.e., within a potential well some electron volts in depth, can be illustrated by a mechanical analog: A ball can be prevented from rolling from a saddle by rotating the saddle just right to bring the ball back to the middle before it can leave the surface via one of the steeply falling sides (Fig. 4.55a). Paul demonstrated the dynamic stabilization of up to three steel balls by such a device in his Nobel lecture [101, 102].

The trajectories of low-mass ions in a QIT were shown to be similar to those observed for charged aluminum dust particles [158–161]. Wuerker recorded Lissajous trajectories, superimposed by the RF drive frequency, as a photomicrograph (Fig. 4.55b) [158]. The complex motion of the ions is the result of the two super-imposed secular oscillations in $r$ and $z$ direction. Calculations of the trajectories yield the same results [162].

### 4.6.4 Mass-Selective Stability Mode

The whole range of ions is generated within or admitted to the QIT, but solely ions of one particular $m/z$ are trapped at a time by setting appropriate parameters of the QIT. Then, the stored ions are pulsed out of the storage volume by applying a negative pulse to one of the end caps [163, 164]. Thus, they hit the detector located behind an opening in the center of one of the end caps. A full-scan mass spectrum is obtained by addition of several hundred single steps, one for each nominal $m/z$ value. This is the so-called *mass-selective stability* mode of the QIT [165, 166]. The mass-selective stability mode is no longer in use, because it is too slow and provides poor sensitivity as most ions are wasted.

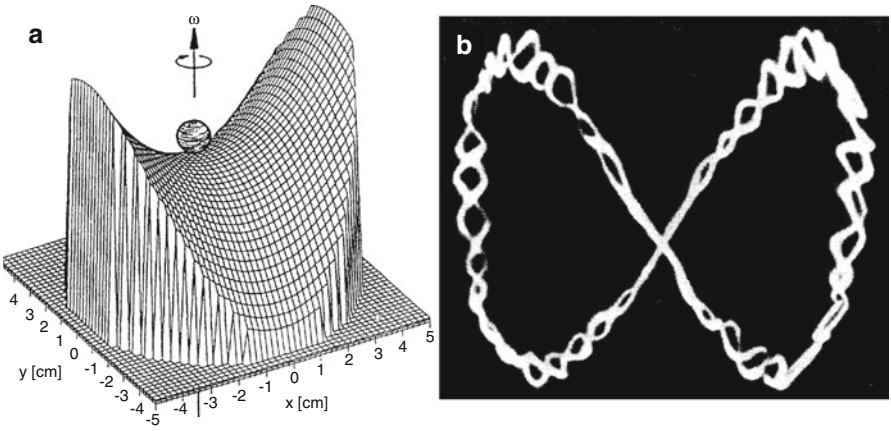


**Fig. 4.55** Visualization of ion motion in the ion trap. (**a**) Mechanical analog of the QIT. (**b**) Photograph of ion trajectories of charged aluminum particles in a quadrupole ion trap ((**a**) Reproduced from Ref. [102] with permission. © World Scientific Publishing, 1993. (**b**) Reproduced from Ref. [158] with permission. © American Institute of Physics, 1959)

### 4.6.5 Mass-Selective Instability Mode

First, the full $m/z$ range of interest is trapped within the QIT. The trapped ions may either be created inside the QIT or externally. Then, with the end caps grounded an RF-voltage scan ($V$) is applied to the ring electrode causing consecutive ejection of ions in the order of their $m/z$ values. This is known as *mass-selective instability* (*ejection*) mode [155, 167]. It can be represented in the stability diagram by a horizontal line from the origin to the point of axial ejection at $q_z = 0.908$. The timing sequence is shown in Fig. 4.56 While easy to understand, this mode is also no longer relevant in QIT operation.

### 4.6.6 Resonant Ejection

Another technique to operate a QITs employs the effects of *resonant ejection* to remove ions of successively increasing $m/z$ value from the storage volume, i.e., to achieve a scan. In an ideal QIT, the motions of the ions in radial and axial directions are mutually independent. Their oscillations can be described by a radial and an axial secular frequency, each of them being a function of the Mathieu trapping parameters $a$ and $q$. If a supplementary RF voltage which matches the axial secular frequency is applied to the end caps, resonant ejection of ions occurs at $q < 0.908$ (Fig. 4.54) [168]. Excitation occurs when the frequency of a supplementary RF signal matches the secular frequency of a trapped ion in $z$ direction. The secular frequency components in axial direction ($\omega_z$) are given by $\omega_z = (n + \beta_z/2)\Omega$, where $\Omega$ represents the angular frequency, $n$ is an integer, and $\beta_z$ is determined by the working point of an ion within the stability diagram [169]. In the special case when

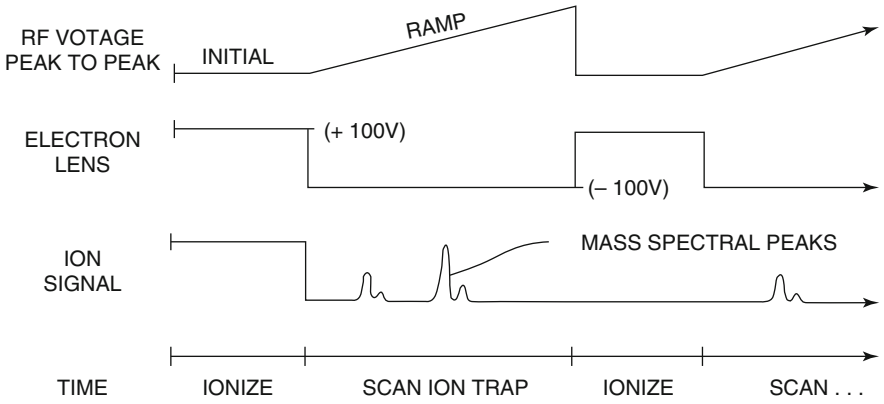


**Fig. 4.56** Timing sequence used for mass-selective instability mode (about 1.5 cycles shown). With an external ion source the ionization time is replaced by the ion injection pulse (Reproduced from Ref. [155] by permission. © Elsevier Science, 1984)

$\beta_z = 1$ and $n = 0$, the fundamental secular frequency is exactly half of the RF drive frequency applied between ring electrode and end caps.

**Scanning by Resonant Ejection** To effect resonant ejection for the set of $\beta_z = 0.5$ and $n = 0$ we have $\omega_z = (0 + 0.5/2) = 0.25\Omega$, i.e., $^1/_4$ of the RF drive frequency has to be applied to eject ions at the $\beta_z = 0.5$ borderline. By scanning the voltage of the RF drive frequency upwards, ions of increasing $m/z$ ratio are successively ejected.

Scans based on resonant ejection may either be carried out in a forward, i.e., from low to high mass, or a reverse direction. However, the scan direction has significant influence on the attainable resolving power, the reverse direction being clearly inferior in that respect. [170, 171] The combination of forward and reverse scanning allows for the selective storage of ions of a certain $m/z$ value by elimination of ions below and above that $m/z$ value from the trap. Thus, it can serve for precursor ion selection in tandem MS experiments [168, 170]. Axial excitation can also be used to cause collision-induced dissociation (CID) of the ions as a result of collisions with the helium buffer gas [155, 168]. A substantial increase of the mass range is realized by reduction of both the RF frequency of the modulation voltage and the physical size of the QIT [166, 172, 173].

### 4.6.7 Axial Modulation and Control of the Ion Population

Ion trapping devices are sensitive to overload because of the detrimental effects of Coulombic repulsion on the ion trajectories. The maximum number of ions that can be stored in a QIT is about $10^6$–$10^7$, but it reduces to about $10^3$–$10^4$ if unit mass resolution in an RF scan is desired. *Axial modulation*, a subtype of resonant ejection, allows to increase the number of ions stored in the QIT by one order of

magnitude while maintaining unit mass resolution [173, 174]. During the RF scan, the modulation voltage with a fixed amplitude and frequency is applied between the end caps. Its frequency is chosen slightly below $^1/_2$ of the fundamental RF frequency, because for $\beta_z \leq 1$, e.g., $\beta_z = 0.98$, we have $\Omega_z = (0 + 0.98/2) \times \Omega = 0.49 \times \Omega$. At the stability boundary, ion motion is in resonance with this modulation voltage, and thus ion ejection is facilitated. Axial modulation basically improves the mass-selective instability mode of operation.

If resolving power is not a major concern, scanning of QITs can be very fast, a property that can be employed to make a *pre-scan*. The actual ion current into the trap is then determined from the pre-scan and the result is used to adjust the number of ions admitted to the QIT by a timed ion gate for the subsequent analytical scan. Thus, the number of ions, and hence, charge density inside the QIT are continuously held close to the optimum. This tool to control the ion population of the QIT has been introduced by Finnigan and referred to as *automatic gain control* (AGC) [146, 175]. AGC gives increased sensitivity at low sample flow and avoids overload of the QIT at high sample flow.

**Importance of the ion population in traps**
Careful control of the ion population, e.g., as implemented by AGC, is not only relevant for QITs but also for all other types of ion traps. The technique is implemented in LITs that are employed as stand-alone devices and also in LITs serving for ion selection and dosing into FT-ICR or Orbitrap analyzers (Sects. 4.7, 4.8, and 4.9).

Provided sufficiently high scan rates are also available whilst resolution is preserved, the pre-scan can be omitted. Instead, a trend analysis based on a set of two or three preceding analytical scans can be performed. This procedure avoids wasting of ions and results in further optimization of the filling level of the QIT. The exploitation of the phenomenon of nonlinear resonances turned out to be of key importance for the realization of this method.

**Tandem MS in a QIT** Tandem mass spectrometric experiments in quadrupole ion traps (more in Sect. 9.8) are performed by combining the techniques of resonant ejection, and forward and reverse scanning to achieve an optimum in precursor ion selection, ion activation, and fragment ion scanning (Fig. 4.57) [168].

### 4.6.8 Nonlinear Resonances

Higher multipole fields, in particular octopole fields, are induced in any real ion trap by deviations from the ideal electrode structure. The trapping potential may then be represented as a sum of an ideal quadrupole field and weak higher order field

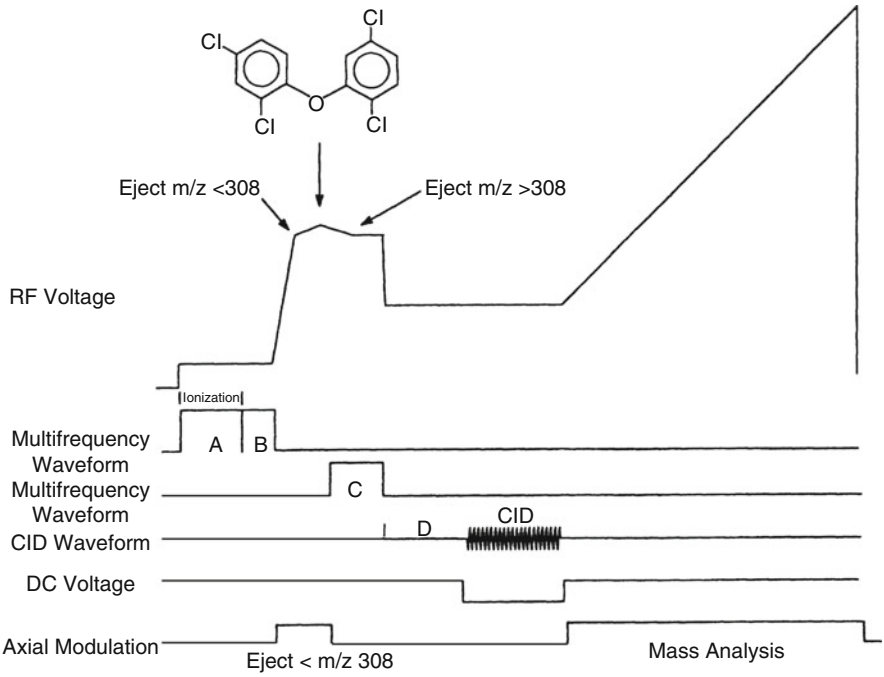


**Fig. 4.57** Complex scan function used for a tandem mass spectrometric study of 2,4,3′,6′-tetrachlorodiphenylether (Reproduced from Ref. [168] by permission. © John Wiley and Sons, 1997)

contributions [154, 176, 177]. Application of an excitation voltage across the end caps induces dipole and hexapole fields in addition. Those higher order fields in the QIT may have beneficial effects such as increase in mass resolution in the resonant ejection mode, but may also result in losses of ions due to nonlinear resonances [178]. Nonlinear resonances have been known for long [179, 180], but useful theoretical descriptions were only recently developed [154, 177, 181, 182]. The condition for the appearance of instabilities is related to certain frequencies through the stability parameters $\beta_r$ and $\beta_z$ and the integer multiples $n_r$ and $n_z$. The locations of instability spread like a net over the stability diagram and have been experimentally verified with astonishing accuracy (Fig. 4.58) [154]. Excitation of ions with a suitable frequency can cause their fast ejection from the trap due to the sudden shift to nonlinear stability. Nonlinear resonances can thus be exploited to realize very fast scans of the QIT (26,000 u $s^{-1}$) while maintaining good resolving power [182], e.g., irradiation of $0.33 \times \Omega$ amplifies hexapole resonances and causes sudden ejection at the $\beta_z = 0.66$ borderline.

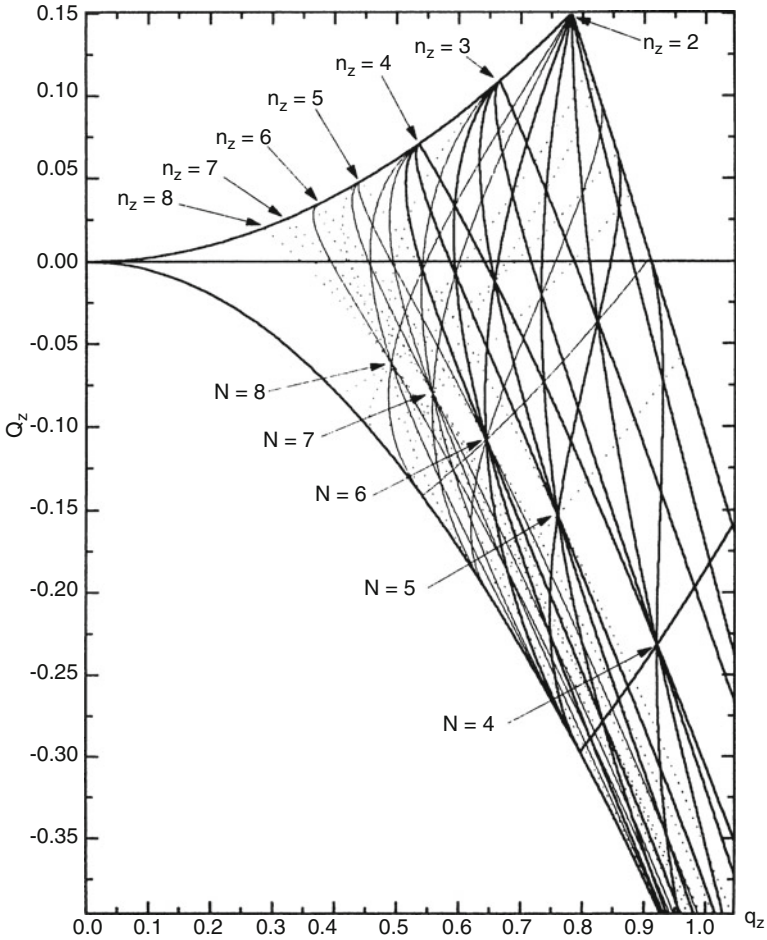


**Fig. 4.58** Plot of theoretical lines of instability corresponding to the relation $n_r/2\beta_r + n_z/2\beta_z = 1$ for different orders $N = n_r + n_z$ (strong resonances represented by *solid lines*, weak ones by *dotted lines*) (Reproduced from Ref. [154] by permission. © Elsevier Science, 1996)

### 4.6.9 Miniaturization and Simplification of Ion Traps

The fabrication of quadrupole mass analyzers of any design necessitates high precision in machining and alignment of the electrodes; the production of hyperbolic electrode surfaces is especially challenging. While quadrupoles are compact, for mobile applications, even smaller and preferably less expensive analyzers are desirable [15, 183, 184]. Additionally, mobile instruments should have reduced vacuum requirements as the generation of high vacuum demands for comparatively heavy and energy-consuming pumps.

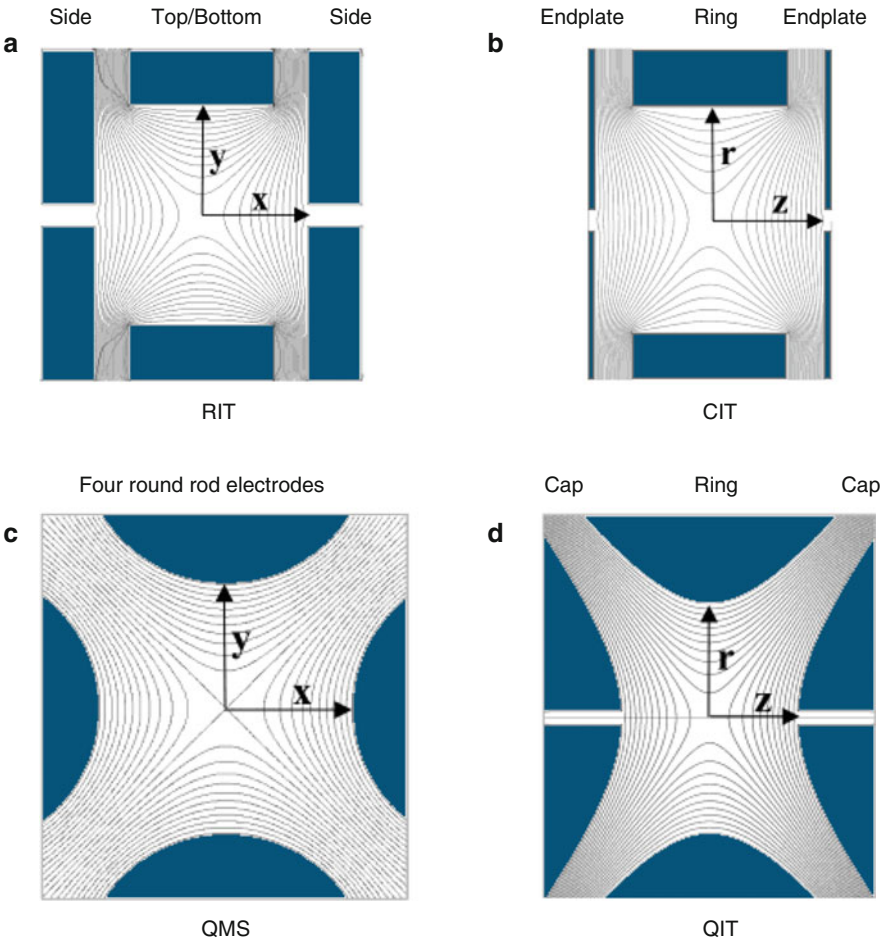


**Fig. 4.59** Calculated trapping fields for (**a**) a rectilinear ion trap, (**b**) a cylindrical ion trap with planar endplates, (**c**) a quadrupole mass filter with round rods, and (**d**) a quadrupole ion trap with hyperbolic electrodes (Paul trap). Analyzer views (**a**) and (**c**) are end-on, (**b**) and (**d**) side-on (Adapted from Ref. [185] with permission. © American Chemical Society, 2004)

It turns out that the electrode geometries of LITs and QITs can largely be simplified without sacrificing too much of their performance. Thus, a *rectilinear ion trap* (RIT) can be constructed that has flat rectangular-shaped electrodes, one pair (top and bottom) being smaller than the other (side walls with slits for ion ejection, Fig. 4.59) [185, 186]. Also the geometry of the Paul trap can be transformed into a simple *cylindrical ion trap* (CIT) built of two planar endplates and a cylindrical ring electrode. Such simplified electrode shapes also allow for

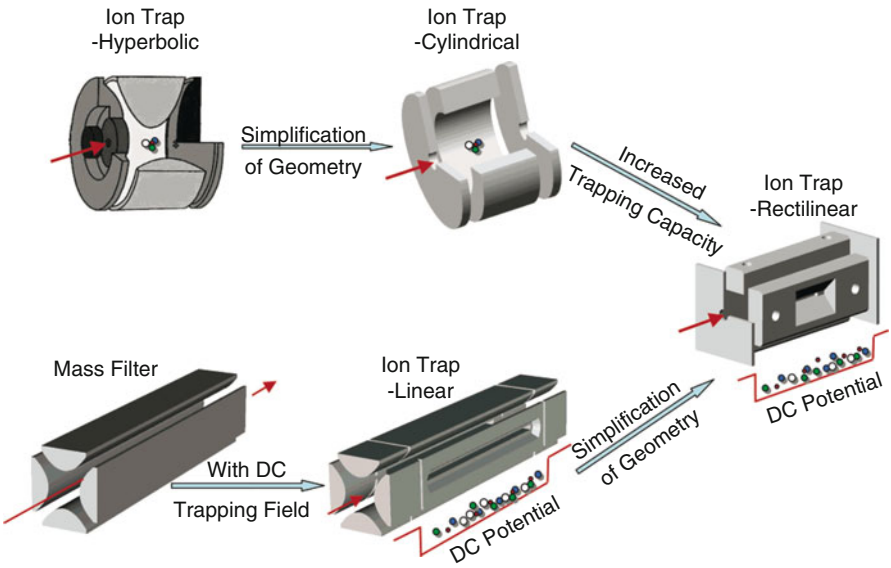


**Fig. 4.60** Conceptual evolution of the rectilinear ion trap and interrelationship to other types of ion traps (Reproduced from Ref. [185] with permission. © American Chemical Society, 2004)

more compact traps to be built. The smaller dimensions then result in shorter ion paths, and thus, shorter mean free paths (poorer vacuum) can easily be tolerated. In turn, this allows vacuum generation to be performed by a single stage.

The evolution of ion traps and subsequent combination of characteristics of two "parent lines" that led to the construction of a RIT has instructively been illustrated in a paper by Ouyang et al. (Fig. 4.60) [185].

### 4.6.10 Digital Waveform Quadrupole Ion Trap

In almost all QITs, the $m/z$ range is extended by lowering the RF drive frequency and/or by resonant ejection at a low $q$ value, e.g., Thermo Fisher Scientific QITs eject the ions at $q = 0.78$–$0.80$ rather than the classical $q = 0.908$. Alternatively to a scan of the drive voltage at constant RF, a frequency scan at constant voltage can be applied to realize scans over an extended $m/z$ range of up to about $m/z$ 20,000. This demands a waveform generator coupled with a power amplifier, which is associated with excessive power consumption and difficulties in obtaining a high voltage output without waveform distortion [171].

The concept of the *digital ion trap* (DIT) makes use of a digital waveform to trap the ions. In this context, the terms *digital ion trap* and *digital waveform* describe a waveform composed of simple rectangular pulses applied to the ring electrode [171, 187]. In practice, a switching circuit is used to generate a pulsed waveform by rapid alternation between discrete DC high-voltage levels ($\pm 250$ to $\pm 1000$ V).

The digital mode of pulse generation affords precise control of the timing. Furthermore, the AC excitation voltage connected across the end-cap electrodes can be delivered by the same digital circuitry. Interestingly, the ion motion under the influence of a digital waveform may still be expressed in terms of the conventional Mathieu parameters [171, 187, 188].

The development of the DIT has been pursued by Shimadzu and has reached a quite impressive level. Recently, an array of DITs, termed *ion trap array* (ITA), has been developed allowing multiple steps of isolation, activation, or scanning in parallel [189].

### 4.6.11 External Ion Sources for the Quadrupole Ion Trap

Chemical ionization (CI) mass spectra were first obtained by using the mass-selective instability mode of the QIT [166, 167, 190]. The reagent gas was admitted into the QIT, ionized and then allowed to react with the analyte.

With external ion sources it became feasible to interface any ionization method to the QIT mass analyzer [191]. However, commercial QITs are chiefly offered for two fields of applications: (*i*) GC-MS systems with EI and CI, because they are either inexpensive or capable of MS/MS to improve selectivity of the analysis (Chap. 14); and (*ii*) instruments equipped with atmospheric pressure ionization (API) methods (Chaps. 12 and 13) offering higher mass range, and some fivefold unit resolution to resolve isotopic patterns of multiply charged ions (Fig. 4.61) [161, 175, 192, 193].

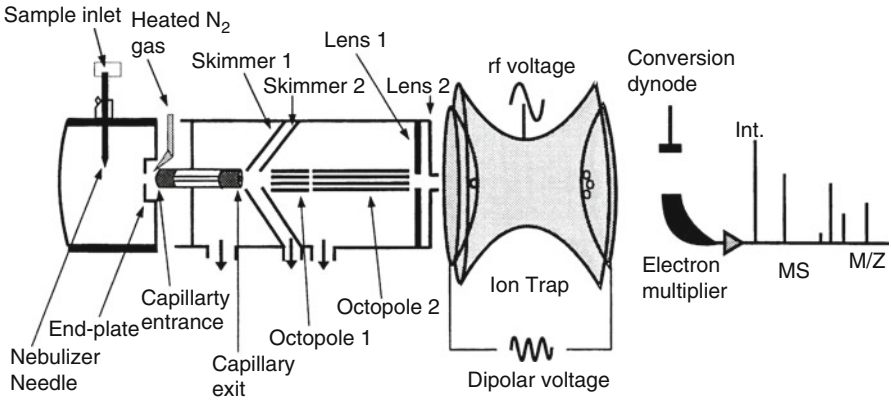


**Fig. 4.61** Layout of a quadrupole ion trap instrument equipped with an external ESI ion source. The analogy to the ESI-LIT configuration shown in Fig. 4.50 is striking (Reproduced from Ref. [193] by permission. © John Wiley & Sons, 2000)

### 4.6.12 Ion Trap Maintenance

The confined volume of quadrupole ion traps and their mode of operation causes a large fraction of the ions to hit the electrodes thereby leading to contamination of their surfaces. Quadrupoles and quadrupole ion traps thus require occasional cleaning, which means that the entire analyzer needs to be disassembled and reassembled afterwards. The photograph in Fig. 4.62a shows the analyzer of a


**Fig. 4.62** Analyzer maintenance of a QIT; here of the Finnigan LCQ. (**a**) Complete QIT analyzer mounted onto the top cover plate of the vacuum manifold, (**b**) after taking it apart for cleaning

Finnigan LCQ instrument after dismounting the entire unit from the instrument frame. Ions would enter from an ESI source on the right (not shown) and be passed across two stages of differential pumping by means of RF-only octopoles. Here, the second octopole also serves as a linear ion trap to dose ion packages into the QIT under AGC control. The polished electrode on the left below the exit endcap of the QIT is the entrance into the detector.

Figure 4.62b shows the analyzer components spread on a clean sheet of lint-free paper. After gentle cleaning with fine metal polish (only if there are permanent dark spots), water with detergent, distilled water, and finally solvent like methanol or isopropanol the parts are allowed to dry. Finally, the analyzer is reassembled, mounted into the vacuum manifold, and evacuated. About 1 h later, the QIT should be ready for performing the full tuning procedure to achieve restored performance.

**Stay grounded**
"Ion traps are also the only type of mass spectrometer that most users can disassemble and reassemble without sacrificing instrument performance." [185].

### 4.6.13 Summary of RF Quadrupole Devices

**Principle of Operation**
In an electric radiofrequency (RF) quadrupole field, ions are forced to oscillate in the open space between the four electrodes creating this field. Suitable frequency and amplitude provided, this motion can be stable in that the ions never hit one of the electrodes and never escape through the gaps in between. RF quadrupoles can be mass-selective as these conditions are only met for ions of a selected $m/z$ value or range of $m/z$ values. The $m/z$ range is adjusted by superimposition of an RF and a DC voltage. Mass-selective operation also requires that ions to be analyzed experience a sufficient number of oscillations or have sufficient dwell time within this field to eject ions outside the boundaries of stability due to their instable trajectories.

**Types of RF Quadrupole Devices**
Linear quadrupoles (Q) are operated as mass filters, while linear RF-only multipoles (q, h, o) are used as ion guides and collision cells. In both cases, a beam of ions is passed through the device so that the duration of interaction is determined by the velocity of the ions and the length of the RF device (Q, q, o, h).

Linear quadrupole ion traps (LIT) as well as quadrupole ion traps with three-dimensional quadrupole fields (QIT) are marked by storing ions inside. They are more flexible as they can either serve to accumulate ions to provide ion packages for other analyzer stages or be run to mass analyze a package of ions. During the

period of ion storage, ions can also be activated by collisions with residual gas inside the LIT or QIT. Fragment ions arising thereof can be stored and mass-analyzed as well (Chap. 9).

**General Characteristics**
As Q, LIT, and QIT are purely driven by RF and DC voltages, operational parameters can be changed at very high rates, typically >10,000 u $s^{-1}$. These analyzers are also very compact (neither requires a long flight tube nor for a heavy magnet), and thus, ideal for use in benchtop instruments. Q, LIT, and QIT are easy to handle and user-friendly. They are typically run at unit resolution but zoom scans to increase the resolving power across a narrow *m*/*z* window are sometimes enabled. None of these analyzers is adequate for accurate mass measurements.

**Use in MS Instrumentation**
Most manufacturers offer a variety of Q, LIT, and QIT instruments for use with the different kinds of ionization methods. The majority of stand-alone Q, LIT, and QIT instruments is used in routine gas chromatography (GC)- and liquid chromatography (LC)-mass spectrometry applications. Additionally, Q, LIT, and QIT devices are frequently incorporated into hybrid instruments to serve as the first of the two mass analyzers.

## 4.7 Fourier Transform Ion Cyclotron Resonance

### 4.7.1 From Ion Cyclotron Resonance to Mass Spectrometry

The development that led to modern *Fourier transform ion cyclotron resonance* (FT-ICR) mass spectrometers began in 1932 when E. O. Lawrence applied a transverse alternating electric field orthogonally to a magnetic field to build a particle accelerator [194, 195]. It was demonstrated that in *ion cyclotron resonance* (ICR) the angular frequency of the circular motion of ions is independent of the radius they are traveling on.

Later, this principle was applied to construct an ICR mass spectrometer [196, 197]. ICR mass spectrometers measuring the power absorption from the exciting oscillator were commercialized in the mid-1960s by Varian. Starting from their application to gas-phase ion chemistry [198], ICR instruments made their way into analytical mass spectrometry [199]. However, it was the introduction of FT-ICR in 1974 that initiated the major breakthrough [200, 201]. Ever since, the performance of FT-ICR instruments has steadily improved [202, 203] to reach unprecedented levels of resolving power and mass accuracy when superconducting magnets are employed [204–209]. The introduction of a dynamically harmonized ICR cell gave new thrust to the technique [210, 211]. Now, more than 40 years after FT-ICR-MS has been introduced [212], the technique can achieve resolving powers of up to $1.2 \times 10^7$ (12 million), and even a 21-Tesla superconducting magnet has

been constructed for FT-ICR-MS to obtain ultrahigh resolving power at high spectral acquisition rates and outstanding sensitivity [213].

FT-ICR analyzers are operated in a way that notably differs from what we have dealt with so far. FT-ICR-MS relies on nondestructive ion detection by registering image currents of circulating ions in the time domain. FT is applied to deliver frequency domain data that can then be converted into the intensity versus $m/z$ data format. This may appear to be quite complex – and in fact, it is. So let's approach this issue step by step – FT-ICR-MS is well worth the extra effort.

**Top-of-the line MS**

Todays FT-ICR mass spectrometers offer ultrahigh resolving power ($R = 10^5$ to $>10^6$) [214–217] and highest mass accuracy ($\Delta m = 10^{-4}$–$10^{-3}$ u, cf. Sects. 3.5 and 3.6) [208, 209], attomol detection limits (with nanoESI or MALDI sources), high mass range and $MS^n$ capabilities [218]. Modern FT-ICR instruments actually represent some sort of hybrids with linear quadrupole or LIT front ends.

### 4.7.2 Ion Cyclotron Motion – Basics

As we know from the discussion of magnetic sectors, an ion of velocity $v$ entering a uniform magnetic field $B$ perpendicular to its direction will, by action of the Lorentz force (Sect. 4.3.2), immediately move on a circular path. Contemplating the path in the direction of the magnetic field reveals that negative ions circulate clockwise while positive ions move counterclockwise (Figs. 4.19 and 4.63).

The radius $r_m$ of the ions' circular motion is determined by Eq. (4.13):

$$r_m = \frac{m_i v}{qB} \tag{4.13}$$

Upon substitution with $v = r_m\omega$ and rearrangement of the resulting term, *the cyclotron angular frequency* $\omega_c$ is obtained as:

$$\omega_c = \frac{qB}{m_i} \tag{4.33}$$

and by substituting with the cyclotron frequency ($f_c = \omega_c/2\pi$) Eq. (4.33) becomes

$$f_c = \frac{qB}{2\pi m_i} \tag{4.34}$$

One realizes that the cyclotron frequency is independent of the ions' initial velocity, but proportional to its charge and the magnetic field, and inversely proportional to its mass. Of any physical quantity, frequencies can be measured at

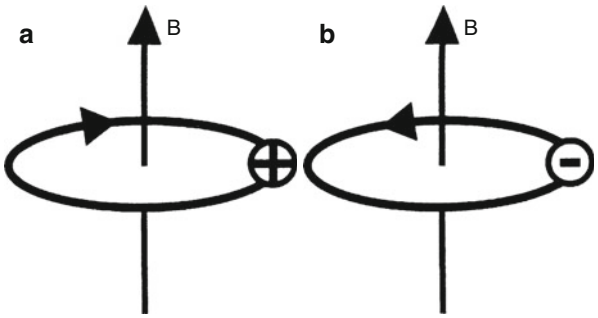


**Fig. 4.63** Circular motion of ions in a magnetic field. Viewing along the direction of the magnetic field one observes (**a**) a counterclockwise motion for positive ions and (**b**) a clockwise motion for negative ions (Adapted from Ref. [219] with permission. © Elsevier Science Publishers, 2002)

the highest accuracy, and thus, cyclotron frequency measurements appear as ideal premises for building powerful *m*/*z* analyzers.

### 4.7.3 Cyclotron Motion: Excitation and Detection

Gaseous ions are not at rest but at least move arbitrarily at their thermal velocities. When such a package of thermal ions is generated within a magnetic field or is injected into it, the resulting small ion cloud contains ions that are all spinning at their respective cyclotron frequencies (circular micromotion) while the cloud as a whole remains stationary provided it has been brought to a halt within the field boundaries. Therefore, the magnetic field not only acts in an *m*/*z*-sensitive way by imposing the cyclotron motion on the ions, but also provides ion trapping in a plane perpendicular to its field lines (*xy*-plane, cf. action of the quadrupolar field in a LIT).

Upon excitation, the circular micromotion is superimposed by the macroscopic cyclotron motion of the whole ion cloud, i.e., the RF excitation field preserves the coherence of ion packages composed of ions of the same *m*/*z* value. As the initial kinetic energy of the ions is small as compared to the energy uptake from the RF field, it is of minor importance for the experiment [220]. Nonetheless, the complexity of the overall motion affects frequency-to-mass calibration if accurate results are required [221].

In practice, mass-selective excitation, so-called *resonant excitation*, is achieved by applying a transverse electric field alternating at the cyclotron frequency $f_c$ ($\omega_c = 2\pi f_c$) to accelerate the ions. Such a field can be applied by a pair of RF electrodes placed on opposite sides of the orbit. As the ions accelerate, the radius of their orbit increases, and the resulting overall motion is a spiral (Fig. 4.64a) [195, 203]. For lighter ions, the spiral reaches the same radius with fewer cycles

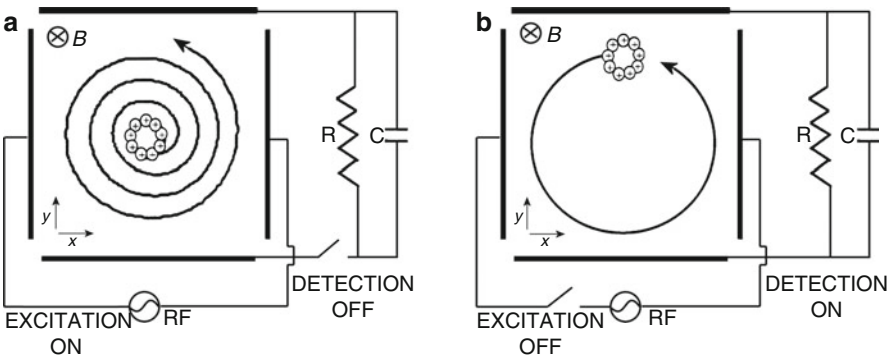


**Fig. 4.64** The sequence of (**a**) excitation (**b**) and image current detection in ICR-MS. The ionic micromotion is indicated by the small circle of ions. The cell is shown along the direction of the magnetic field. (**a**) Illustrates the spiral trajectory of the ion cloud as induced by excitation of the ions by an RF electric field oscillating at the cyclotron resonance frequency. Note that the radius is a function of ion velocity, but the frequency $f_c$ of circulation is not and that the radius remains constant during detection

than in case of heavier ones, i.e., the spiral is steeper, because low-mass ions need less energy than high-mass ions to accelerate to a certain velocity.

**Ion kinetic energy in ICR** Consider a singly charged ion of a mass of 100 u at thermal energy. Assuming a temperature of 300 K, its average velocity (Boltzmann distribution) is about 230 m $s^{-1}$. In a 3-T magnetic field it will circulate at $r_m \approx 0.08$ mm. To increase the radius to 1 cm, Eq. (4.13) demands the velocity to rise by a factor of 125, i.e., to 28,750 m $s^{-1}$. Rearranging Eq. (4.3) delivers $eU = v^2 m_i/2$, and thus, we calculate a kinetic energy of about 430 eV. Definitely, the translational energy of ions in an ICR cell is high enough to effect activating collisions (Fig. 4.65 and Chap. 9) [220].

**Omegatron** The so-called *omegatron* was an early ICR motion-based mass spectrometer. The ions in an omegatron are generated by electron ionization of a gaseous sample inside the cell (Fig. 4.66). The electric RF field causes ions fulfilling the resonance condition, i.e., those of $f_c = f_{RF}$, to accelerate and consequently to increase the radius of their orbit. The $m/z$ value is derived from the number of half cycles (proportional to ion kinetic energy) until the ions strike the electrometer plate at $r = r_{cell}$ [196, 197]. Thus, the omegatron essentially measures ion kinetic energy. To analyze a $m/z$ range either the RF frequency (adaptation of $f_{RF}$ to $f_c$) or the magnetic field (shifting of $f_c$ to $f_{RF}$) are varied. Omegatrons were small ($r_{cell} \approx 1$ cm) and mainly used as compact residual gas analyzers.

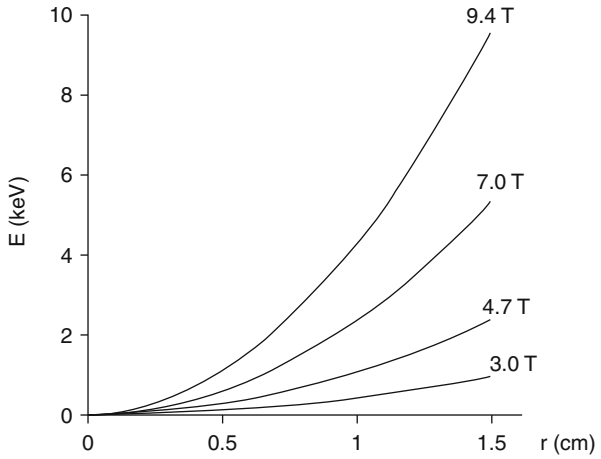


**Fig. 4.65** Kinetic energy of $m/z$ 100 ions in an ICR cell vs. orbital radius at magnetic field strengths from 3.0 to 9.4 T (Adapted from Ref. [220] with permission. © John Wiley and Sons, Inc., 1998)

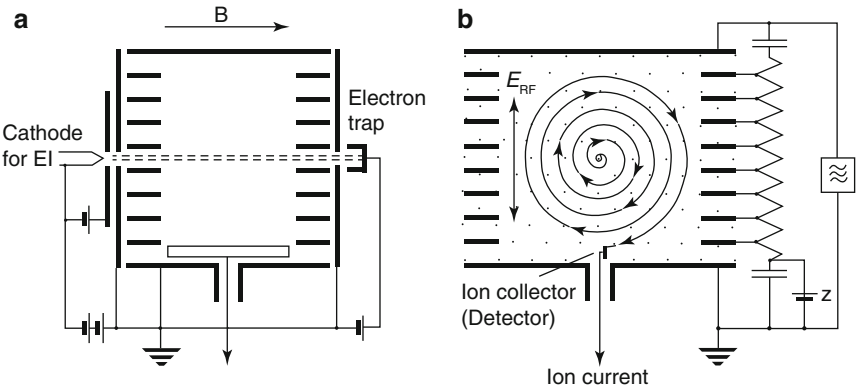


**Fig. 4.66** Omegatron. (**a**) View parallel to $B$ (*horizontal*) and parallel to the electron beam (*horizontal*) used to generate ions by EI inside the cell. The accelerating electric RF field acts vertical to $B$. (**b**) View on-axis to $B$ shows the spiral motion of accelerating ions until the radius of their orbit approaches that of the cell where the ions hit an ion collector for detection (Adapted from Ref. [91] with kind permission of Curt Brunnée)

**Mission half-accomplished**

The disadvantages of the omegatron for use as a mass analyzer are clear: (*i*) mass accuracy and resolving power are limited to $1/N_c$ ($N_c$ = number of half cycles); (*ii*) the electric signal for ion detection is solely due to neutralization

(continued)

of the ions, and there is no amplification as obtained with multiplier-type detectors used with all other analyzers; and (*iii*) the ions are removed from the cell upon detection precluding the use for MS/MS.

Moving from destructive detection by discharging the ions on the detection plates to nondestructive *image current detection* allows to switch from energy scanning to – indirect – cyclotron frequency measurement (Fig. 4.64b) [222, 223]. Image current detection relies on the fact that an ion cloud repeatedly attracts (positive ions) or repels (negative ions) the electrons of the detection electrodes upon its passage. The resulting minuscule image current can be amplified, transformed into a voltage signal and recorded as long as the ion motion exhibits sufficient coherence. In other words, a transient periodic signal is recorded in the time domain.

**Observing swarms in flight**
In ICR cells, the ions circulate like separate swarms of birds rather than like matter in the rings of Saturn. If ions of the same $m/z$ non-coherently circulated at the same frequency and radius, but occupied the total orbit rather than a small sector of it, there would be no image current induced upon their passage at the detector plates, i.e., coherence of the circulating ion motion is crucial.

### 4.7.4 Cyclotron Frequency Bandwidth and Energy-Time Uncertainty

The *frequency bandwidth* to be covered by an ICR instrument is governed by the $m/z$ range to be analyzed. Assuming a 9.4-T superconducting magnet, which currently represents the "upper-middle class", we may now use Eq. (4.34) to calculate $f_c$ for singly charged ions of $m/z$ 50 ($m_i = 8.30 \times 10^{-26}$ kg) as $f_c = (1.66 \times 10^{-19}\ \text{C} \times 9.4\ \text{T})/(2\pi \times 8.30 \times 10^{-26}\ \text{kg}) = 3.00$ MHz. For an ion of $m/z$ 500 ($8.30 \times 10^{-25}$ kg) we get a 10 times lower value, $f_c = 300$ kHz, and for an ion of $m/z$ 5000 ($8.30 \times 10^{-24}$ kg) we arrive at 30 kHz. To handle ions in the range $m/z$ 50–5000, the ICR frequency band has to span from 30 kHz to 3.0 MHz. In other words, an ICR instrument needs to cover a frequency range from several tens of kilohertz to a few megahertz (Fig. 4.67). The tremendous bandwidth has severe implications on both the mode of operation to achieve homogeneous excitation and detection and on the electronics to deliver the required level of performance over the entire range.

Following the above calculation, it takes a frequency resolution of 3 Hz (300 kHz/100,000) to achieve a resolving power of $R = 100{,}000$ at $m/z$ 500. The *energy-time uncertainty principle* states that $\Delta E \times \Delta t \approx h$. With $\Delta E = h\Delta v$ we

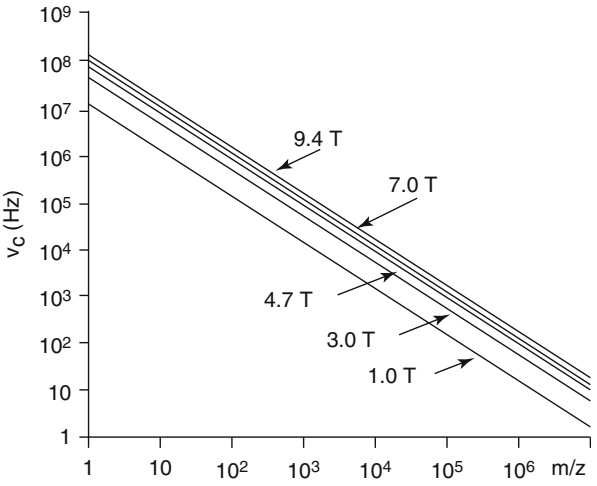


**Fig. 4.67** Plot of ICR frequencies vs. *m*/*z* for different magnetic field strengths from 1.0 to 9.4 T (Reproduced from Ref. [220] with permission. © John Wiley and Sons, Inc., 1998)

derive $h\Delta\nu \times \Delta t \approx h$ or $\Delta\nu \times \Delta t \approx 1$. Accordingly, the above frequency resolution of 3 Hz in 0.3 MHz corresponds to a measurement time of 0.33 s per data point of the scan range. Operation of an ICR instrument in *continuous wave mode*, i.e., scanning in the frequency domain, is obviously unrealistic as soon as high resolving power is to be achieved. Therefore, the only practical way to acquire high-resolution ICR spectra would be to realize a broad band detection of all frequencies in parallel.

Although discouraging for ion detection, the energy-time uncertainty principle opens up new perspectives for ion excitation. According to $\Delta\nu \times \Delta t \approx 1$, a rectangular pulse of 1 ms duration covers a frequency bandwidth of 1000 Hz; a pulse of even 1 μs should correspond to a bandwidth (frequency uncertainty) of 1 MHz, i.e., shorter pulses cover increasingly broader ranges. This has been employed in so-called *pulse excitation*.

**The "bell model"**
To understand pulse excitation, it is helpful to consider a mechanical comparison – a bell, for example, does not require excitation at its resonance frequency. Instead, a short strike with a hammer (pulse excitation) is fully sufficient. The bell takes up the energy with no specified frequency (all potential frequencies are contained) and automatically "finds" its own frequency plus its overtones to resonate and, thus, to sound.

According to the above considerations, the resolving power $R$ that can theoretically be achieved depends on the smallest $\Delta\nu$ that can be resolved, and thus, increases the longer $\Delta t$ used for acquiring the transient, $t_{acq}$. Further, it depends

on $m/z$ of the ion and the magnetic field $B$. A simple numerical-value equation may be used to calculate the theoretical maximum $R$ [220, 224]:

$$R = \frac{v}{\Delta v} = \frac{m}{\Delta m} = 1.274 \times 10^7 \frac{z B t_{\text{acq}}}{m} \tag{4.35}$$

For example, for an ion of $m/z$ 400, $B = 7$ T, and $t_{\text{acq}} = 1$ s, we obtain $R = 222{,}950 \approx 230{,}000$. A transient of 0.2 s would therefore reduce it to one fifth, $R = 46{,}000$, while recording the transient for 10 s could deliver $R = 2{,}300{,}000$.

**Resolving power's interdependence**
Obviously, the resolving power of any FT-ICR instrument can only be stated along with $m/z$ of the ion of interest, the magnetic field, and the acquisition interval of the transient. A high rate of spectral acquisition sacrifices resolving power, while a long transient can yield ultrahigh resolving power at the expense of speed and duty cycle.

### 4.7.5 Fourier Transform – Basic Properties

Some knowledge of the basic properties of the *Fourier transform* (FT) will be helpful prior to discussing FT-ICR instrumentation [225]. The Fourier transform is a mathematical operation that transforms one complex-valued function of a real variable into another. The domain of the original function is typically time (as is here) and accordingly is termed the *time domain*. The domain of the function generated upon FT is frequency. The product of FT then is the *frequency domain* representation of the original function. The frequency domain function describes which frequencies are contained in the original function. For example, FT applied to a chord of music comprising several fundamental frequencies (and overtones) as represented by the notes would deliver all contributing frequencies and their amplitudes. The Fourier transform makes the move from a wave and its amplitude to its frequency and its amplitude (Fig. 4.68a, b).

FT of a transient signal, i.e., a signal vanishing to zero amplitude at the end of the observation time span, delivers a Lorentzian curve in the frequency domain (Fig. 4.68c, d). In accordance with the energy-time uncertainty principle, the frequency domain output becomes increasingly sharper the longer the observation time span, because the frequency is more accurately determined the more cycles are recorded in the transient.

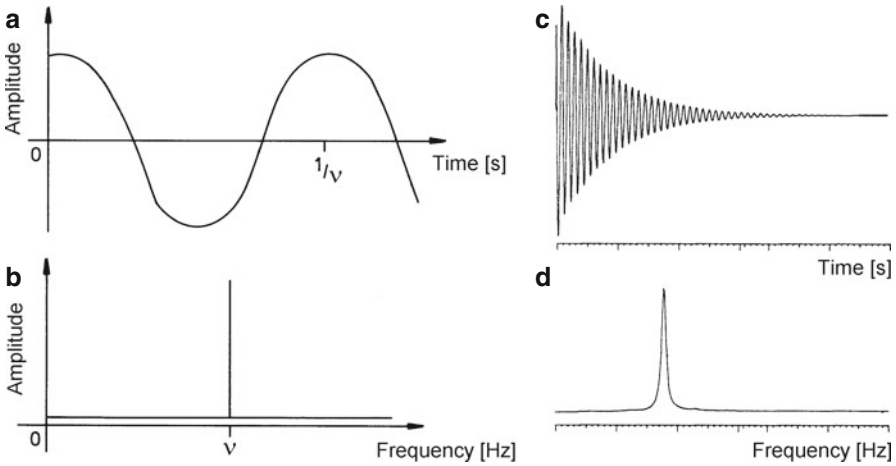


**Fig. 4.68** Illustration of the principle of FT. (**a**) A time domain wave, infinite in time, is transformed by FT to (**b**) reveal its frequency. The amplitude is conserved. (**c**) FT of a transient time domain signal into (**d**) a frequency domain signal of Lorentzian shape. FT works equally well if an extremely large number of frequencies and amplitudes is contained in the time domain signal

**Jean-Baptiste Joseph Fourier**
Fourier was a French mathematician (1768–1830). Besides Fourier transformation, his influential work concerns the mathematical description of the conduction of heat in solids and the development of infinite series (Fourier series). He witnessed the French revolution and accompanied Napoleon on his expedition to Egypt.

In FT-ICR experiments, the observation time span is normally shorter than the time required to damp down the transient to zero. Instead, the detection is abruptly ended when the preset transient length is reached. The duration of the transient is generally determined by the product of the number of data points that is to be recorded and the rate at which those data points are being sampled. The minimum *sampling rate* is in turn determined by the highest cyclotron frequency to be observed. Typical values in FT-ICR-MS are 0.5–2 s transients of 512 k to 2 M ($2 \times 10^6$) data points at 250 kHz to 1 MHz sampling frequency. Thus, the arbitrary truncation of the transient causes the transient to represent a combination of a step function and a perfectly dampened signal (Fig. 4.69). As FT yields sinc ($x$) from a step function, the FT output from a truncated signal is a Lorentzian main peak accompanied by side bands, so-called *wiggles*.

To reduce the side band-creating effect of truncation, the transient is normally subjected to *apodization* prior to FT. Apodization means the multiplication of the signal by a mathematical function that causes the values to smooth out to zero.

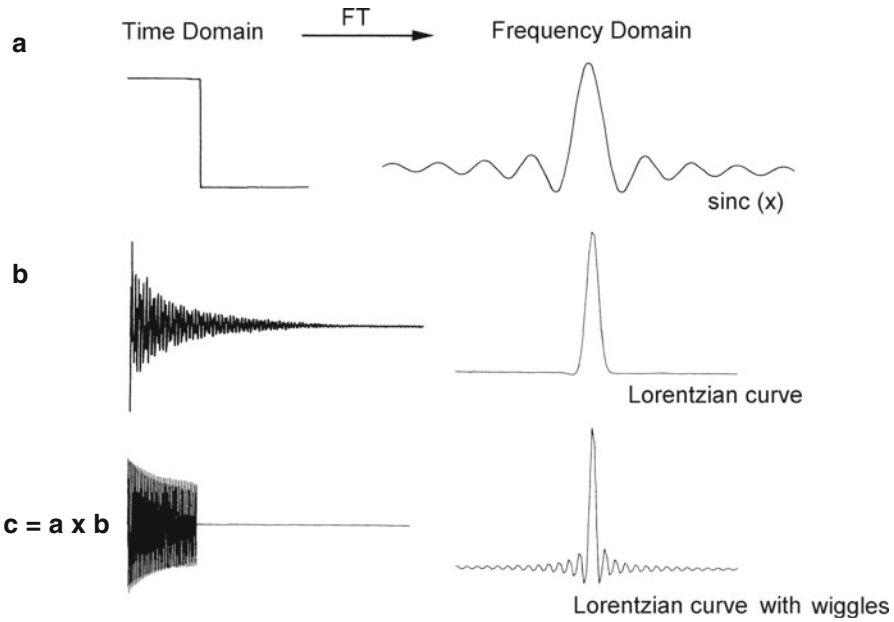


**Fig. 4.69** The effects of Fourier transforms on different input signals. (**a**) A step function is converted to sinc ($x$), (**b**) a fully dampened transient signal containing only one frequency yields a single Lorentzian curve, and (**c**) the truncated transient can be regarded as a combination of (**a**) and (**b**) and yields a Lorentzian curve accompanied by "wiggles"

Some sophisticated apodization methods are in use to deliver the ultimate resolution, nonetheless, simple sin ($x$) or $\sin^2$ ($x$) functions work well.

Another feature of FT is to yield better resolved frequency spectra from larger data sets, which not necessarily need to contain real data. Simply adding a row of zeros to the end of the experimental transient is beneficial in that it smoothes the peak shape by increasing the number of data points per $m/z$ interval. This "trick" is known as *zero-filling*. The number of attached zeros normally equals the number of data points, sometimes even twice as many are filled in (*double zero-filling*).

### 4.7.6 Nyquist Criterion

The actual shape of a peak not only depends on the capabilities of the mass analyzer in use but is also determined by the sampling rate applied to collect the signal (Sects. 4.12 and 11.5). The sampling rate is even more relevant for periodic signals such as from the cyclotron motion in FT-ICR. The minimum sampling rate needed to correctly detect any periodic signal is governed by the *Nyquist criterion*, according to which the sampling rate, $\nu_{\text{samp}}$, must have at least twice the frequency of the process, $\nu_{\text{proc}}$, that is to be recorded

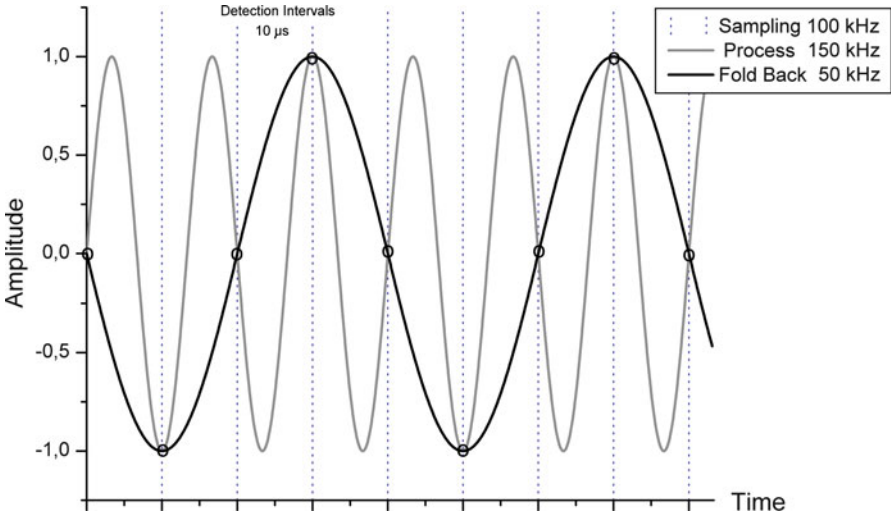


**Fig. 4.70** The aliasing phenomenon. Detection points are where the *dotted* verticals cross the *light gray* signal curve (**o**). The process (150 kHz) occurs at $v_{proc} = 1.5 \times v_{samp}$ (100 kHz or 10 µs per point) instead of $\leq 0.5\ v_{samp}$. This causes the output of an aliased signal at $v_{fold} = 50$ kHz as determined by Eq. (4.37) (*dark curve*). In this special case setting $n = 1$ just delivers $v_{fold} = v_{nyq}$

$$v_{samp} \geq 2 \times v_{proc} \tag{4.36}$$

Vice versa, the Nyquist limit frequency, $v_{nyq}$, up to which a process can just be correctly detected is given as

$$v_{nyq} = v_{samp}/2 \tag{4.37}$$

*aliasing* (or *folding back*) occurs beyond the Nyquist limit. Then, the detected signal pretends the process to proceed at a foldback frequency, $v_{fold}$, described by

$$v_{fold} = \left| n \times v_{samp} - v_{proc} \right| \tag{4.38}$$

where the factor $n$ is an integer selected as to fulfill the condition $0 < v_{fold} \leq v_{nyq}$ An illustration of the folding back phenomenon is given in Fig. 4.70.

### 4.7.7 Excitation Modes in FT-ICR-MS

In the ICR cell, there is a stringent correlation of cyclotron frequency $f_c$ and $m/z$ value. For simplicity, the very first FT-ICR experiment was therefore performed with an excitation pulse of a fixed $f_c$ tailored to fit the model analyte, methane molecular ion [200]. However, useful measurements require the simultaneous excitation of all ions in the cell, and this in turn demands for a large RF bandwidth.

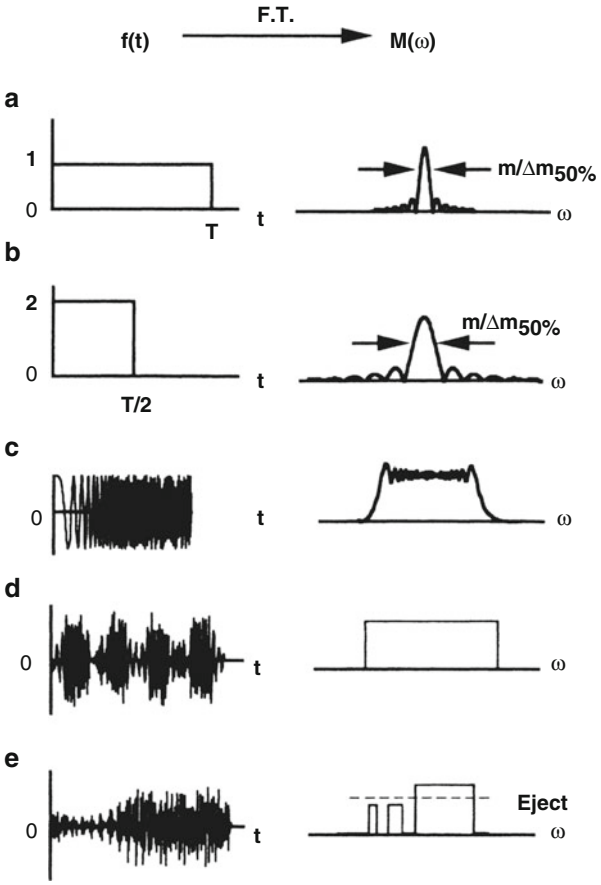


**Fig. 4.71** Time-domain (*left*) and frequency-domain (*right*) excitation waveforms: (**a**, **b**) rectangular pulses yield inhomogeneous and rather narrow excitation windows; (**c**) "chirp" excitation; (**d**, **e**) SWIFT excitations, with (**e**) designed to eject a certain mass range from the cell (Reproduced from Ref. [220] by permission. © John Wiley & Sons, 1998)

Several excitation methods have been developed to cope with this technically nontrivial task. The differences between these methods can easily be judged from the shape of the frequency-domain excitation waveforms (Fig. 4.71) [203, 220]. The simplest approach is to irradiate a single frequency (resonant excitation) for some time, i.e., as a *rectangular pulse*, but this selectively excites ions of a single mass [200]. Applying such a narrow band excitation as a short pulse yields some expansion of the range. The effect of a *frequency sweep* or *"chirp" excitation* is much better [201]. Chirp excitation sequentially affects ions across the *m*/*z* range although it never delivers a defined frequency. Instead, the chirp exploits the wide band character of rushing across the frequencies. Chirp excitation is not perfectly homogeneous as it gives some distortions close to the borders of the range, nonetheless is it successfully employed in commercial FT-ICR instruments.

The best results are to be expected from *stored waveform inverse Fourier transform* (SWIFT) excitation [226]. First, the ideal excitation waveform is tailored to the needs of the intended experiment and then produced by an RF generator. SWIFT excitation also allows to remove ions of predefined *m*/*z* ranges from the ICR

cell. This results in storage of a small $m/z$ range, or after repeated SWIFT pulsing of a single nominal mass out of a broad band spectrum. Those ions are then accessible for ultrahigh resolution measurements or as precursors for tandem MS.

### 4.7.8 Axial Trapping

Our basic considerations of ICR (Sect. 4.7.3 and Fig. 4.64) were so far restricted to the $xy$-plane of a cell. Two of the four side walls ($x$-axis) of the ICR cell are connected to the RF power supply during the period of excitation. Then, the image current induced in the detector plates ($y$-axis) is recorded as transient signal for some period of time (0.5–30 s). The excitation of the ions within the ICR cell has to stop at a level low enough to avoid wall collisions of the lightest ions to be measured [206, 219, 220].

At a first glance, the $z$-dimension of the cell seems to be of no importance for the function of an FT-ICR mass spectrometer. However, the $z$-component of thermal energy and the kinetic energy of ion injection into the ICR cell in case of an external ion source both would lead to rapid loss of the $xy$-trapped ions along that axis, because they would pass through the cell along the $z$-axis on a helical trajectory. It is therefore important to establish a trapping potential in $z$-direction. The simplest way is to place DC trapping electrodes at the open ends [197]. Furthermore, our initial treatment of the ICR cell was also done with the implicit understanding that this would be a cubic cell.

### 4.7.9 Magnetron Motion and Reduced Cyclotron Frequency

Trapping of ions in a potential well implies reflection of ions between the trapping plates that induces an oscillatory motion along the $z$-axis the frequency $\omega_z$ of which is given by

$$\omega_z = \sqrt{\frac{2qV_{\text{trap}}\alpha}{ma^2}} \tag{4.39}$$

where $a$ is the physical $z$-dimension of the trap and $\alpha$ represents a shape parameter that depends on the trap design [220]. The curved electric field close to the borders also produces an outward-bound radial force $F_\text{r} = qE_{(\text{r})}$ opposed to the action of the Lorentz force $F_\text{L}$ that is given by

$$F_r = qE_{(r)} = \frac{qV_{\text{trap}}\alpha}{a^2} r \tag{4.40}$$

The magnetic field now acts by transforming the radial force component into another circular motion of the trapped ions. The total force on an ion then is

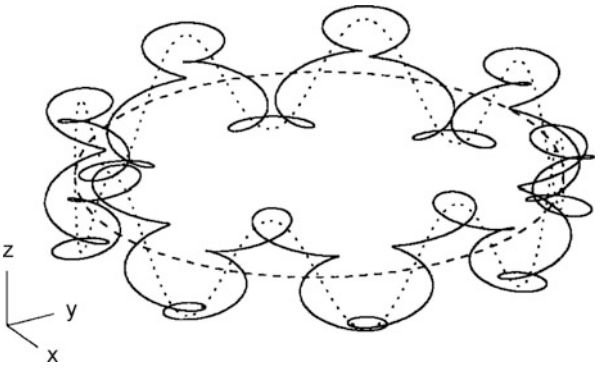


**Fig. 4.72** Ion motion for $\omega_+ = 4\omega_z$ and $\omega_z = 8\omega_-$ in an ICR cell. Pure magnetron motion (*dashed*), magnetron plus trapping motion (*dotted*), and the resulting overall motion (*solid*) (Reproduced from Ref. [227] by permission. © Elsevier Science Publishers, 1995)

$$F_{\text{tot}} = F_L - F_r = m_i\omega^2 r = qB\omega r - \frac{qV_{\text{trap}}\alpha}{a^2}r \tag{4.41}$$

which can be rewritten to reveal its character of a quadratic equation in ω

$$\omega^2 - \frac{qB\omega}{m_i} + \frac{qV_{trap}\alpha}{a^2} = 0 \tag{4.42}$$

This quadratic equation has two solutions, the first of them representing the *reduced cyclotron frequency* $\omega_+$

$$\omega_+ = \frac{\omega_c}{2} + \sqrt{\left(\frac{\omega_c}{2}\right)^2 - \frac{{\omega_z}^2}{2}} \tag{4.43}$$

and the second the *magnetron frequency* $\omega_-$

$$\omega_- = \frac{\omega_c}{2} - \sqrt{\left(\frac{\omega_c}{2}\right)^2 - \frac{{\omega_z}^2}{2}} \tag{4.44}$$

where $\omega_z$ is obtained from Eq. (4.39) and $\omega_c$ from Eq. (4.33). The obvious consequence for the ionic motion in an ICR cell is that the simple description of $\omega_c$ by Eq. (4.33) only yields the so-called *unperturbed cyclotron frequency*, whereas the real motion is by far more complex. Figure 4.72 shows the overall motion of ions in an ICR cell taking $\omega_z$, $\omega_+$ and $\omega_-$ into account [227]. It should be noted that the radius of the magnetron motion is generally larger than that of the cyclotron motion. In many cases the magnetron motion also causes a small side peak in the vicinity of the main peak.

### 4.7.10 Detection and Accuracy in FT-ICR-MS

An FT-ICR experiment requires full temporal separation of excitation and subsequent detection of the trapped ions. Detection is based on the measurement

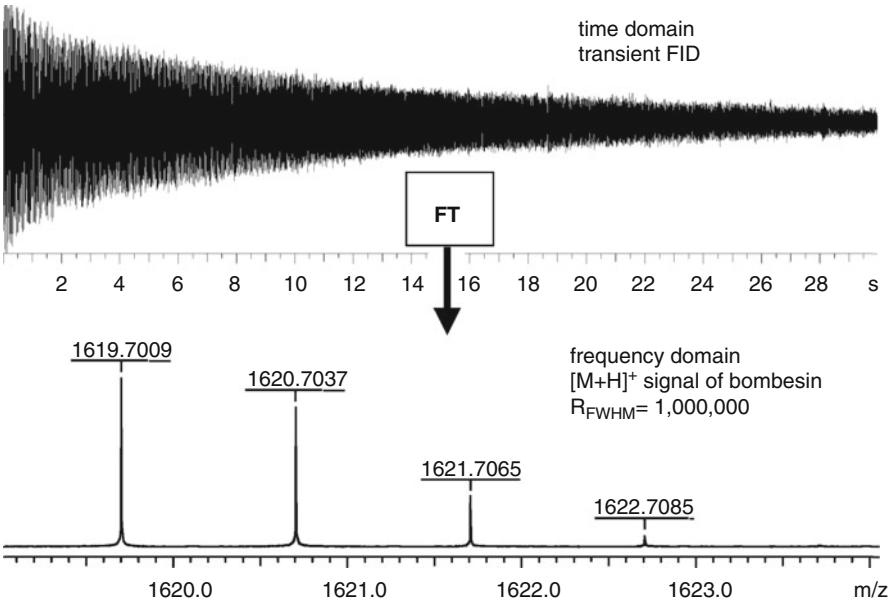


**Fig. 4.73** The principle of FT-ICR-MS. In detail, the procedure includes recording the transient, apodization of the transient, zero-filling, FT, and finally the calculation of *m*/*z* values from the cyclotron frequencies. The longer the detection interval the higher the attainable resolving power. This example shows the $[M + H]^+$ ion of the peptide bombesin, *m*/*z* 1619.7009, where a 30 s transient resulted in a spectrum at $R = 10^6$ (By courtesy of Bruker Daltonik, Bremen)

of image currents in the detector plates. An image current is induced by each ion package when repeatedly passing the detector plates at its individual cyclotron frequency, i.e., detection in FT-ICR means "listening to the circulating ions". The transient signal or *free induction decay* (FID) is recorded, and afterwards, the FID is converted from the *time domain* to the *frequency domain* by means of Fourier transformation. This means that the complex FID caused by superimposition of many single frequencies is deconvoluted to reveal the single contributing frequencies and their respective amplitudes. Using Eq. (4.34), the frequencies are converted to *m*/*z* values; their amplitudes now representing the abundances of the corresponding ions (Fig. 4.73) [195, 200, 203, 228, 229].

There is a correlation between the transient signal and the pressure in the ICR cell [220, 228]. In perfect vacuum, the orbiting motion would solely be dampened by induction, whereas in the presence of residual gas collisions will finally slow down the ions to thermal energy. As the resolving power in FT-ICR-MS is also proportional to the acquisition time of the transient signal, ultrahigh vacuum in the range of $\approx 10^{-10}$ mbar is a prerequisite in the ICR cell. Based on a 7-T magnet and Eq. (4.35), the theoretical resolution for the example in Fig. 4.73 is $R \approx 1.6 \times 10^6$, which shows the influence of residual gas and other factors causing loss of coherence on actual resolving power.

**Ultrahigh vacuum required**
The need for extremely long mean free paths in FT-ICR mass spectrometers arises from the combination of high ion velocities of several $10^3$ m $s^{-1}$ and observation intervals in the order of seconds. Coherent swarms of ions thus need to travel hundreds of meters during the detection interval. Collisions would be detrimental for peak shape. The typical ICR cell pressure therefore is $10^{-10}$ to $10^{-9}$ mbar.

The detection efficiency is greatly improved for cylindrical cells as compared to cubic cells, because the ions pass the detection electrodes at almost constant distance to their surface. This results in stronger image currents due to on the average closer passages and sharper detection wave forms as their entering and exiting from the detection zone causes more sudden changes.

The ICR voltage signal strength at the detector plates is inversely proportional to ion mass if the monitoring circuit is predominantly resistive, and is independent of ion mass if the circuit is predominantly capacitive [229]. Image current detection at room temperature is typically less sensitive than ion counting techniques in beam instruments. Nonetheless, for modern FT-ICR instruments the detection limit to yield a signal-to-noise ratio of 3:1 corresponds to roughly 200 ions, provided these are excited to travel at half of the maximum cyclotron radius [211, 219].

The advantages of FT-ICR detection over ICR are obvious:

- The $1/N_c$ limit vanishes because every ion undergoes some $10^4$–$10^8$ cycles during the detection interval.
- Sensitivity improves because the ions give rise to a detectable image charge during each passage of a detector plate.
- Ion detection is nondestructive, i.e., ions are not lost upon detection (this enabling MS/MS experiments).
- Elongated recording of the FID provides for extremely precise determination of all cyclotron frequencies, thereby yielding the highest values of resolution and mass accuracy available [214, 215, 230].

External calibration is most effective when the level of excitation and the number of trapped ions of calibrant ions closely approaches that of the analyte ions [219]. The latest FT-ICR instruments can routinely attain mass accuracies of better than 1 ppm. Internal calibration can yield further improvement.

Although resolution and mass accuracy are already high in broadband spectra ($R = 3 \times 10^4$–$10^5$, $\Delta m < 10^{-3}$ u), the performance of FT-ICR instruments further improves by storing only narrow $m/z$ ranges, because fewer ions in the cell mean less distortion by coulombic interactions.

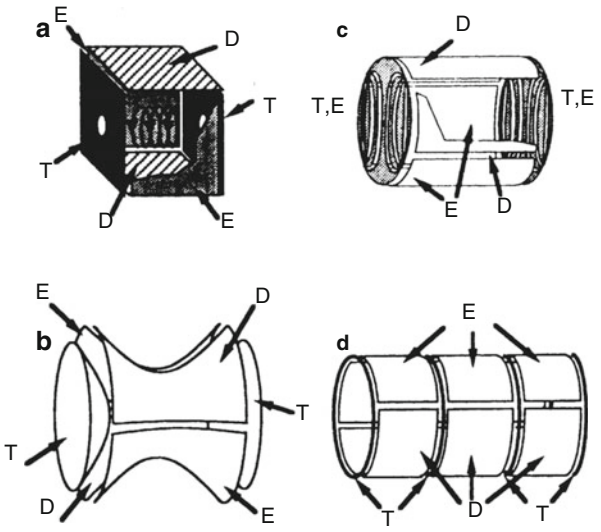


**Fig. 4.74** Important ICR cell types; electrodes are labeled with *E* excitation, *D* detection, *T* trapping; (**a**) classic cubic cell, (**b**) Penning cell with hyperbolic electrodes, (**c**) infinity Cell™ with segmented trapping plates, and (**d**) triple cell. The latter two aim at virtually expanding the potentials in the trapping zone along the *z*-axis (Adapted from Ref. [232] with permission. © Elsevier Science Publishers, 1995)

### 4.7.11 Design of ICR Cells

We have seen that ion motion and detection in FT-ICR are affected by various parameters. Axial trapping oscillation, resulting magnetron motion, and disturbances leading to loss of coherence – or dephasing – strongly depend on the geometry of the ICR cell and on the homogeneity of the magnetic field. The simple cubic cell (the ICR cell of the pioneers) severely suffers from field imperfections. Therefore, numerous other designs have been developed offering remarkable improvements over the cubic cell (Fig. 4.74) [219, 220].

A nearly ideal hyperbolic field is created inside a hyperbolic trap, also known as *Penning trap* or *Penning cell* (Fig. 4.74b). However, this shape requires a small inner volume for the ions to circulate and the performance soon suffers from space charge effects as the number of ions increases. While capable of extremely high performance with 10–1000 ions, Penning cells are not suited for analytical work where a cell has to accommodate large ion populations to offer a high dynamic range and to deal with complex mixtures.

As in the case of segmented LITs with radial ejection (Sect. 4.5.3 and Figs. 4.48 and 4.49), the distortion of the electric field can be avoided when the trapping sections are properly designed and operated; then the ICR cell displays itself to the ions as being of virtually infinite length. Thus, triple-segmented cylindrical cells [231] and many others have been developed [232]. Another approach, the *infinity cell* makes use of segmented end caps on a cylindrical cell (Fig. 4.74c) [233].

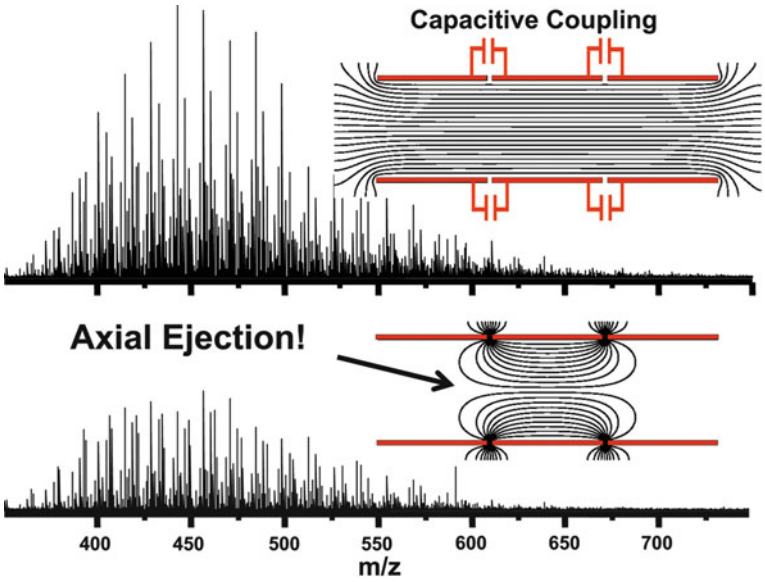


**Fig. 4.75** Comparison of a cylindrical cell having both capacitively-coupled (*top*) and noncoupled trapping electrodes (*bottom*) to the resulting spectra of a complex sample. The curvature of the RF excitation isopotentials for the single electrode pair (*bottom*) produces axial RF excitation leading to *m*/*z*-dependent axial ejection. Capacitive coupling of the RF excitation to the end cap electrodes effectively eliminates axial ejection and yields an improved spectrum. (Reproduced with permission from Ref. [212]. © Elsevier Science Publishers, 2015)

The advantageous effect of capacitive coupling of trapping segments in a triple-segmented cylindrical cell are shown in Fig. 4.75. The figure not only depicts the field flattening effect of the capacitive coupling but also shows its correlation to the enhancement of FT-ICR spectra due to this design [212]. ICR cells of this type are used in the Thermo Scientific LTQ-FT Ultra series.

A recently designed cell by E. Nikoleav extends the region of harmonic potential to almost its full volume. This is achieved by subdivision of the walls of a long cylindrical cell (150 × 56 mm) into alternating convexly and concavely shaped segments [210, 224, 234]. The convex segments stay grounded while the trapping potential is applied to the concave parts. The trapping plates are slightly spherical in shape. Overall, this causes ions to experience an on-average harmonic potential per full cycle of cyclotron motion (Fig. 4.76). This fact gives rise to its description as a *dynamically harmonized ICR cell*. For excitation and detection the cylinder is classically divided into four sections of 90° with the dividing cuts slicing every second convex electrode into halves. This design provides a major boost in

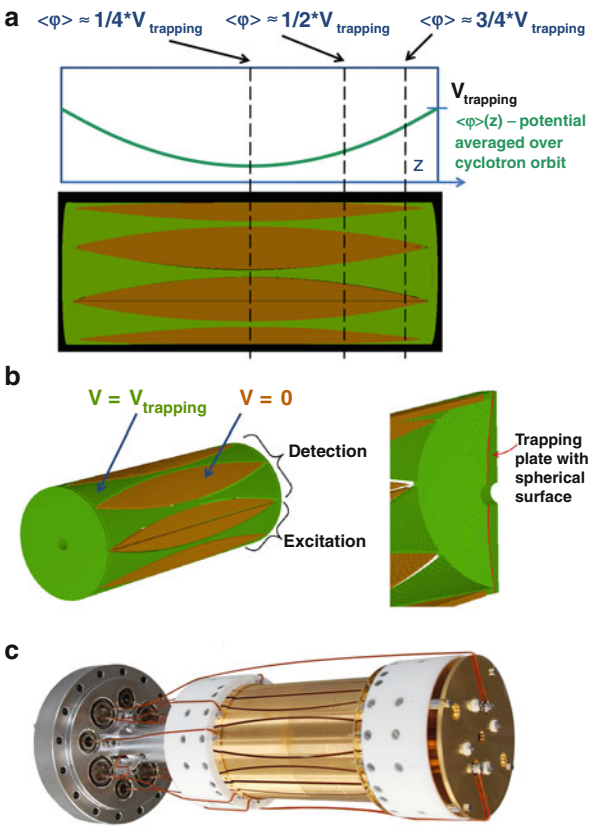


**Fig. 4.76** Dynamically harmonized ICR cell. (**a**) Axial cross section showing the segmented cell walls and the hyperbolic trapping potential experienced by ions on average per full cycle. (**b**) Division into four 90° sections to accomplish excitation and detection plus detail of a trapping plate. (**c**) Photograph of the Paracell; gold plating is used to minimize electrode oxidation. (Figure compiled from material by courtesy of Bruker Daltonik, Bremen)

resolving power whilst maintaining high ion capacity and dynamic range [216, 217, 235]. It is commercialized as Paracell by Bruker Daltonik.

### 4.7.12 FT-ICR Instruments

Ion traps, ICR cells as well as QITs, are best operated with the number of trapped ions close to their respective optimum, because otherwise ion trajectories are distorted by coulombic repulsion. Hence, external ion sources in combination with ion transfer optics capable of controlling the number of injected ions are ideally attached to ion traps. Currently, MALDI [236] and even more so ESI [207, 214, 215, 230, 237] and other atmospheric pressure ionization sources predominate in FT-ICR.

The ion current is not solely regulated by the source but by some device to collect and store the desired amount of ions until the package is ready for injection

into the ICR cell. Linear RF-multipole ion traps are normally employed for that purpose (Sect. 4.5.1) [119, 238, 239], but other systems are also in use [218]. RF-only multipoles are commonly used to transfer the ions through the boundaries of the magnetic field into the ICR cell (Sect. 4.4.4) [238]. For their injection, it is important to adjust the conditions so that the ions have low kinetic energy in $z$-direction in order not to overcome the shallow trapping potential. While some buffer gas is beneficial in case of LITs and QITs, ICR cells are operated at the lowest achievable pressure. The typical path from an external ion source into the ICR cell is therefore characterized by multistep differential pumping to achieve some $10^{-8}$–$10^{-7}$ Pa inside the ICR cell.

FT-ICR instruments are always equipped with superconducting magnets usually having 7 T and 9.4 T field strength; while 12 T and 15 T is also occasionally available. The advantages of increased field strengths are numerous: resolving power and scan speed, for example, increase linearly with $B$. Moreover, upper mass limit, ion trapping time, ion energy, and number of trapped ions even increase with $B^2$.

At the time of writing, FT-ICR instruments as considered here are provided by just two manufacturers: (*i*) the Qh-FT-ICR type as by the Bruker Solarix series (Fig. 4.77) and LIT-FT-ICR hybrid instruments as by the Thermo Scientific LTQ FT Ultra series (Sect. 4.8 and Fig. 4.86).

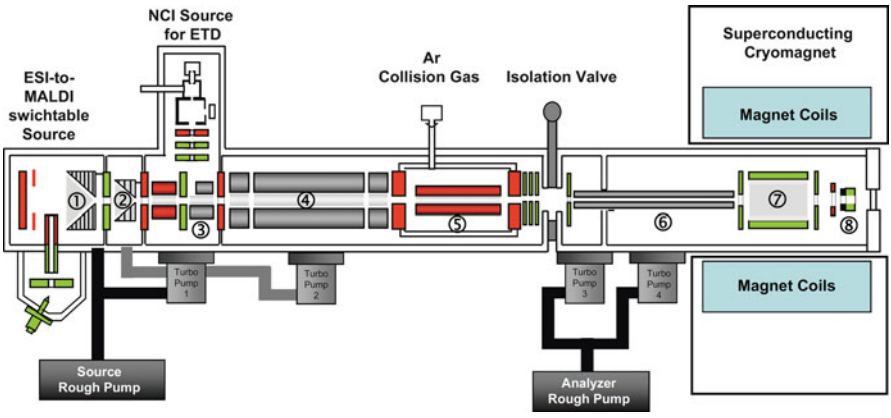


**Fig. 4.77** A hQh-ICR hybrid instrument. This instrument is equipped with an ESI-to-MALDI switchable ion source that makes use of a two-stage ion funnel (①, ②) to focus ions into a RF hexapole ion guide (h, ③). The ions then pass a quadrupole (④) that may either be run as band pass (q) or as mass-selective device (Q) and then reach a multifunctional RF hexapole ion trap (h, ⑤) where they can be (*i*) accumulated, (*ii*) collisionally activated, or (*iii*) reacted with radical anions from the NCI source to effect ETD as required. For mass analysis the ions are then guided via an RF-only hexapole (⑥) into the ICR cell (⑦) where a hollow cathode (⑧) is attached for ECD. RF-only hexapole (⑥) and magnet are not to scale but shown relatively much smaller (Schematic of Bruker Solarix instrument series by courtesy of Bruker Daltonik, Bremen)

### 4.7.13 Summary of FT-ICR Instrumentation

**Principle of Operation**
Ions moving on a plane orthogonal to the direction of a magnetic field are forced on circular orbits by action of the Lorentz force. The radius of their orbit depends on ion kinetic energy, while the frequency of oscillation – the so-called cyclotron frequency – depends on the mass of the ions. To induce this mass-dependent ion motion, ions that are transferred into a magnetic field need to be excited by an RF electric field of a frequency equaling that of their cyclotron frequency. Once excited, ions of equal $m/z$ coherently circulate inside the ICR cell. Upon their passage, the ion swarms induce image currents in the detection plates making up about half of the inner wall surface of the ICR cell. The image currents are recorded in the time domain (for 0.2–20 s), transformed into frequency domain by means of Fourier transformation (FT), and finally used to calculate the corresponding $m/z$ values.

**Performance Characteristics**
FT-ICR instruments are the best-performing mass spectrometers in terms of resolving power ($10^5$ to $>10^6$) and mass accuracy (typically 0.1–2 ppm). The level that is achieved depends on the actual instrument, the duration of the transient, and numerous other parameters. Due to the long detection interval and the use of image current detection, FT-ICR-MS offers comparatively low sensitivity. This is counterbalanced by the fact that modern instruments can accommodate different ionization techniques, offer a variety of tandem-MS capabilities, and may even serve for sophisticated experiments in gas-phase ion chemistry. The extraordinary resolving power and mass accuracy enable the analysis of complex mixtures like crude oil or dissolved organic matter. Tandem-MS may serve to solve complex problems in protein analysis.

**General Considerations**
Mostly due to the prerequisite of using high-field superconducting magnets and the need for ultrahigh vacuum, FT-ICR instruments are large, heavy, and expensive in terms of both investment and cost of operation. While it may be challenging to exploit an instrument's full potential, modern FT-ICR instruments are nonetheless suitable for routine use. In fact, there are problems that can only be solved by FT-ICR-MS.

**FT-MS**
Occasionally, FT-ICR-MS is referred to as FT-MS or even FTMS. Apparently, FT-MS is most frequently used by mass spectrometrists who have dealt with FT-ICR-MS since the early days of the technique. Of course, ICR-MS without Fourier transformation would never have become as successful, but Fourier transformation alone cannot separate ions according to $m/z$. With the advent of the Orbitrap analyzer (Sect. 4.8), there is a second system making use of Fourier transformation of a time domain signal, although the prefix FT finds no mention in that name.

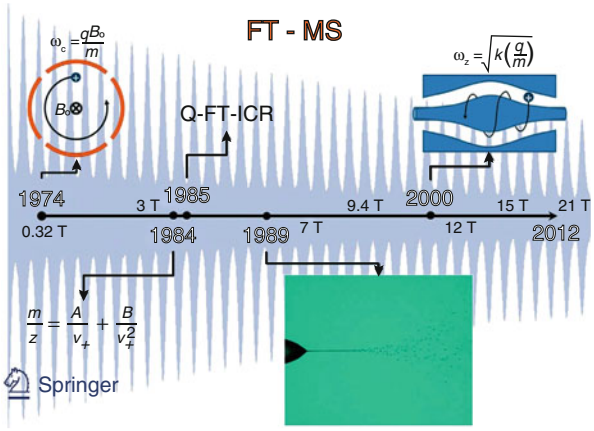


**Fig. 4.78** FT-MS timeline as displayed on the journal cover of an issue dedicated to HR-MS. The journey starts with the introduction of FT-ICR and proceeds via *m*/*z* calibration, introduction of RF quadrupole transfer optics, external ESI source, and the first papers dealing with Orbitrap development. The magnetic fields available for FT-ICR-MS are also included (Adapted from *Analytical and Bioanalytical Chemistry* **403(5)** 2012 with permission. © Springer-Verlag, Heidelberg, 2012)

The acronym FT-MS is hence proposed as a collective term summarizing all FT-based MS techniques, i.e., FT-ICR-MS *and* Orbitrap-MS. Figure 4.78 taken from a journal cover of a special issue dedicated to HR-MS presents a welcome transition from FT-ICR to Orbitraps and also presents a compact timeline of developments.

## 4.8 Orbitrap Analyzer

The Orbitrap analyzer incorporates a concept of *m*/*z* analysis of its own [20, 240]. Commercialized by Thermo Fisher Scientific in 2005, the Orbitrap™ delivers high resolving power and accurate mass measurement at a level rivaling FT-ICR to a certain extent [20, 241–245]. It is the special charm of the Orbitrap to operate without a magnetic field, and therefore, to be available at a lower price and having fewer installation room requirements than FT-ICR instruments. Nonetheless, it has one important feature in common with FT-ICR: the Orbitrap also employs image current detection of ion oscillations and Fourier transformation for the conversion of the transient into the frequency domain. As we already have dealt with the very basics of FT in the context of FT-ICR-MS we may now concentrate on design and operation of the Orbitrap analyzer itself.

**Orbiting in an electrostatic field**
The Orbitrap is also an ion trap, but there is neither a magnet to hold ions inside nor is there any sort of RF excitation to initiate their motion. Instead, moving ions are trapped in a constant radial electrostatic field. The electrostatic attraction towards the central electrode is compensated by a centrifugal force that arises from the initial tangential velocity of ions: very much like a satellite in orbit [241].

### 4.8.1 Orbitrap – Principle of Operation

In 1923, Kingdon constructed an ion trapping device based on a straight wire along the axis of a surrounding cylindrical electrode having flanges that enclosed the trapping volume. Ions tangentially approaching the wire that is set to attractive electric potential would not hit the wire but become captured in a rotational motion around it. Their trajectory is then defined by an equilibrium of the centrifugal force and the electrostatic force generated by applying a voltage between wire and enclosing cylinder. Axial motion along the wire is confined by the field curvature introduced by the flanges of the cylinder. This became known as the *Kingdon trap* [246]. Later, Knight refined the outer electrode shapes to a design with large radius in the center that continuously decreased toward both ends. The outer electrode was symmetrically split into halves in a fashion similar to the end caps of the QIT. This trap design is often called *ideal Kingdon trap* [247]. Knight's trap could store ions and eject them onto a detector, but did not perform any $m/z$ analysis [245]. The first proposal to build a Kingdon trap-based mass analyzer with image current detection addressed the ion rotational frequencies, but it suffered from the poor definition of those frequencies due to the influence of initial ion velocity upon entering the trap [248]. Finally, the concept of Makarov exploited the periodic back and forth motion of ions along the central electrode [240]. This setup requires a precisely defined field composed of a quadrupole field of the ion trap and the logarithmic field of a cylindrical capacitor that is split into two halves. This mass analyzer was termed *Orbitrap* [240] and can be considered as a refined Knight-style Kingdon trap. It has a spindle-like central electrode and a barrel-like outer electrode (Fig. 4.79) [245].

The electric field resulting from the complex shape of the Orbitrap electrodes may be termed quadrologarithmic field and has the potential distribution $U(r,z)$

$$U(r,z) = \frac{k}{2}\left(z^2 - \frac{r^2}{2}\right) + \frac{k}{2}(R_m)^2 \ln\left[\frac{r}{R_m}\right] + C \tag{4.45}$$

where $r$ and $z$ are cylindrical coordinates ($z = 0$ being the plane of symmetry of the field), $k$ is the field curvature, $R_\mathrm{m}$ the characteristic radius, and $C$ is a constant [240, 249]. Equation (4.44) determines the electrostatic field experienced by ions inside the Orbitrap that forces them to move in complex spiral patterns. Stable ion trajectories combine rotation around the central axis with axial oscillations, the

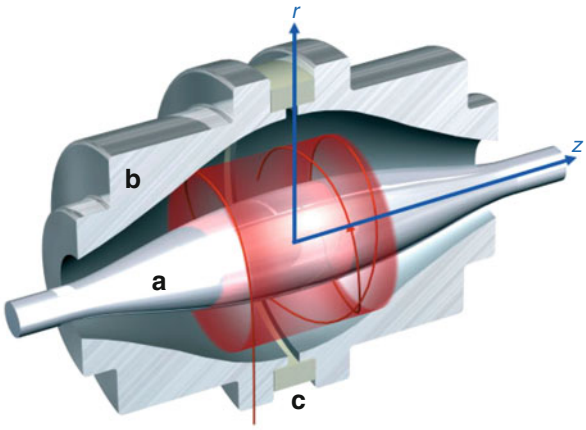


**Fig. 4.79** A cut-away view of the Thermo Fisher Orbitrap™ mass analyzer. Ions are moving in spirals around a spindle-like-shaped central electrode (**a**) that creates an axial field gradient. An outer electrode (**b**) is split in half by an insulating ceramic ring (**c**). An image current induced by moving ions is detected via a differential amplifier between the two halves of the outer Orbitrap electrode. The *m*/*z* of different ions in the Orbitrap can be determined from respective frequencies of oscillation after a Fourier transform (Reproduced from Ref. [241] with permission. © Wiley-VCH, Weinheim, 2006)

frequency $\omega_z$ of which solely depends on the ratio of ionic charge $q$ to ionic mass $m_i$ and the field curvature, but is independent of the tangential velocity and spatial spread of the ions [241].

A detailed mathematical treatment of the Orbitrap can be found in Refs. [20, 240]. It delivers this important frequency of axial oscillations $\omega_z$ (in rad $s^{-1}$) as given by

$$\omega_z = \sqrt{k \left(\frac{q}{m_i}\right)} \tag{4.46}$$

The frequency of the harmonic axial oscillation $\omega_z$ is inversely proportional to the square root of the mass-to-charge ratio of the ions.

Another two characteristic frequencies can be derived for ions inside the Orbitrap. First the frequency of rotation $\omega_\varphi$ around the central electrode

$$\omega_\phi = \frac{\omega_z}{\sqrt{2}} \sqrt{\left(\frac{R_m}{R}\right)^2 - 1} \tag{4.47}$$

and second, the frequency of radial oscillation $\omega_r$, i.e., the "pumping motion" of the orbit as the ions move along the variable radius of the central electrode:

$$\omega_r = \omega_z \sqrt{\left(\frac{R_m}{R}\right)^2 - 2} \tag{4.48}$$

### 4.8.2 Ion Detection and Resolving Power of the Orbitrap

The frequency of the harmonic axial oscillation $\omega_z$ can be determined by image current detection from a differential amplifier connected to the halves of the outer electrode; for each $m/z$ value a sine wave is produced. Analogous to FT-ICR, the image current signal is monitored, stored, and translated into a frequency domain signal by fast Fourier transform resulting in an accurate reading of their $m/z$ (Fig. 4.80) [241, 250]. Different from FT-ICR, there is no excitation prior to the detection period. Instead, the electric field gradient induces the axial oscillation when ions are injected tangentially but off-center with respect to plane of symmetry. All ions have exactly the same amplitude whereas the frequency of axial motion is dictated by their $m/z$ value. Again, there is an analogy to FT-ICR in that packets of ions of common $m/z$ exhibit discrete motions with some interference by interpenetration of ion clouds of different $m/z$ that are simultaneously occupying the trapping volume [20].

In an Orbitrap, the mass resolving power $R$ is half the frequency resolving power due to the square root in Eq. (4.46) [245, 249]. It can be calculated as

$$R = \frac{m}{\Delta m} = \frac{1}{2\,\Delta\omega_z} \sqrt{\frac{k\,q}{m}} \tag{4.49}$$

**Orbitrap versus FT-ICR** While the frequency of the axial oscillation $\omega_z$ in an Orbitrap is proportional to $(q/m)^{1/2}$, the cyclotron frequency $\omega_c$ in FT-ICR is proportional to $q/m$. Accordingly, FT-ICR offers higher resolving power for lower $m/z$ ions whereas the Orbitrap may outperform it at high $m/z$ values. For example, in case of an FT-ICR instrument with a 7-T magnet, the Orbitrap has an edge over FT-ICR above $m/z$ 800 (Fig. 4.81) [241, 245].

### 4.8.3 Ion Injection into the Orbitrap

The Orbitrap alone does not present a very practical instrument. While it serves as a high performance $m/z$ analyzer, its operation demands for proper ion injection and it requires ultra-high vacuum in order to realize sufficiently long transients. Ion injection has to comply with several conditions and restrictions:

- Geometric prerequisites have to be met, such as injection angle, angular spread, and position with respect to the electrodes.

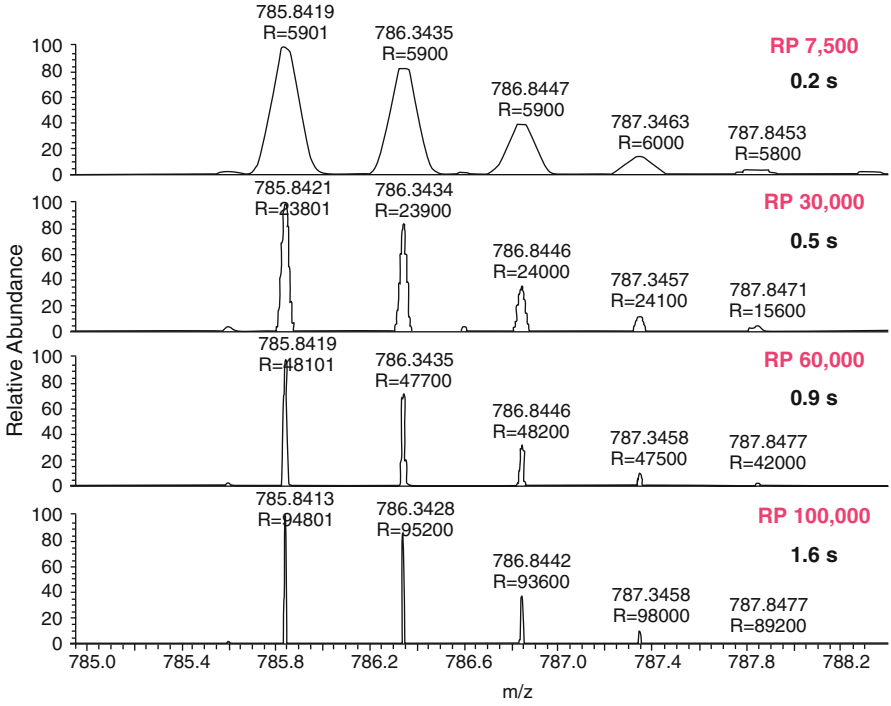


**Fig. 4.80** Resolving power of a commercial Orbitrap instrument as achieved for doubly charged peptide ions at detection intervals ranging from 95 to 1267 ms resulting in cycle times from 0.2 to 1.6 s. The cycle times are longer than pure detection intervals due to preparation of ion packets, data processing etc. The values specified are calculated with reference to the manufacturer's standard value of *m*/*z* 400 (Reproduced from Ref. [241] with permission. © Wiley-VCH, Weinheim, 2006)

- Initial ion velocity and velocity distribution are important.
- Timing of the injection and its duration need to be carefully adjusted.
- Dosage of ions to achieve optimum ion population in the Orbitrap is required.
- Ultrahigh vacuum may not be interrupted to warrant the mean free path for tens to hundreds of thousands of undisturbed revolutions around the central electrode.

Thus, a bent RF-only quadrupole is employed to accumulate, store, and thermalize the ions by a low pressure of nitrogen prior to injection. Derived from the shape of the RF section in the form of the letter "C" this part has been termed the *C-trap*. The C-trap can be filled with about a million elementary charges. Collisional damping is important, because this way the ions are brought to rest in the middle of the C-trap. Nitrogen is used for that purpose as it is already used in the source region of the instrument and it is efficient at capturing and cooling the ions. In other words, the C-trap decouples the Orbitrap from all preceding steps of ion generation, desolvation, and eventually precursor ion selection [250].

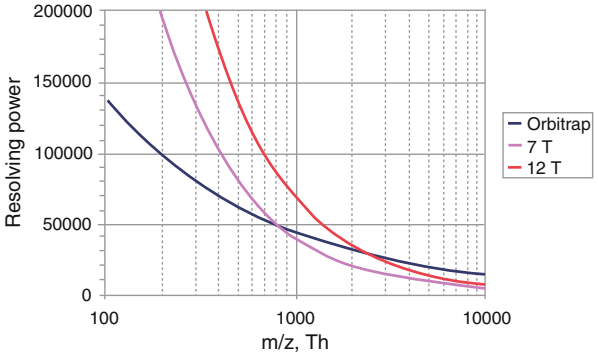


**Fig. 4.81** For an Orbitrap analyzer the drop in resolving power with increasing $m/z$ is less pronounced than for FT-ICR instruments. While FT-ICR clearly outperforms Orbitraps up to $m/z$ 8000 (7 T, *pink line*) or even $m/z$ 2500 (12 T, *red line*) the Orbitrap can deliver somewhat better resolving power in the high mass range (*blue line*) (Reproduced from Ref. [241] with permission. © Wiley-VCH, Weinheim, 2006)

High-voltage electric pulses with short rise times in the order of few hundreds of nanoseconds serve to eject the ions from the C-trap through the gap between the inner pair of quadrupole rods along lines converging on the entrance of the Orbitrap. By lowering the electric potential of the central electrode simultaneously with the entry of the ion packets, ions are captured and start circling. Typically, the ions are injected at kinetic energies of about 1.3 keV while the central electrode is set to −3.4 kV (for positive-ion mode) [245]. The initial bunches become reshaped into rings that oscillate axially along the central electrode. The amplitude of these oscillations is determined by the initial offset of ion injection from the Orbitrap center, whereas coherency of axial oscillations, i.e., maintenance of thin rings, is ensured by the short temporal duration of ion packet injection (Fig. 4.82).

**One Orbitrap cycle**
Ions are collected and thermalized in the C-trap and are injected as a focused beam off-center into the Orbitrap. The electric field of the Orbitrap is increased during the period of injection to compress the ion cloud towards the center. The ions thus are rotating around the central spindle electrode, and in addition, perform radial as well as axial oscillations. After stabilization of the high voltage, the axial oscillation proportional to $(q/m)^{½}$ is recorded via image current detection using the pair of outer electrodes.

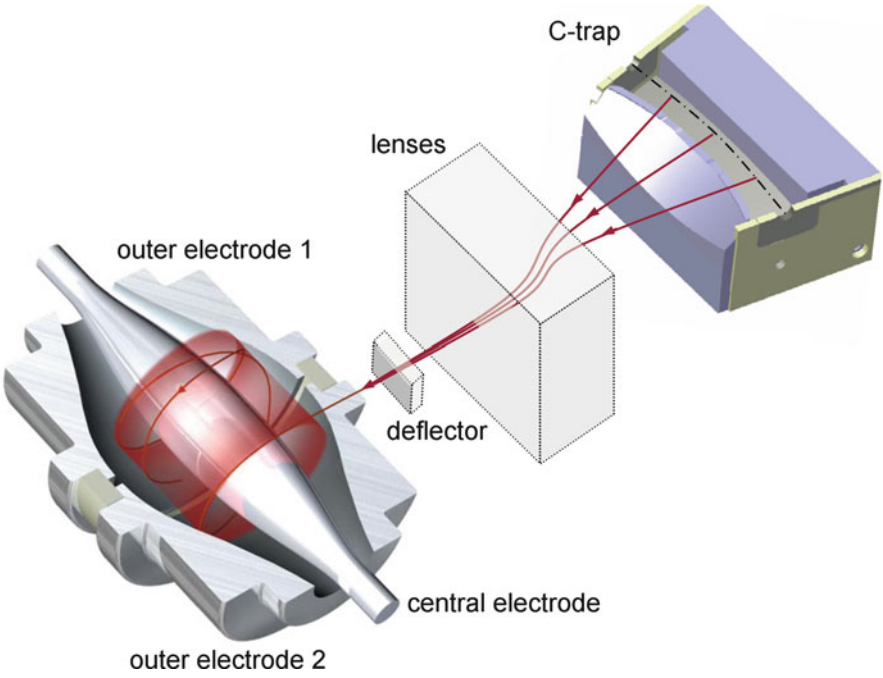


**Fig. 4.82** The Orbitrap mass analyzer with ions being injected from the C-trap through lenses and a deflector. During injection, the C-trap acts as a convex lens with the outer rods pushing and the inner short rods pulling the ions by a DC pulse. Trapping voltage is applied to the central electrode (Courtesy of A. Makarov, Thermo Fisher Scientific)

### 4.8.4 Hybridization with a Linear Quadrupole Ion Trap

To become an analytically useful mass spectrometer, the above combination still needs to be interfaced to an ion source. The prototype implementation of the Orbitrap made use of laser desorption/ionization in the immediate vicinity of the Orbitrap [240], but soon, an external electrospray ion source followed [249]. For highest versatility, the Orbitrap has been attached to the rear of a fully functional Thermo Fisher LTQ instrument (cf. Sect. 4.5.4 and Fig. 4.50). The LIT may either be operated on its own as it still is equipped with SEM detectors or it may be axially emptied into the C-trap via an RF-only transfer octopole. The entire setup, dubbed LTQ-Orbitrap, is shown in Fig. 4.83. This instrument offers both low-resolution MS and $MS^n$ operation in the LTQ section and final high-resolving $m/z$ analysis at ppm-accuracy of whatever ions decided to be sent into the Orbitrap [241–244, 250]. A differential pumping system reduces the pressure along the instrument to achieve about $2 \times 10^{-10}$ mbar in the Orbitrap. While Orbitrap technology has strongly advanced, there is still ongoing research for further improvements [251–255].

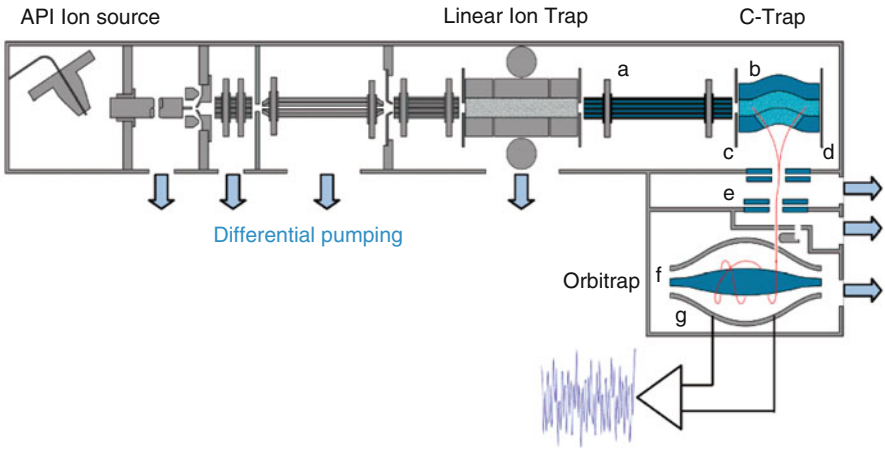


**Fig. 4.83** The Thermo Scientific LTQ Orbitrap mass spectrometer. The front end up to the LIT is identical to the LTQ instrument introduced in Sect. 4.5.3 and Fig. 4.41. Ions axially ejected from the LIT are entering (**a**) a transfer octopole to (**b**) a curved RF-only quadrupole known as C-trap, from where they are injected via (**c**) gate electrode, (**d**) trap electrode, and (**e**) ion optics into the Orbitrap comprising (**f**) the inner electrode and (**g**) outer electrodes for detection. Note that there are four ports for differential pumping along the LTQ section and another three sideways to reduce the pressure from the C-trap to the Orbitrap (Adapted from Ref. [243] with permission. © American Chemical Society, 2006)

### 4.8.5 Orbitrap at a Glance

**Mass Analysis in the Orbitrap**

In an Orbitrap ions are captured by electrostatic attraction of a spindle-shaped central electrode provided they are entering the trapping field in a tangential direction. Proper ion injection in terms of kinetic energy, spatial focusing, and timing is achieved by radial ejection of ion bunches from a C-shaped quadrupole ion trap. The resulting ionic motion inside the Orbitrap is a superimposition of circulation around the central electrode and oscillation along the axis of the same. The longitudinal oscillation is caused by the electric field gradient along the spindle axis. The oscillation is recorded in the time domain via image current detection by two outer electrodes. The frequency is then obtained by FT of the recorded transient and used to calculate $m/z$ and abundance of the ions in the Orbitrap.

**Performance Characteristics**

The main features of the Orbitrap are high resolving power and accurate mass. The level of both depends on the actual Orbitrap model and the exact mode of operation. Typically, spectra are acquired at a resolving power of $R = 20{,}000–200{,}000$ and mass accuracy is in the order of 0.5–3 ppm.

**Growing Orbitrap Family**
Since the introduction of the first instrument featuring an Orbitrap mass analyzer, the array of instruments has continuously been growing. In between, the range includes benchtop systems purely offering HR-MS for routine LC-MS and lately also GC-MS plus benchtop systems with tandem MS capabilities due to a Q-Orbitrap design. Instruments of increasing sophistication with LIT and even dual-LIT frontends and other features complement the Orbitrap family of instruments. Some of them will be discussed in the context of tandem MS (Sect. 9.10). The Orbitrap is set apart from all other types of mass analyzers not only by its unique working principle but also by the fact of being exclusively commercialized by a single company, Thermo Fisher.

## 4.9 Hybrid Instruments

As anticipated in the sections on linear ion traps (Sect. 4.5.4), modern Fourier transform-ion cyclotron resonance (Sect. 4.7.12), and LIT-Orbitrap mass spectrometers (Sect. 4.8.4), instruments can efficiently be designed by combining different types of mass analyzers and ion-guiding devices in a single so-called *hybrid instrument* [256, 257]. By these means one can obtain mass spectrometers that unite the advantageous properties of each mass analyzer they are composed of.

Hybrid mass spectrometers combine the expertise of the various highly developed dedicated devices and mass-analyzing, ion-guiding, ion-accumulating, and ion-focusing elements in a way that ensures the most versatile and yet economic solution. The design of a hybrid instrument may aim at:

- achieving highest resolving power and accuracy,
- boosting speed and sensitivity,
- realizing a compact and versatile yet affordable multi-purpose instrument.

Budgetary aspects are an important issue in favor of hybridization because each stage is selected as to deliver optimum performance at lowest cost. Hybrids are ideally employed for tandem mass spectrometry, for instance. In tandem mass spectrometers the first stage of $m/z$ analysis (MS1) is used to select ions for further fragmentation and subsequent analysis of the product ions in a second $m/z$ analyzer (MS2, Chap. 9). It is generally sufficient to combine a low-resolution MS1 unit with a high-resolution MS2.

**Table 4.2** Hybrid mass analyzers.

| MS1 | Properties of MS1 | MS2 | Properties of MS2 |
|---|---|---|---|
| BE or EB | LR and HR | qQ | LR, low energy CID |
| BE or EB | LR and HR | QIT | LR, low energy CID, $MS^n$ |
| EB or EBE | LR and HR | oaTOF | LR, low energy CID, high sensitivity |
| Qq | LR, low-energy CID | oaTOF | high resolution and mass accuracy, high sensitivity |
| Qq | LR, low-energy CID | LIT | LR, higher sensitivity than QqQ, MS/MS in LIT |
| Qq | LR, low-energy CID | Orbitrap | High resolution and mass accuracy |
| QIT | LR, low-energy CID, $MS^n$ | TOF | HR, high sensitivity |
| LIT | LR, low-energy CID, $MS^n$ | Orbitrap | High to ultrahigh resolution and mass accuracy |
| Qq | LR, low-energy CID, $MS^2$ | ICR | Ultrahigh resolution and mass accuracy, MS/MS in ICR |
| LIT | LR, low-energy CID, $MS^n$ | ICR | Ultrahigh resolution and mass accuracy, MS/MS in ICR |

### 4.9.1 Evolution of Hybrid Mass Spectrometers

The development of hybrid instruments started from magnetic sector-quadrupole hybrids, either BqQ [258, 259], EBqQ, [260] or BEqQ [261–263]. Numerous other systems such as magnetic sector-QIT [264], magnetic sector-oaTOF [265, 266], QITTOF [159, 267, 268], QqTOF [55, 269–271], QqLIT [129], LIT-ICR, and QqICR followed. LIT-Orbitraps present the most recent addition [241, 242, 252, 253] (Table 4.2).

The adaptation of conceptually different mass analyzers to each other may demand for sophisticated interfaces, because of the largely differing requirements concerning ion kinetic energies. The magnetic sector-quadrupole or magnetic sector-QIT hybrids, for example, require keV ions exiting the sector to be decelerated to some 10 eV before entering the qQ section, or to be slowed down and pulsed into the QIT, respectively. Due to the bulky and demanding magnetic sector analyzer, hybrids of that type do not anymore play a role.

Geometries composed of an oaTOF as second analyzer bear the advantage that advanced TOFs offer accurate mass measurements equaling the accuracy of magnetic sector instruments. While their linear quadrupole front end serves as MS1 in tandem MS experiments, it is operated in RF-only mode when tandem MS is not intended, because this allows to acquire full-range spectra at high resolution using the TOF analyzer (MS2, Fig. 4.84). It should be noted that the first quadrupole of hybrids with Qq as MS1, i.e., Qq-TOF hybrids, typically offers mass-selective operation covering an $m/z$ range different from the range in RF-only operation, e.g., $m/z$ 50–4000 in mass-selective and $m/z$ 50–10,000 in RF-only transmission mode.

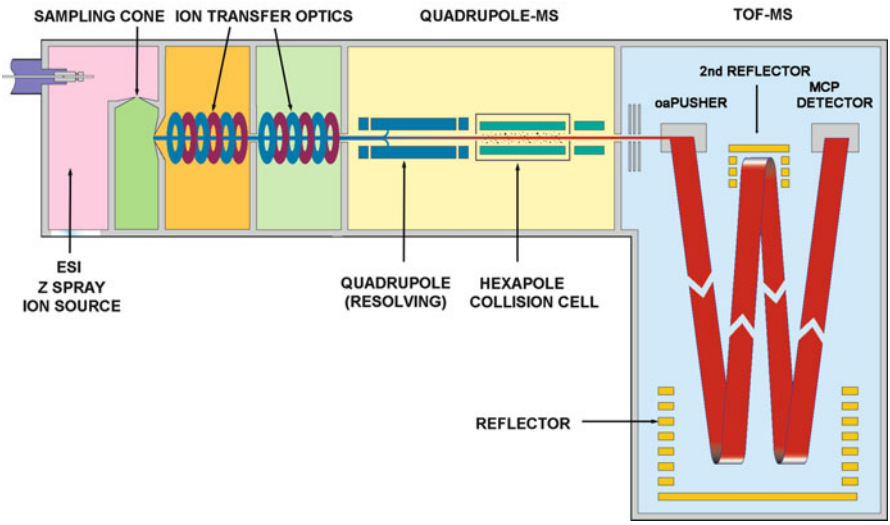


**Fig. 4.84** The Q-TOF Ultima, Qh-oaTOF design, with ESI ion source in MS/MS mode. The TOF analyzer has a reflector that can either be operated using the large reflector alone (V-mode) or adding a second stage of ion reflection (W-mode) for higher resolving power (Courtesy of Waters Corporation, MS Technologies, Manchester, UK)

**Widespread in use**

Besides accommodating to their versatility, there is nothing new to understand with hybrid instruments. Exotic at a first glance, hybrids are governing today's market of mass spectrometers [133–135].

There is very strong competition between high-end QqTOF instruments, on the one side, and Qq-Orbitrap and LIT-Orbitrap hybrid instruments like the aforementioned LTQ-Orbitrap (Fig. 4.83), on the other. The Orbitrap instrument family shows remarkable flexibility in terms of how the Orbitrap analyzer is implemented as part of a complex hybrid system. The range not only includes Qq-Orbitrap and LIT-Orbitrap hybrids but recently even a Q-Orbitrap-tandemLIT configuration. The latter instrument, the Orbitrap Fusion is marketed as a *tribrid* because it incorporates three different types of mass analyzers (Fig. 4.85) [254, 255]. The purpose of the tandem LIT is to provide a higher-pressure LIT for precursor ion selection and ion fragmentation plus a lower-pressure LIT for effective mass analysis. The Orbitrap Fusion architecture permits a multitude of operational modes that allow tandem MS experiments to be run in parallel while a full range survey scan delivers accurate mass data of the next package of precursors to be interrogated or accurate mass of fragments.

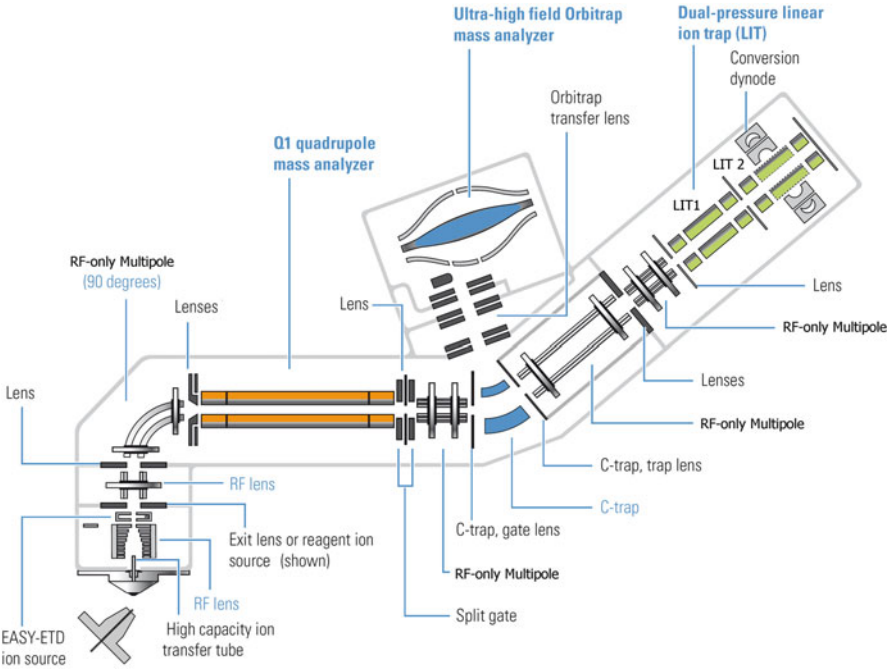


**Fig. 4.85** The Orbitrap Fusion Lumos tribrid mass spectrometer. The first RF-only multipole is bent by 90° to get rid of neutrals before ions are entering the analyzer section comprising quadrupole (*orange*), Orbitrap (*blue*), and LIT/LIT (*green*) (Adapted from Thermo Fisher technical documentation with kind permission. © Thermo Fisher Scientific, Bremen, 2015)

The highest level of resolving power and mass accuracy can be achieved by replacing the oaTOF section with a FT-ICR analyzer. Those high-end hybrid instruments are either available as Qh-ICR by employing a quadrupole as first mass analyzer (Bruker Daltonik APEX-Q and Solarix instruments, Fig. 4.78) or as LIT-ICR, i.e., with a linear ion trap in front of the ICR cell (Thermo Scientific LTQ-FT series, Fig. 4.86).

## 4.10 Ion Mobility-Mass Spectrometry Systems

There is an increasing interest in *ion mobility spectrometry* (IMS) as it presents an effective means of separating gaseous ions [272, 273]. In IMS an electric field forces the ions to drift along a path through a countercurrent inert gas atmosphere whereby they are separated due to their collision cross sections. IMS does for gaseous ions what gas chromatography does for gaseous neutrals, and in fact, IMS was initially referred to as *plasma chromatography* (PC). IMS can separate isobaric ions of different charge state (size-to-charge ratio) resulting from their distinct speed of propagation along the electric field of the ion mobility tube or

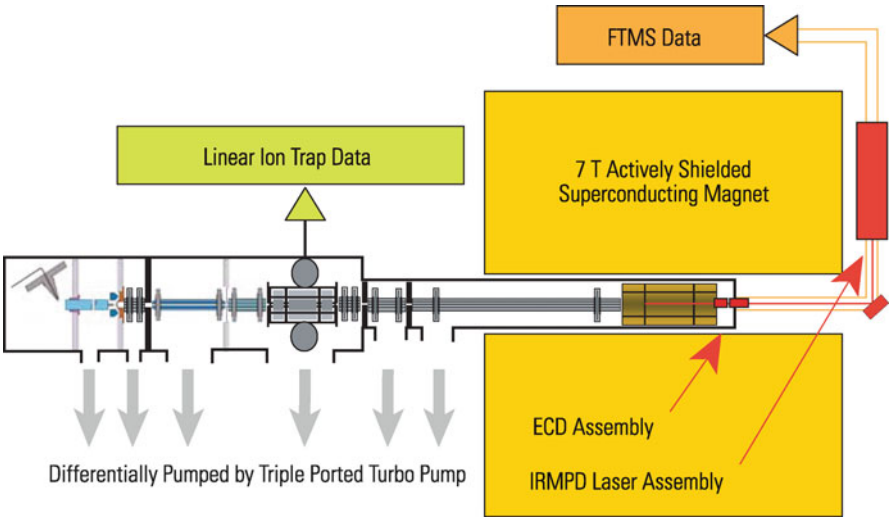


**Fig. 4.86** Schematic of a LIT-FT-ICR hybrid instrument, the Thermo Scientific LTQ FT Ultra, incorporating a fully functional LTQ front end (as in LTQ Orbitrap) for highest versatility (Courtesy Thermo Fisher Scientific, Bremen)

distinguish isobars of the same charge state by their steric properties, i.e., it separates isomers and conformers alike by their shape. Thus, IMS is a valuable aid in biomolecular analysis [274–276].

Clearly, mass spectrometry is perfectly suited for the detection for gaseous ions eluting from an ion mobility device. Therefore, *ion mobility-mass spectrometry* (IM-MS) coupling has received considerable attention since the 1970s [277–279]. The IM-MS instrument provides the following functional features [272]:

- transfer of gaseous sample into the ion source,
- ion formation from neutral sample molecules at atmospheric pressure,
- accumulation of an ion package and injection into the drift region,
- measurement of drift velocities of the swarms of ions while passing the electric field of the drift region in a drift gas atmosphere, and
- detection of ions by a mass analyzer coupled to the IMS stage.

**Hybrid, hyphenation, or something in between?**
While a detailed treatment of ion mobility spectrometry is beyond the scope of this book, it is certainly useful to provide a brief description of the technique [272, 273]. In principle, IM-MS systems can be regarded as hyphenated instrumentation (for applications cf. Sect. 14.6) because the peculiarities of ion mobility demand an integrated instrumental approach.

(continued)

This distinguishes IM-MS from gas or liquid chromatography couplings to MS that may be coupled to and decoupled from a mass spectrometer as required [274, 280]. Therefore, IM-MS is dealt with here as a special case of hybridization.

### 4.10.1 Ion Mobility Separation

Ion mobility effects separation of ions based on their different velocities when accelerated by a constant electric field along a drift tube with a countercurrent inert gas, typically helium or nitrogen. The average velocity, $v_D$, of a drifting ion is then governed by the number of soft collisions it experiences within the drift tube. This number of collisions with the neutrals is directly proportional to the electric field strength, $E$, and the ion mobility constant $K$ (in $cm^2\ V^{-1}\ s^{-1}$).

$$v_D = K\,E \tag{4.50}$$

The value of $K$ depends on the ion and the drift gas. Equation (4.50) is only valid up to field strengths of about 1000 V $cm^{-1}$, whereas above that electric field strength the proportionality between $K$ and $E$ is canceled [274].

The electric field needs to be weak enough so that collisions at given gas density dampen the ions to achieve an internal ion energy in equilibrium with the temperature of the bath gas [276]. Furthermore, gas discharges have strictly to be avoided. In the high-pressure regime (133–1013 mbar or 100–760 Torr) drift tubes are operated at 100–300 V $cm^{-1}$ to deliver what in IMS is considered as high resolving power of 100–300. In the low-pressure regime, field strengths are limited to 10–30 V $cm^{-1}$. Unfortunately, lower pressure goes along with reduced resolving power of the device while coupling to mass analyzers is simplified due to reduced load on the vacuum system [276].

In the low-field regime, the value of $K$ can be calculated from

$$K = \frac{3q}{16N}\ \sqrt{\frac{2\pi}{kT}}\ \sqrt{\left(\frac{m_g + m_i}{m_g\,m_i}\right)}\ \left(\frac{1}{\Omega}\right) \tag{4.51}$$

where $q$ is the ionic charge, $N$ the number density of the buffer gas, $k$ is Boltzmann's constant, $T$ is the absolute temperature, $m_g$ is the mass of the buffer gas molecules, and $m_i$ is the mass of the ions that have the collision cross section $\Omega$ [275, 280].

In the IM-MS experiment, $q$ and $\Omega$ are a priori unknown, but $m_i$ is derived from $m/z$ as soon as the charge state $z$ has been identified, which in turn delivers $q$ from

$q = ze$. As hundreds of TOF mass spectra can be acquired during the tens of milliseconds required for one ion mobility run, the setup easily delivers high-quality MS data to identify the drift time-separated ions.

The reduced mobility, $K_0$, is calculated for comparing IMS data between runs obtained at different buffer gas temperature and pressure and also across different instruments. The reduced mobility, $K_0$, is obtained from:

$$K_0 = \frac{{l_D}^2}{t_D U_D} \quad \frac{T_0}{T} \quad \frac{p}{p_0} \tag{4.52}$$

where $l_D$ is the length of the drift tube and $U_D$ the voltage applied along it; the temperature is given in units of Kelvin ($T_0 = 273.2$ K) and the pressure in units of millibar ($p_0 = 1013$ mbar). $K_0$ has the physical dimension of $cm^2\ V^{-1}\ s^{-1}$. Depending on the source, the equation for the reduced mobility may also be stated in the literature using the electric field strength instead of the voltage and the pressure in Torr:

$$K_0 = \frac{l_D}{t_D E_D} \quad \frac{273.2\,\mathrm{K}}{T} \quad \frac{p}{760\,\mathrm{Torr}} \tag{4.52a}$$

where $l_D$ is the length of the drift tube and $E_D$ the voltage applied divided by $l_D$ [276].

For this classical approach to IMS, the theory of ion propagation is very well developed and allows to calculate the orientationally averaged collision cross sections with high confidence [275].

**IM-TOF-MS** The mass analyzer of an IM-MS instrument must be able to deliver a spectral acquisition rate that allows to collect mass spectra faster than the time span for elution of an IMS peak. As ion mobility separation proceeds in the order of tens of milliseconds, a typical IMS resolving power in the order of 100 implies that at least 100 mass spectra have to be acquired per IMS run. Only TOF analyzers are capable of delivering spectra at 100–1000 Hz, and thus, the IM-TOF-MS hybrid presents the natural combination for IM-MS (Fig. 4.87).

### 4.10.2 Stacked Ring Ion Guide

As an alternative to RF-only multipole ion guides, the *stacked ring ion guide* (SRIG) has been newly recognized since 2004. Ring electrodes (2–3 mm i.d.) are aligned with 1–2 mm insulating ceramics spacers in between them and supplied with an RF drive voltage ($U_{RF} \approx 100$ V at 1 MHz) that is reversed in phase between adjacent rings (Fig. 4.88) [118, 281]. Ions entering the SRIG experience a deep radial potential well with comparatively steep walls towards the inner ring surfaces when traveling though the apertures. The SRIG offers high transmission if operated with a thermalizing buffer gas at around 3 mbar. Interestingly, the SRIG not merely

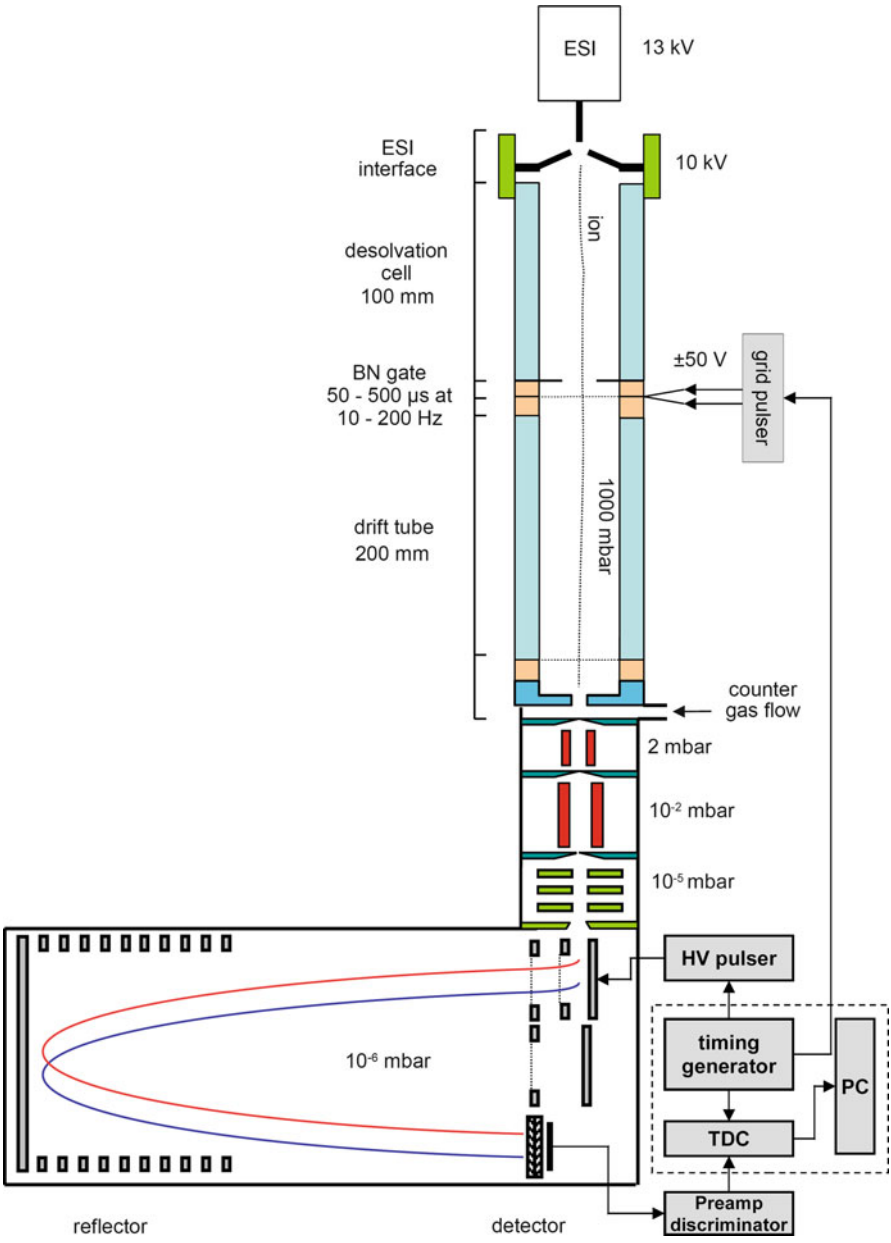


**Fig. 4.87** Basic design of an ambient-pressure IMS-TOF mass spectrometer. Ions from an electrospray source are entering a desolvation chamber from where packets are pulsed into the ion mobility tube by means of a Bradbury-Nielsen (BN) ion gate. The ion path is shown uneven to indicate diffusion of ions. After ion mobility separation the ions are transferred into the reflector oaTOF analyzer via a differentially pumped interface (Courtesy of TofWerk AG, Thun, Switzerland)

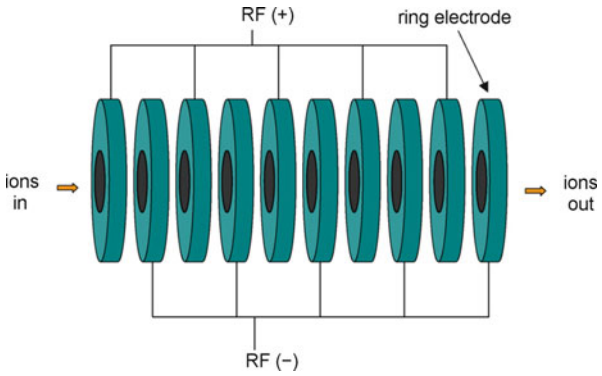


**Fig. 4.88** A stacked ring ion guide. Rings are connected to an RF drive voltage in alteration of the phase. Normally tens of pairs are used to build one ion guide. Ions entering from the left experience a deep radial potential well with comparatively steep walls toward the inner ring surfaces when traveling though the apertures (Reproduced from Ref. [281] with permission. © Elsevier Science Publishers, 2007)

forms a kind of pipe for the ions, its effective potential more resembles a corrugated hose where the grooves act as low potential wells in axial direction, which are deep enough to restrain axial drift of thermalized ions by soft trapping.

To avoid stopping of the ions, a DC pulse can be delivered to a pair of rings causing the ions to move forth to the next potential groove. If the DC pulse makes a progression from pair to pair it creates a traveling wave (T-wave) that makes the ions "surf" along the SRIG (Fig. 4.89).

Such *traveling wave ion guides* (TWIGs) are incorporated in many Waters instruments to replace the more traditional RF-only multipoles as ion guides and collision cells, e.g., in the "triplequadrupoles" of the Xevo™ and Quattro Premier™ series that essentially are of Q-TWIG-Q design. The wave created by a potential of about 2 V is generally propagating at around 300 m $s^{-1}$. This provides an effective means of minimizing dwell times in the corresponding compartment.

### 4.10.3 Traveling Wave Ion Guides for IMS

When ions differing either in charge state or collision cross sections, or both, are entering the TWIG, the less mobile ones may occasionally transverse a wave in backward direction. Those ions lagging behind the traveling wave will exit later than those surfing on the wave. This makes the TWIG become an ion mobility separator.

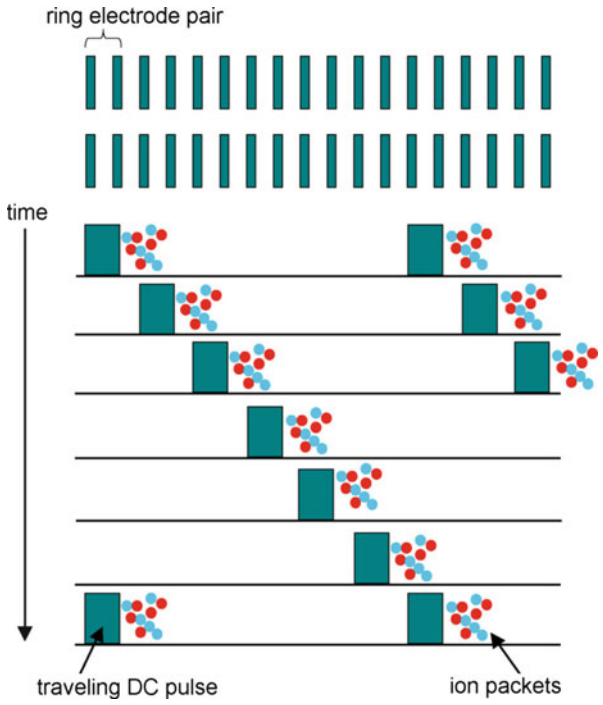


**Fig. 4.89** Effect of a traveling wave DC pulse along a stacked ring ion guide. Ions in front of the DC pulse are moving along from stack to stack and are thus propulsed through the device (T-wave ion guide). A buffer gas is required to narrow down the thermal energy distribution (Reproduced from Ref. [281] with permission. © Elsevier Science Publishers, 2007)

**Traveling wave**
A specific type of IM-MS instrumentation using a *traveling-wave* (T-wave™) approach is available from Waters. In a T-wave ion mobility device ions are pushed by low-voltage waves established along a large stack of paired ring electrodes. However, the theory of ion mobility separation in the T-wave is not as fully understood as in traditional IMS devices [275, 280].

Obviously, multi-RF-ring electrode devices can be designed, optimized, and operated in numerous ways to

- guide ions on their transit from one instrument stage to another or across a pumping stage,
- keep ions on track while they are subjected to collisions with gas for excitation and fragmentation,


**Fig. 4.90** Waters TriWave as incorporated in Synapt G2 instruments for ion mobility separation. Ions entering from the *left* are accumulated in the first section acting as the ion trap, then batch wise admitted into the ion mobility separation zone, and finally collected for transfer into the oaTOF analyzer (Adapted with permission. Courtesy of Waters MS Technologies)

- admit, stop, and collect ions to accumulate packets for subsequent IMS or mass analysis,
- provide ion mobility separation.

Compartments serving either purpose can be combined to form a linear operational unit as part of a more complex hybrid mass spectrometer (Fig. 4.90). With the exception of IMS, which is performed at 100–200 mbar of buffer gas countercurrent to the ion motion, multi-RF-ring electrode devices are typically operated in the 0.1–10 mbar pressure range. Thus, they are compatible with all sorts of applications of RF multipole ion guides.

### 4.10.4 Hybrid Instruments with IMS

A hybrid instrument comprising a mass-selecting quadrupole, a traveling wave ion mobility separator, and an oaTOF analyzer has been marketed by Waters as Synapt series of instruments (Fig. 4.91) [118, 281]. Additionally, this instrument incorporates a RF-ring electrode device in the interface region from ion source to the first mass-analyzing quadrupole. We will resume this topic in the context of interface design for electrospray ionization (Sect. 12.2).

Waters was the first company to offer IMS-tandem MS combinations and still seems to have the widest range of IM-MS instruments. More recently, Agilent (6560 Ion Mobility Q-TOF LC/MS) as well as Bruker with a new concept of *trapped ion mobility* (timsTOF) have also included this type of instrumentation in their portfolio. The designs are becoming more diverse as the technique receives more widespread use. Nonetheless, all IMS-tandem MS instruments rely on oaTOF as the final stage of mass analysis due to its unique combination of acquisition rate and resolving power.

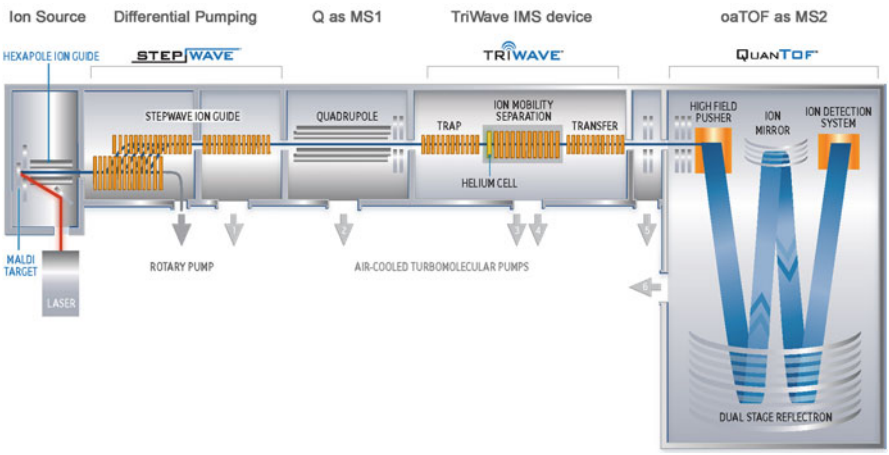


**Fig. 4.91** The Waters Synapt G2-Si, a Q-IMS-oaTOF hybrid, here shown with MALDI source. The combination of three ring ion guide sections is used to build a complete IMS device comprising a trap at the entrance to supply ion packages, the IMS itself, and an ion guide for transfer to the mass analyzer (cf. TriWave in Fig. 4.89) (Adapted with permission. Courtesy of Waters MS Technologies)

## 4.10.5 Overview of Hybrid Instrumentation Including IM-MS

**Classification**

Mass spectrometers composed of different types of mass analyzers and ion-guiding devices are termed *hybrid instruments*. The components are combined in a way as to obtain mass spectrometers uniting the advantages of each subunit they are composed of. Thus, hybrids incorporate mass-analyzing, ion-guiding, ion-accumulating, ion separating, and ion-focusing elements in a way that ensures the most versatile and yet economic solution to obtaining a certain type of instrument.

**Types of IMS**

*Drift tube ion mobility* (DT-IMS) is the classical form of IMS. *Travelling-wave ion mobility* (TW-IMS) has been introduced and is marketed by Waters. In addition, there are *field asymmetric ion mobility* (FAIMS) and *differential ion mobility* (DMS) [282–284]. FAIMS devices are very compact and can externally be fitted to existing instruments with electrospray interface.

**Relevant Representatives of Hybrid Instruments**

Most newly introduced mass spectrometers are hybrid instruments in one way or another. Typically, they are designed as tandem mass spectrometers with a low-resolving first stage of $m/z$ analysis (MS1) for precursor ion selection, e.g., Q, QIT, or LIT, and a high-resolving second stage for product ion analysis (MS2), e.g., oaTOF, Orbitrap, or FT-ICR.

Another family of hybrids includes ion mobility separation either in front of the mass spectrometer section or between MS1 and MS2. More widespread acceptance of IM-MS and instrument design by different manufacturers is leading to an increased diversity of instrumentation and modes of operation. Due to speed and sensitivity requirements, all dedicated IMS-tandem MS instruments rely on oaTOF as the final stage of mass analysis due to its unique combination of acquisition rate, duty cycle, and resolving power.

## 4.11 Ion Detection

The simplest detector is a *Faraday cup*, i.e., an electrode where the ions deposit their charge. The electric current flowing away from that electrode results in a voltage when passing through a resistor of high impedance. Faraday cups are still in use to measure abundance ratios with highest accuracy in *isotope ratio mass spectrometry* (IR-MS) [285]. Early in the era of Mattauch-Herzog-type instruments, the *photographic plate* has been the standard detection system (Sect. 4.3.5). With the advent of scanning mass spectrometers, *secondary electron multipliers* (SEM) became predominant [286]. These rely on the emission of secondary electrons from surfaces upon impact of energetic ions. Ion-counting detectors are not used in FT-ICR and Orbitrap instruments where *image current detection* is employed instead.

### 4.11.1 Analog-to-Digital Conversion

Ion packages of adjacent $m/z$ values hit the detector very shortly after each other causing the signal to change at very high frequency. This requires the use of GHz-frequency digitizers for *analog-to-digital conversion*. Obviously, the final peak shape directly depends on the speed of the *analog-to-digital converter* (ADC) [45].

In case of an 8-bit ADC, for example, the intensity of the detector output is converted into a numerical value of 0–255 [287]. The *dynamic range* is the ratio obtained by dividing the intensity of the most intense signal by that of the weakest while both are correctly detected in the same spectrum. To improve the small dynamic range delivered by 8-bit ADCs (0–255), several tens to a few hundred single spectra are usually summed up. Most recent TOF and oaTOF instruments are therefore equipped with 8-bit or even 10-bit ADCs to provide a dynamic range of $10^4$–$10^5$ after summation of several individual spectra.

Slower scanning instruments such as quadrupole, quadrupole ion trap, and magnetic sector instruments are typically equipped with 16–20-bit ADCs corresponding to intensity values of 0–65,535 ($2^{16}$–1) and 0–1,048,575 ($2^{20}$–1),

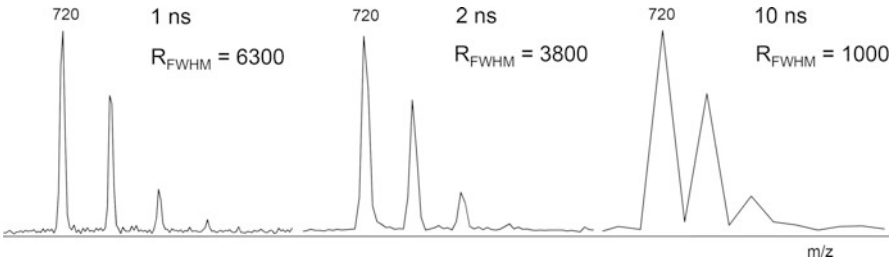


**Fig. 4.92** The [60]fullerene molecular ion peak depicted at different settings of the dwell time per data point of the analog-to-digital converter obtained on the aforementioned instrument after PIE upgrade. At 1 ns per data point (1 GHz) the peaks are well resolved and resolution is limited by the analyzer. At 2 ns (500 MHz) some broadening occurs. At 10 ns (100 MHz) peak shapes are reduced to triangles because detection provides just about two points per *m*/*z*

respectively. This explains their advantage when a high linear dynamic range is required, e.g., for quantitation.

### 4.11.2 Digitization Rate

In particular, the resolving power of advanced TOF analyzers creates a need for high-speed ADCs. Modern TOF instruments incorporate 8-bit ADCs with a digitization rate of 4–5 GHz to suit their resolving power of up to $R = 45{,}000$. The *digitization rate* or *sampling rate* of an ADC may be reported as dwell time per data point, e.g., 1 ns, or as sampling frequency, e.g., 1 GHz (Fig. 4.92). Data points are also shown on a spectrum in Sect. 11.5.

**General relevance**
These considerations concerning the digitization rate are in no way restricted to TOF instruments but apply to any process of data acquisition. As a rule of thumb, good peak shapes require 6–10 data points per peak. This rule applies analogously to the number of single spectra per eluting chromatographic peak.

### 4.11.3 Time-to-Digital Conversion

*Time-to-digital converters* (TDC) had been employed in some early oaTOF instruments instead of analog-to-digital converters because of the much higher speed of TDCs. Speed in terms of sampling rate is needed to reach the high resolution of oaTOF analyzers, and speed in terms of data flow is a prerequisite to handle the enormous number of spectra per second. However, a TDC is a pulse-counting device that offers only 1 bit dynamic range (value 0 or 1) [287]. Detector–

TDC combinations easily suffer from saturation effects as they cannot distinguish the arrival of a single ion from that of several ions arriving simultaneously. The TDC response is therefore not proportional to ion flux. Thus, summation of many single spectra is also necessary to obtain a higher dynamic range via improved signal statistics. Nevertheless, the result is still unsatisfactory for quantitative analysis and for correct isotopic patterns. Furthermore, the dead time between subsequent counting events causes the second of a pair of ions having almost equal arrival times to remain undetected. Dead time effects within ion packages of a given $m/z$ even cause $m/z$ values to shift to the low-mass side (detection of early incoming ions only), which makes empirical dead-time corrections necessary for accurate mass measurements [287, 288].

### 4.11.4 Discrete Dynode Electron Multipliers

When an energetic particle impinges on the surface of a metal or a semiconductor, secondary electrons are emitted from that surface. The ease of such an emission is determined by the *electron(ic) work function* of the respective material, e.g., BeCu alloy oxide ($w_e \approx 2.4$ eV) [289]. The higher the velocity of the impacting particle [286, 290] and the lower the electron work function of the surface, the larger the number of secondary electrons. If an electrode opposite to the location of emission is held at more positive potential, all emitted electrons will be accelerated towards and hit that surface where they in turn cause the release of several electrons each. The avalanche of electrons produced over 12–18 discrete dynode stages held at about 100 V more positive potential each causes an electric current large enough to be detected by a sensitive preamplifier. Such a detector is called *secondary electron multiplier* (SEM, Fig. 4.93) [291]. The dynodes are normally cup-shaped, but stacks of Venetian blind-like dynodes have also been in use. Due to a certain air sensitivity of the emissive layer and in order to prevent arcing due to the high voltage, electron multipliers require operation in high vacuum.

The ion currents actually reaching the first dynode are chiefly in the picoampere range, but may span over a $10^{-18}$–$10^{-9}$ A range. Depending on the applied voltage, SEMs provide a gain of $10^6$–$10^8$ [291]. The resulting current at the electron trap is the input of a nearby preamplifier providing another $10^6$–$10^9$ gain. Its output current is then converted to a voltage signal which finally can be translated to an intensity value by means of an analog-to-digital converter (ADC).

**How many ions per peak?** A singly-charged ion corresponds to a charge of $1.6 \times 10^{-19}$ C, and 1 A is equal to 1 C $s^{-1}$. Thus, an ion current of $10^{-15}$ A $= 10^{-15}$ C $s^{-1}$ is provided by about 6000 ions per second. If the detection of these ions during a scan in a GC-MS run taking 1 s over the $m/z$ 40–400 range yields a mass spectrum consisting of some 30–60 peaks, this corresponds to 100–200 ions per peak. Such conditions define the detection limit of a scanning mass spectrometer.

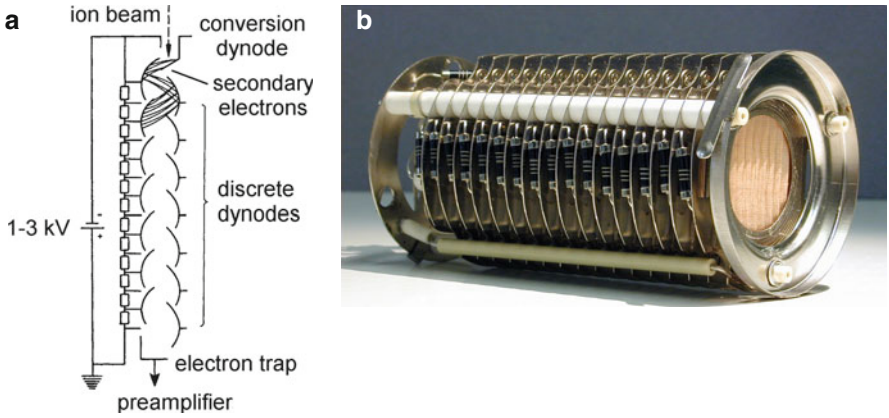


**Fig. 4.93** Discrete dynode electron multipliers. (**a**) Schematic of a 14-stage SEM. (**b**) An old-fashioned 16-stage Venetian blind-type SEM clearly showing the resistors and ceramics insulators between the stacking dynodes at its side ((**a**) Adapted from Ref. [292] by permission. © Springer-Verlag Heidelberg, 1991)

**Replacement may be on order**
All types of secondary electron multipliers have limited life-time. They can deliver 0.1–10 C of extracted charge and are also limited by beam-induced destruction of the first dynode.

### 4.11.5 Channel Electron Multipliers

The cascade of secondary electrons can also be produced in a continuous tube. Such detectors, known as *channel electron multipliers* (CEM) or just *channeltrons*, are more compact and less expensive than discrete dynode SEMs. CEMs are preferably used in benchtop instruments. Their gain depends on the length-to-diameter ratio with an optimum ratio around 40–80 [293]. In a CEM, the high voltage drops continuously from the ion entrance to the electron exit of the tube requiring a sufficiently high resistance of the semiconducting material to withstand high voltage of about 2 kV. This is accomplished by an emissive layer of silicon dioxide overlying a conductive layer of lead oxide on the supporting heavily lead-doped glass tube [291, 294]. Straight CEMs are unstable at gains exceeding $10^4$ because positive ions created inside by EI of residual gas are accelerated towards the input side of the tube where they randomly contribute to the signal causing spurious output pulses [294, 295]. A curved design shortens the free path for ion acceleration thereby suppressing noise from this so-called *ion-feedback*. Curved CEMs provide gains of up to $10^8$ (Figs. 4.94 and 4.95).

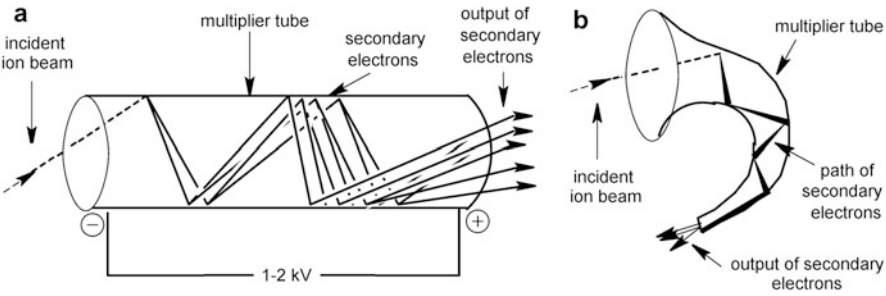


**Fig. 4.94** Linear channel electron multiplier (**a**) and curved channel electron multiplier (**b**) (By courtesy of Waters Corporation, MS Technologies, Manchester, UK)

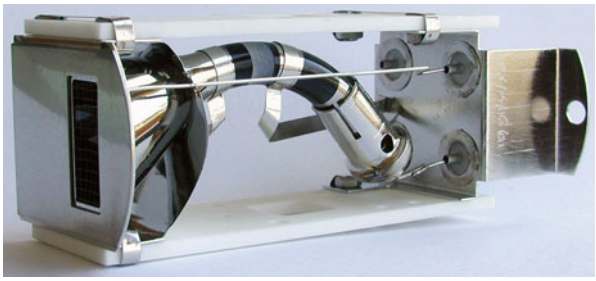

**Fig. 4.95** Channeltron multiplier. Ions or electrons from a conversion dynode would enter from the left side. Amplification of secondary electrons occurs down the bent tube

**Counting all sorts**
Ion counting detectors also produce signals upon impact of energetic neutrals, electrons, or photons. Therefore, care has to be taken, not to allow other particles than the mass-analyzed ions to hit the detector.

### 4.11.6 Microchannel Plates

An extreme reduction of the size of a linear channeltron tube to some micrometers in diameter can be achieved. The cross section of such a single tube is by far too small to be of any use, however, millions of these tubes put together in a "bundle" yield a *channel electron multiplier array*; more common terms are *microchannel plate* or *multichannel plate* (MCP, Fig. 4.96). To avoid that the ions enter the microchannels parallel to their axis, these are inclined by some degrees from the perpendicular to the plate's surface. The gain of an MCP is $10^3$–$10^4$, i.e., much lower than that of a SEM or CEM. Instead of a single MCP, two MCPs are often sandwiched together in such a way that the small angles oppose each other

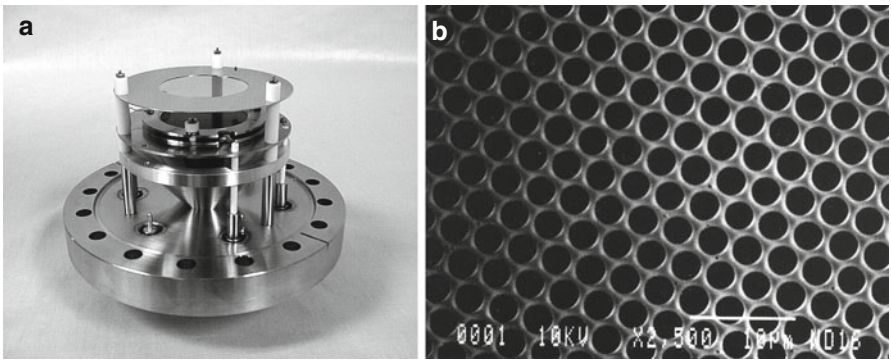


**Fig. 4.96** MCP detector (top inner, glossy disk) mounted on top of a flange (**a**) and SEM micrograph of a high-resolving MCP showing channels of 2 µm diameter (**b**) (By courtesy of (**a**) R.M. Jordan Company, Grass Valley, CA and of (**b**) Burle Industries, Baesweiler)

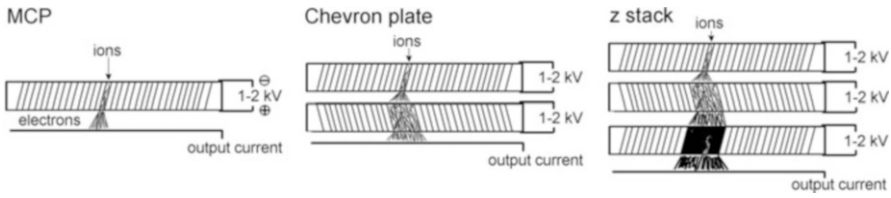


**Fig. 4.97** Stacking of MCPs to increase gain. *From left*: single MCP, Chevron plate, and z-stack configuration. Note the loss of spatial resolution upon stacking

(*Chevron plate*, Fig. 4.97) to obtain gains of $10^6$–$10^7$. Occasionally, even three MCPs are stacked analogously (*z-stack*, gain up to $10^8$) [295, 296].

MCPs are produced as round plates of various sizes. Those of 2–5 cm in diameter are typically employed in mass spectrometers. An MCP may either be operated to give an integral output for all incident ions during a certain time interval, or the location of the impact may be conserved by connecting sectors of the MCP to individual registration channels. The first setup is more widespread, e.g., in TOF-MS to detect the electron current every nanosecond while the ions are arriving at the detector. The second setup can be used for imaging purposes, e.g., to construct an array detector (below).

### 4.11.7 Post-acceleration and Conversion Dynode

Discrimination of slower ions as compared to faster ions is observed with SEMs [297], CEMs, and MCPs as well [293, 298, 299]. This means a reduction in sensitivity upon reduction of the acceleration voltage of a mass spectrometer, and of course, with increasing ion mass. *Post-acceleration detectors* can reduce such effects and especially help to improve the sensitivity for high-mass ions [290, 299]. In post-

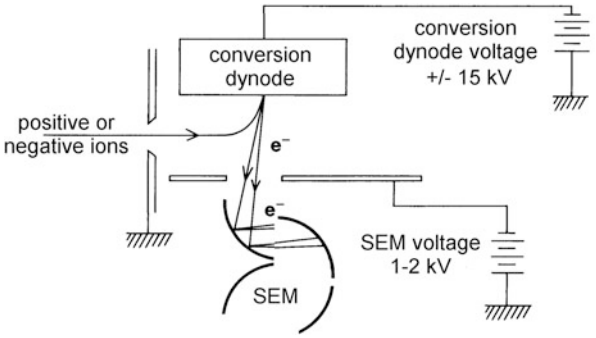


**Fig. 4.98** Detector configuration with conversion dynode (By courtesy of JEOL, Tokyo)

acceleration detectors the ions are accelerated immediately in front of the detector by a voltage of 10–30 kV before they hit the first dynode or the first MCP.

The electron output of ion-counting detectors is usually measured with reference to ground potential, i.e., the first dynode is set to negative high voltage as to achieve acceleration of the electrons down the dynode assembly. In case of sector or TOF instruments, the deceleration of keV negative ions by the detector voltage is of comparatively minor importance. However, the slow ions exiting from quadrupole mass analyzers would stop before they reached the detector. Therefore, *conversion dynodes* are frequently placed in front of the SEM or CEM (Fig. 4.98) [291]. These are robust electrodes set to high potential (5–20 kV) of a polarity suitable to attract the ions actually exiting from the mass analyzer. Their impact on the conversion dynode creates secondary ions or electrons that can be used for subsequent detection. A conversion dynode detector also serves as a post-acceleration detector and gives almost equal sensitivity for positive and negative ion detection. In addition, neutrals and photons cannot reach the detector if the conversion dynode is placed out of the line of sight.

### 4.11.8 Focal Plane Detectors

Magnetic sector instruments are scanning devices usually focusing ions of one $m/z$ value after the other onto a point detector. However, the mass-dispersive element of these instruments, i.e., the magnetic sector, is capable of producing an image of several neighboring $m/z$ values simultaneously. *Focal plane detectors* (FPD) or *array detectors*, as they are often termed, can detect a small $m/z$ range, i.e., $\pm$2–5% of the center mass, at a time [293, 300, 301]. The ions impinging along the focal plane on the surface of an MCP (usually a Chevron plate) are converted to electrons. The electrons from the backside of the MCP stack are then converted into photons by a phosphor screen, and the light image is guided onto a photodiode array or a CCD detector by means of a fiber optical device. Such a multichannel electro-optical detection system typically improves sensitivity or signal-to-noise

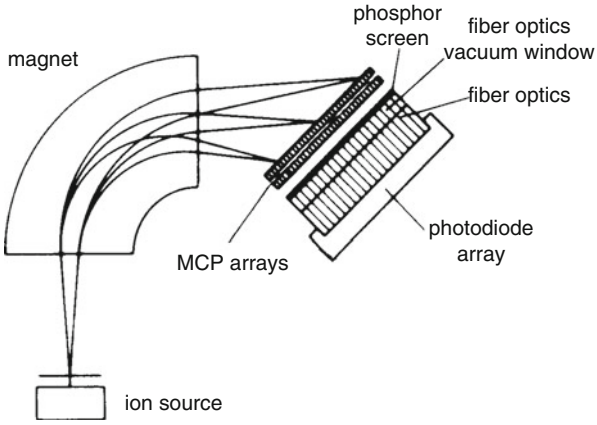


**Fig. 4.99** Array detector in the focal plane of a magnetic sector to detect a small mass range simultaneously (By courtesy of Thermo Electron (Bremen) GmbH)

ratio, respectively, by a factor of 20–100, because less of the ion current is lost without being detected and fluctuations in the ion current are compensated [302, 303].

The resolution of an FPD is theoretically limited by the number of channels (512–2048). In practice, it is even less because the image suffers some broadening as it passes from the first MCP to the photodiode array (Fig. 4.99). Therefore, instruments with FPD can normally be switched from FPD to SEM detection, e.g., by vertical electrostatic deflection of the ion beam (Finnigan MAT900). Furthermore, quadrupole lenses or an inhomogeneous ESA behind the magnet are employed to achieve variable dispersion, i.e., to zoom the $m/z$ range of simultaneous detection. Recent developments point towards fully integrated FPDs on a silicon chip [304].

## 4.12 Vacuum Technology

Vacuum systems are integral parts of any mass spectrometer, but vacuum technology definitely is a field of its own [305–309]. Thus the discussion of mass spectrometer vacuum systems will be restricted to the very basics.

### 4.12.1 Basic Mass Spectrometer Vacuum System

Generally, two pumping stages are employed to generate the high vacuum of a mass spectrometer. Usually, *rotary vane pumps* having *pumping speeds* of about 4–16 $m^3\ h^{-1}$ are used to generate a medium vacuum of several Pascals. They are then connected to high-vacuum pumps in a way that their high-pressure side exhales into the medium vacuum of the rotary vane pumps, i.e., they are operated as *backing pumps*. This way, each pumping stage contributes a compression of some $10^4$–$10^5$ to the total factor of $10^9$–$10^{10}$ between atmospheric pressure and the

**Table 4.3** Pressure ranges in vacuum technology

| Pressure range [Pa] | Pressure range [mbar] | Pressure range [mtorr] | Vacuum | Gas flow |
|---|---|---|---|---|
| $10^5$–$10^2$ | 1 bar–1 mbar | 750 torr–750 mtorr | Rough vacuum (RV) | Viscous flow |
| $10^2$–$10^{-1}$ | 1–$10^{-3}$ | 750–0.75 | Medium vacuum (MV) | Knudsen flow |
| $10^{-1}$–$10^{-5}$ | $10^{-3}$–$10^{-7}$ | 0.75–7.5 × $10^{-5}$ | High vacuum (HV) | Molecular flow |
| $<10^{-5}$ | $<10^{-7}$ | $<7.5 \times 10^{-5}$ | Ultrahigh vacuum (UHV) | Molecular flow |

high vacuum of $10^{-4}$–$10^{-5}$ Pa (Table 4.3). The high-vacuum pumps can either be *turbomolecular pumps*, *oil diffusion pumps*, or *cryopumps* [310, 311].

**Typical vacuum system** The vacuum system of non-benchtop mass spectrometers consists of one to three rotary vane pumps and two or three turbo pumps. Rotary vane pumps are used for the inlet system(s) and as backing pumps for the turbo pumps. One turbo pump is mounted to the ion source housing, another one or two are operated at the analyzer. Thereby, a differentially pumped system is provided where local changes in pressure, e.g., from reagent gas in CI or collision gas in CID, do not notably influence the whole vacuum chamber.

### 4.12.2 High Vacuum Pumps

*Turbomolecular pumps* or *turbo pumps* having pumping speeds of 200–500 l $s^{-1}$ are currently the standard high vacuum pumps in mass spectrometry. A high-speed rotor (50,000–60,000 rpm) is employed to transport the molecules out of the *vacuum manifold* (*vacuum chamber*). Turbo pumps can be switched on and off in minutes, have low power consumption (about 100 W), and thus can be operated either air- or water cooled. Furthermore, they provide clean, in particular oil-free, high vacuum, are compact, and can be mounted either vertically below or horizontally at the sides of the vacuum manifold. Their disadvantages are the risk of sudden damage (similar to hard disk drives) and potential high frequency noise. Fortunately, modern turbo pumps run for many years and their noise is negligible.

Special turbo pump designs provide more than one port to allow for their simultaneous connection to different pressure regions, e.g., ca. $10^{-5}$ mbar and ca. $10^{-3}$ mbar. Such multistage turbo pumps are very useful as one unit is able to support differential pumping of atmospheric pressure ionization interfaces.

Furthermore, newer turbo pumps are equipped with magnetic bearings rather than with oil-lubricated bearings. This cuts down on maintenance, as the yearly exchange of lubricant becomes needless and also guaranties oil-free high vacuum.

Recent turbo pump designs also accept higher pressure at their exhaust thereby allowing for replacement of rotary vane pumps by membrane pumps. This results in

truly oil-free vacuum and offers more comfortable maintenance of the roughing pumps.

*Oil diffusion pumps* offer high pumping speeds (600–2000 l $s^{-1}$) at the cost of high power consumption (0.4–2 kW) and the need for a strong cooling water flow. The oil (perfluoropolypropylene glycols; Fomblin™, Santovac™) is thermally evaporated and the oil vapor supplies transport of gas molecules that enter it by diffusion. The gas-loaded oil vapor is condensed and the gas is removed from the liquid by the action of the backing pump. As diffusion pumps have no moving mechanical parts they are highly reliable and extremely silent. However, elongated use as well as sudden venting causes severe oil contaminations of the vacuum manifold. Diffusion pumps have almost been abandoned from modern mass spectrometers.

*Cryopumps* adsorb (freeze) residual gas to a surface cooled to the temperature of liquid nitrogen. They are highly efficient and provide clean vacuum, but cannot be operated without interruptions to recover the adsorber. Cryopumps are typically operated in combination with turbo pumps because they are only started after high-vacuum conditions are reached. Otherwise, the adsorber would soon be saturated.

## 4.13 Purchasing an Instrument

To some of us it can unexpectedly happen that we are faced with the task of having to buy a mass spectrometer, eventually for ourselves or on behalf of someone else. References to certain commercial instruments made in this chapter were in no way intended to preclude such a 100,000–1,000,000 € decision. The below guide may be useful in selecting an instrument that meets your requirements best.

**Purpose**
Define the tasks the mass spectrometer is going to be acquired for:

- Need for one dedicated or for several ionization methods?
- GC-MS, LC-MS, or ion mobility separation required?
- High resolution and accurate mass needed?
- Is tandem MS an issue or even a must?
- What sensitivity is needed?
- Is quantitative work important?
- Are you going to do mass spectral imaging?

**Budget**
Check your budget. A powerful and versatile second-hand machine from a proven company can be better than a toy-like single-purpose benchtop system.

**Contact Sales**
Get into contact with sales persons of all manufacturers offering suitable systems. Compare prices and modalities of customer training and support. Try to get information concerning longevity and product cycle (5, 10, 15 years?).

**Demonstration**
Make appointments for demonstration of those instruments that are likely to be acquired, e.g., for the top three of your ranking. Do not use completely unknown samples for this purpose. Otherwise, problems associated with your analyte might erroneously be regarded as a lack of instrumental performance.

**Data System**
Modern instruments form a unit with their data system. Does this offer the features you want? Does it allow for customization, "manual" settings, or corrections?

**Analyzing Data**
The software provided for analyzing the data is also of high relevance. Can you customize plots, lists, and reports, obtain molecular formulas, extract

**Table 4.4** Rough estimates correlating instrumentation and factors affecting its cost

| | Acquisition | Installation room requirements | | Operation and long-term usage | |
|---|---|---|---|---|---|
| | Price of instrument | Footprint and weight | Power consumption, air conditioning load | Qualification of personnel | Maintenance |
| Time-of-flight | S–L | S–L | S–M | S–L | S–L |
| Magnetic sector | L–XL | L–XL | L–XL | L–XL | L |
| Linear quadrupole | S–M | S–M | S–M | S–M | S–M |
| Quadrupole ion trap | S–M | S – M | S–M | S–M | S–M |
| Linear quadrupole ion trap | M–L | S–M | S–M | M–L | M |
| Fourier transform-ion cyclotron resonance | XL–XXL | XL–XXL | XL–XXL | L–XL | XL–XXL |
| Orbitrap | L–XL | L | L | L–XL | L |
| Quadrupole-TOF hybrid | M–XL | M–L | L | M–L | L |
| Ion mobility-TOF hybrid | XL | L | L | L–XL | L–XL |

Classified in the format of American dress sizes as S, M, L, XL, XXL

chromatograms, get sophisticated output of data like Kendrick or van Krevelen plots?

**Other Opinions**
Use independent information from the published literature and ask current users of your top-choice mass spectrometers for the special strengths and shortcomings of those systems.

**Investment and Cost of Ownership**
Cost is not only affected by the price of acquisition of a mass spectrometer but also by operation in that it may have highly variable requirements of room, power, air conditioning, and operational skills (Table 4.4).

**Avoid Buyer's Remorse**
Keep in mind that any instrument acquisition inherently presents some compromise – none is perfect. Anyway, try to find the best for your needs and decide to be happy with your purchase afterwards.

## References


1. Ligon WV Jr (1979) Molecular Analysis by Mass Spectrometry. Science 205:151–159. doi:10.1126/science.205.4402.151
2. Brunnée C (1987) The Ideal Mass Analyzer: Fact or Fiction? Int J Mass Spectrom Ion Proc 76:125–237. doi:10.1016/0168-1176(87)80030-7
3. Beynon JH (1960) Instruments. In: Beynon JH (ed) Mass Spectrometry and Its Applications to Organic Chemistry. Elsevier, Amsterdam
4. Habfast K, Aulinger F (1968) Massenspektrometrische Apparate. In: Kienitz H (ed) Massenspektrometrie. Weinheim, Verlag Chemie
5. Aulinger F (1968) Massenspektroskopische Geräte. In: Kienitz H (ed) Massenspektrometrie. Weinheim, Verlag Chemie
6. Brunnée C (1982) New Instrumentation in Mass Spectrometry. Int J Mass Spectrom Ion Phys 45:51–86. doi:10.1016/0020-7381(82)80100-9
7. Brunnée C (1997) 50 Years of MAT in Bremen. Rapid Commun Mass Spectrom 11:694–707. doi:10.1002/(SICI)1097-0231(199704)11:6<694::AID-RCM888>3.0.CO;2-K
8. Chapman JR, Errock GA, Race JA (1997) Science and Technology in Manchester: The Nurture of Mass Spectrometry. Rapid Commun Mass Spectrom 11:1575–1586. doi:10.1002/(SICI)1097-0231(199709)11:14<1575::AID-RCM22>3.0.CO;2-0
9. McLuckey SA (1998) Intrumentation for mass spectrometry. In: Hesso AE, Karjalainen UP, Jalonen JE, Karjalainen EJ (eds) Advances in Mass Spectrometry: Proc 14th Intl Mass Spectrometry Conf. Tampere, Finland, 1997. Elsevier, Amsterdam
10. Grayson MA (ed) (2002) Measuring Mass – From Positive Rays to Proteins. ASMS and CHF, Santa Fe and Philadelphia
11. Jennings KR (ed) (2012) A History of European Mass Spectrometry. IM Publications, Charlton Mill
12. Muenzenberg G (2013) Development of Mass Spectrometers from Thomson and Aston to Present. Int J Mass Spectrom 349–350:9–18
13. Doerr A, Finkelstein J, Jarchum I, Goodman C, Dekker B (2015) Nature Milestones: Mass Spectrometry. Nature Meth 12:1–21. www.nature.com/milestones/mass-spec

14. Badman ER, Cooks RG (2000) Miniature Mass Analyzers. J Mass Spectrom 35:659–671. doi:10.1002/1096-9888(200006)35:6<659::AID-JMS5>3.0.CO;2-V
15. Le Gac S, van den Berg A (eds) (2009) Miniaturization and Mass Spectrometry. The Royal Society of Chemistry, Cambridge
16. Baykut G, Franzen J (1994) Mobile Mass Spectrometry: A Decade of Field Applications. Trends Anal Chem 13:267–275. doi:10.1016/0165-9936(94)87063-2
17. Prieto MC, Kovtoun VV, Cotter RJ (2002) Miniaturized Linear Time-of-Flight Mass Spectrometer with Pulsed Extraction. J Mass Spectrom 37:1158–1162. doi:10.1002/jms.386
18. Arkin CR, Griffin TP, Ottens AK, Diaz JA, Follistein DW, Adams FW, Helms WR (2002) Evaluation of Small Mass Spectrometer Systems for Permanent Gas Analysis. J Am Soc Mass Spectrom 13:1004–1012. doi:10.1016/S1044-0305(02)00422-1
19. Fenselau C, Caprioli R (2003) Mass Spectrometry in the Exploration of Mars. J Mass Spectrom 38:1–10. doi:10.1002/jms.396
20. Hu Q, Noll RJ, Li H, Makarov A, Hardman M, Cooks RG (2005) The Orbitrap: A New Mass Spectrometer. J Mass Spectrom 40:430–443. doi:10.1002/jms.856
21. Wiley WC, McLaren IH (1955) Time-of-Flight Mass Spectrometer with Improved Resolution. Rev Sci Instrum 26:1150–1157. doi:10.1063/1.1715212
22. Stephens WE (1946) A Pulsed Mass Spectrometer with Time Dispersion. Phys Rev 69:691
23. Cameron AE, Eggers DF (1948) An Ion "Velocitron". Rev Sci Instrum 19:605–607. doi:10.1063/1.1741336
24. Wolff MM, Stephens WE (1953) A Pulsed Mass Spectrometer with Time Dispersion. Rev Sci Instrum 24:616–617. doi:10.1063/1.1770801
25. Wiley WC, McLaren IH (1997) Reprint of: Time-of-Flight Mass Spectrometer with Improved Resolution. J Mass Spectrom 32:4–11. doi:10.1002/(SICI)1096-9888(199701)32:1<1::AID-JMS467>3.0.CO;2-6
26. Harrington DB (1959) The time-of-flight mass spectrometer. In: Waldron JD (ed) Advances in Mass Spectrometry. Pergamon Press, Oxford
27. Gohlke RS, McLafferty FW (1993) Early Gas Chromatography/Mass Spectrometry. J Am Soc Mass Spectrom 4:367–371. doi:10.1016/1044-0305(93)85001-E
28. Guilhaus M (1995) The Return of Time-of-Flight to Analytical Mass Spectrometry. Adv Mass Spectrom 13:213–226
29. Guilhaus M, Mlynski V, Selby D (1997) Perfect Timing: Time-of-Flight Mass Spectrometry. Rapid Commun Mass Spectrom 11:951–962. doi:10.1002/(SICI)1097-0231(19970615)11:9<951::AID-RCM785>3.0.CO;2-H
30. Karas M, Hillenkamp F (1988) Laser Desorption Ionization of Proteins with Molecular Masses Exceeding 10000 Daltons. Anal Chem 60:2299–2301. doi:10.1021/ac00171a028
31. Weickhardt C, Moritz F, Grotemeyer J (1997) Time-of-Flight Mass Spectrometry: State-of-the-Art in Chemical Analysis and Molecular Science. Mass Spectrom Rev 15:139–162. doi:10.1002/(SICI)1098-2787(1996)15:3<139::AID-MAS1>3.0.CO;2-J
32. Cotter RJ (1997) Time-of-Flight Mass Spectrometry: Instrumentation and Applications in Biological Research. American Chemical Society, Washington, DC
33. Enke CG (1998) The Unique Capabilities of Time-of-Flight Mass Analyzers. Adv Mass Spectrom 14:197–219
34. Fuerstenau SD, Benner WH (1995) Molecular Weight Determination of Megadalton DNA Electrospray Ions Using Charge Detection Time-of-Flight Mass Spectrometry. Rapid Commun Mass Spectrom 9:1528–1538. doi:10.1002/rcm.1290091513
35. Fuerstenau SD, Benner WH, Thomas JJ, Brugidou C, Bothner B, Suizdak G (2001) Mass Spectrometry of an Intact Virus. Angew Chem Int Ed 40:541–544. doi:10.1002/1521-3773(20010202)40:3<541::AID-ANIE541>3.0.CO;2-K
36. Vestal ML (2009) Modern MALDI Time-of-Flight Mass Spectrometry. J Mass Spectrom 44:303–317. doi:10.1002/jms.1537

37. Guilhaus M (1995) Principles and Instrumentation in Time-of-Flight Mass Spectrometry. Physical and Instrumental Concepts. J Mass Spectrom 30:1519–1532. doi:10.1002/jms.1190301102
38. Ioanoviciu D (1995) Ion-Optical Solutions in Time-of-Flight Mass Spectrometry. Rapid Commun Mass Spectrom 9:985–997. doi:10.1002/rcm.1290091104
39. Cotter RJ (1992) Time-of-Flight Mass Spectrometry for the Analysis of Biological Molecules. Anal Chem 64:1027A–1039A. doi:10.1021/ac00045a726
40. Takach EJ, Hines WM, Patterson DH, Juhasz P, Falick AM, Vestal ML, Martin SA (1997) Accurate Mass Measurements Using MALDI-TOF with Delayed Extraction. J Protein Res 16:363–369. doi:10.1023/A:1026376403468
41. Vestal M, Juhasz P (1998) Resolution and Mass Accuracy in Matrix-Assisted Laser Desorption Ionization-Time-of-Flight. J Am Soc Mass Spectrom 9:892–911. doi:10.1016/S1044-0305(98)00069-5
42. Vestal M, Hayden K (2007) High Performance MALDI-TOF Mass Spectrometry for Proteomics. Int J Mass Spectrom 268:83–92. doi:10.1016/j.ijms.2007.06.21
43. Beavis RC, Chait BT (1989) Factors Affecting the Ultraviolet Laser Desorption of Proteins. Rapid Commun Mass Spectrom 3:233–237. doi:10.1002/rcm.1290030708
44. Toyoda M, Okumura D, Ishihara M, Katakuse I (2003) Multi-Turn Time-of-Flight Mass Spectrometers With Electrostatic Sectors. J Mass Spectrom 38:1125–1142. doi:10.1002/jms.546
45. Schuerch S, Schaer M, Boernsen KO, Schlunegger UP (1994) Enhanced Mass Resolution in Matrix-Assisted Laser Desorption/Ionization Linear Time-of-Flight Mass Spectrometry. Biol Mass Spectrom 23:695–700. doi:10.1002/bms.1200231108
46. Mamyrin BA (1994) Laser Assisted Reflectron Time-of-Flight Mass Spectrometry. Int J Mass Spectrom Ion Proc 131:1–19. doi:10.1016/0168-1176(93)03891-O
47. Brown RS, Lennon JJ (1995) Mass Resolution Improvement by Incorporation of Pulsed Ion Extraction in a Matrix-Assisted Laser Desorption/Ionization Linear Time-of-Flight Mass Spectrometer. Anal Chem 67:1998–2003. doi:10.1021/ac00109a015
48. Colby SM, King TB, Reilly JP (1994) Improving the Resolution of Matrix-Assisted Laser Desorption/Ionization Time-of-Flight Mass Spectrometry by Exploiting the Correlation Between Ion Position and Velocity. Rapid Commun Mass Spectrom 8:865–868. doi:10.1002/rcm.1290081102
49. Whittal RM, Li L (1995) High-Resolution Matrix-Assisted Laser Desorption-Ionization in a Linear Time-of-Flight Mass Spectrometer. Anal Chem 67:1950–1954. doi:10.1021/ac00109a007
50. Vestal ML, Juhasz P, Martin SA (1995) Delayed Extraction Matrix-Assisted Laser Desorption Time-of-Flight Mass Spectrometry. Rapid Commun Mass Spectrom 9:1044–1050. doi:10.1002/rcm.1290091115
51. Dawson JHJ, Guilhaus M (1989) Orthogonal-Acceleration Time-of-Flight Mass Spectrometer. Rapid Commun Mass Spectrom 3:155–159. doi:10.1002/rcm.1290030511
52. Mirgorodskaya OA, Shevchenko AA, Chernushevich IV, Dodonov AF, Miroshnikov AI (1994) Electrospray-Ionization Time-of-Flight Mass Spectrometry in Protein Chemistry. Anal Chem 66:99–107. doi:10.1021/ac00073a018
53. Coles J, Guilhaus M (1993) Orthogonal Acceleration – A New Direction for Time-of-Flight Mass Spectrometry: Fast, Sensitive Mass Analysis for Continuous Ion Sources. Trends Anal Chem 12:203–213. doi:10.1016/0165-9936(93)80021-B
54. Selby DS, Mlynski V, Guilhaus M (2001) A 20 KV Orthogonal Acceleration Time-of-Flight Mass Spectrometer for Matrix-Assisted Laser Desorption/Ionization. Int J Mass Spectrom 210(211):89–100. doi:10.1016/S1387-3806(01)00438-9
55. Guilhaus M, Selby D, Mlynski V (2000) Orthogonal Acceleration Time-of-Flight Mass Spectrometry. Mass Spectrom Rev 19:65–107. doi:10.1002/(SICI)1098-2787(2000)19:2<65::AID-MAS1>3.0.CO;2-E

56. Selditz U, Nilsson S, Barnidge D, Markides KE (1999) ESI/TOF-MS Detection for Microseparation Techniques. Chimia 53:506–510
57. Charles L (2008) Influence of Internal Standard Charge State on the Accuracy of Mass Measurements in Orthogonal Acceleration Time-of-Flight Mass Spectrometers. Rapid Commun Mass Spectrom 22:151–155. doi:10.1002/rcm.3347
58. Guo C, Huang Z, Gao W, Nian H, Chen H, Dong J, Shen G, Fu J, Zhou Z (2008) A Homemade High-Resolution Orthogonal-Injection Time-of-Flight Mass Spectrometer with a Heated Capillary Inlet. Rev Sci Instrum 79:013109-1-013109/8. doi:10.1063/1.2832334
59. Prazen BJ, Bruckner CA, Synovec RE, Kowalski BR (1999) Enhanced Chemical Analysis Using Parallel Column Gas Chromatography with Single-Detector Time-of-Flight Mass Spectrometry and Chemometric Analysis. Analytical Chemistry 71:1093–1099. doi:10.1021/ac980814m
60. Hirsch R, Ternes TA, Bobeldijk I, Weck RA (2001) Determination of Environmentally Relevant Compounds Using Fast GC/TOF-MS. Chimia 55:19–22
61. Hsu CS, Green M (2001) Fragment-Free Accurate Mass Measurement of Complex Mixture Components by Gas Chromatography/Field Ionization-Orthogonal Acceleration Time-of-Flight Mass Spectrometry: An Unprecedented Capability for Mixture Analysis. Rapid Commun Mass Spectrom 15:236–239. doi:10.1002/1097-0231(20010215)15:3<236::AID-RCM197>3.0.CO;2-B
62. Chernushevich IV (2000) Duty Cycle Improvement for a Quadrupole-Time-of-Flight Mass Spectrometer and Its Use for Precursor Ion Scans. Eur J Mass Spectrom 6:471–479. doi:10.1255/ejms.377
63. Toyoda M (2010) Development of Multi-Turn Time-of-Flight Mass Spectrometers and Their Applications. Eur J Mass Spectrom 16:397–406. doi:10.1255/ejms.1076
64. Toyoda M, Shimma S, Aoki J, Ishihara M (2012) Multi-Turn Time-of-Flight Mass Spectrometers. J Mass Spectrom Soc Jpn 60:87–102. doi:10.5702/massspec.12-47
65. Ichihara T, Uchida S, Ishihara M, Katakuse I, Toyoda M (2007) Construction of a Palmtop Size Multi-Turn Time-of-Flight Mass Spectrometer "MULTUM-S". J Mass Spectrom Soc Jpn 55:363–368. doi:10.5702/massspec.55.363
66. Goesmann F, Rosenbauer H, Bredehoeft JH, Cabane M, Ehrenfreund P, Gautier T, Giri C, Krueger H, Le Roy L, MacDermott AJ, McKenna-Lawlor S, Meierhenrich UJ, Caro GMM, Raulin F, Roll R, Steele A, Steininger H, Sternberg R, Szopa C, Thiemann W, Ulamec S (2015) Organic Compounds on Comet 67P/Churyumov-Gerasimenko Revealed by COSAC Mass Spectrometry. Science 349:497–499. doi:10.1126/science.aab0689
67. Satoh T, Tsuno H, Iwanaga M, Kammei Y (2006) A New Spiral Time-of-Flight Mass Spectrometer for High Mass Analysis. J Mass Spectrom Soc Jpn 54:11–17. doi:10.5702/massspec.54.11
68. Satoh T, Sato T, Tamura J (2007) Development of a High-Performance MALDI-TOF Mass Spectrometer Utilizing a Spiral Ion Trajectory. J Am Soc Mass Spectrom 18:1318–1323. doi:10.1016/j.jasms.2007.04.010
69. Satoh T (2009) Development of a Time-of-Flight Mass Spectrometer Utilizing a Spiral Ion Trajectory. J Mass Spectrom Soc Jpn 57:363–369. doi:10.5702/massspec.57.363
70. Satoh T, Kubo A, Shimma S, Toyoda M (2012) Mass Spectrometry Imaging and Structural Analysis of Lipids Directly on Tissue Specimens by Using a Spiral Orbit Type Tandem Time-of-Flight Mass Spectrometer, SpiralTOF-TOF. Mass Spectrom 1:A0013. doi:10.5702/massspectrometry.A0013
71. Satoh T, Kubo A, Hazama H, Awazu K, Toyoda M (2014) Separation of Isobaric Compounds Using a Spiral Orbit Type Time-of-Flight Mass Spectrometer, MALDI-SpiralTOF. Mass Spectrom 3:S0027-1-S0027/5. doi:10.5702/massspectrometry.S0027
72. Sato H, Nakamura S, Teramoto K, Sato T (2014) Structural Characterization of Polymers by MALDI Spiral-TOF Mass Spectrometry Combined with Kendrick Mass Defect Analysis. J Am Soc Mass Spectrom 25:1346–1355. doi:10.1007/s13361-014-0915-y

73. Casares A, Kholomeev A, Wollnik H (2001) Multipass Time-of-Flight Mass Spectrometers with High Resolving Powers. Int J Mass Spectrom 206:267–273. doi:10.1016/S1387-3806(00)00391-2
74. Wollnik H, Casares A (2003) An Energy-Isochronous Multi-Pass Time-of-Flight Mass Spectrometer Consisting of Two Coaxial Electrostatic Mirrors. Int J Mass Spectrom 227:217–222. doi:10.1016/S1387-3806(03)00127-1
75. Yavor M, Verentchikov A, Hasin J, Kozlov B, Gavrik M, Trufanov A (2008) Planar Multi-Reflecting Time-of-Flight Mass Analyzer with a Jig-Saw Ion Path. Phys Procedia 1:391–400. doi:10.1016/j.phpro.2008.07.120
76. Klitzke CF, Corilo YE, Siek K, Binkley J, Patrick J, Eberlin MN (2012) Petroleomics by Ultrahigh-Resolution Time-of-Flight Mass Spectrometry. Energy & Fuels 26:5787–5794. doi:10.1021/ef300961c
77. Polyakova OV, Mazur DM, Artaev VB, Lebedev AT (2016) Rapid Liquid-Liquid Extraction for the Reliable GC/MS Analysis of Volatile Priority Pollutants. Environ Chem Lett 14:251–257. doi:10.1007/s10311-015-0544-0
78. Wolf RN, Wienholtz F, Atanasov D, Beck D, Blaum K, Borgmann C, Herfurth F, Kowalska M, Kreim S, Litvinov Y, Lunney D, Manea V, Neidherr D, Rosenbusch M, Schweikhard L, Stanja J, Zuber K (2013) ISOLTRAP's Multi-Reflection Time-of-Flight Mass Separator/Spectrometer. Int J Mass Spectrom 349–350:123–133. doi:10.1016/j.ijms.2013.03.020
79. Wolf RN, Eritt M, Marx G, Schweikhard L (2011) A Multi-Reflection Time-of-Flight Mass Separator for Isobaric Purification of Radioactive Ion Beams. Hyperfine Interact 199:115–122. doi:10.1007/s10751-011-0306-8
80. Wolf RN, Marx G, Rosenbusch M, Schweikhard L (2012) Static-Mirror Ion Capture and Time Focusing for Electrostatic Ion-Beam Traps and Multi-Reflection Time-of-Flight Mass Analyzers by Use of an In-Trap Potential Lift. Int J Mass Spectrom 313:8–14. doi:10.1016/j.ijms.2011.12.006
81. Nier AO (1991) The Development of a High Resolution Mass Spectrometer: A Reminiscence. J Am Soc Mass Spectrom 2:447–452. doi:10.1016/1044-0305(91)80029-7
82. Nier AO (1989) Some Reminiscences of Mass Spectrometry and the Manhattan Project. J Chem Educ 66:385–388. doi:10.1021/ed066p385
83. Nier AO (1990) Some Reflections on the Early Days of Mass Spectrometry at the University of Minnesota. Int J Mass Spectrom Ion Proc 100:1–13. doi:10.1016/0168-1176(90)85063-8
84. Duckworth HE, Barber RC, Venkatasubramanian VS (1986) Mass Spectroscopy. Cambridge University Press, Cambridge
85. Cooks RG, Beynon JH, Caprioli RM (1973) Instrumentation. In: Cooks RG, Beynon JH, Caprioli RM, Lester GR (eds) Metastable Ions. Elsevier, Amsterdam
86. Morrison JD (1986) Ion Focusing, Mass Analysis, and Detection. In: Futrell JH (ed) Gaseous Ion Chemistry and Mass Spectrometry. Wiley, New York
87. Dempster AJ (1918) A New Method of Positive Ray Analysis. Phys Rev 11:316–325. doi:10.1103/PhysRev.11.316
88. Cooks RG, Chen G, Wong P, Wollnik H (2014) Spectrometers Mass. In: Digital Encyclopedia of Applied Physics. Wiley-VCH, Weinheim. doi:10.1002/3527600434
89. Mattauch J, Herzog R (1934) Über Einen Neuen Massenspektrographen. Z Phys 89:786–795. doi:10.1007/BF01341392
90. Prohaska T, Irrgeher J, Zitek A, Jakubowski N (eds) (2015) Sector Field Mass Spectrometry for Elemental and Isotopic Analysis. Royal Society of Chemistry, Cambridge
91. Brunnée C, Voshage H (1964) Massenspektrometrie. Karl Thiemig Verlag KG, München
92. Bainbridge KT, Jordan EB (1936) Mass-Spectrum Analysis. 1. The Mass Spectrograph. 2. The Existence of Isobars of Adjacent Elements. Phys Rev 50:282–296. doi:10.1103/PhysRev.50.282
93. Johnson EG, Nier AO (1953) Angular Aberrations in Sector Shaped Electromagnetic Lenses for Focusing Beams of Charged Particles. Phys Rev 91:10–17. doi:10.1103/PhysRev.91.10

94. Todd JFJ (1995) Recommendations for Nomenclature and Symbolism for Mass Spectroscopy Including an Appendix of Terms Used in Vacuum Technology. Int J Mass Spectrom Ion Proc 142:211–240. doi:10.1016/0168-1176(95)93811-F
95. Morgan RP, Beynon JH, Bateman RH, Green BN (1978) The MM-ZAB-2F Double-Focussing Mass Spectrometer and MIKE Spectrometer. Int J Mass Spectrom Ion Phys 28:171–191. doi:10.1016/0020-7381(78)80124-7
96. Hintenberger H, König LA (1957) Über Massenspektrometer mit vollständiger Doppelfokussierung zweiter Ordnung. Z Naturforsch 12:773–785. doi:10.1515/zna-1957-1004
97. Guilhaus M, Boyd RK, Brenton AG, Beynon JH (1985) Advantages of a Second Electric Sector on a Double-Focusing Mass Spectrometer of Reversed Configuration. Int J Mass Spectrom Ion Proc 67:209–227. doi:10.1016/0168-1176(85)80020-3
98. Bill JC, Green BN, Lewis IAS (1983) A High Field Magnet with Fast Scanning Capabilities. Int J Mass Spectrom Ion Phys 46:147–150. doi:10.1016/0020-7381(83)80075-8
99. Matsuda H (1985) High-Resolution High-Transmission Mass Spectrometer. Int J Mass Spectrom Ion Proc 66:209–215. doi:10.1016/0168-1176(85)83010-X
100. Matsuda H (1989) Double-Focusing Mass Spectrometers of Short Path Length. Int J Mass Spectrom Ion Proc 93:315–321. doi:10.1016/0168-1176(89)80120-X
101. Paul W (1990) Electromagnetic Traps for Charged and Neutral Particles (Nobel Lecture). Angew Chem Int Ed 29:739–748. doi:10.1002/anie.199007391
102. Paul W (1993) Electromagnetic traps for charged and neutral particles. In: Nobel Prize Lectures in Physics. World Scientific Publishing, Singapore, pp 1981–1990
103. Paul W, Steinwedel H (1953) A New Mass Spectrometer Without Magnetic Field. Z Naturforsch 8A:448–450. doi:10.1515/zna-1953-0710
104. Paul W, Raether M (1955) Das elektrische Massenfilter. Z Phys 140:262–273. doi:10.1007/BF01328923
105. Lawson G, Todd JFJ (1972) Radio-Frequency Quadrupole Mass Spectrometers. Chem Brit 8:373–380
106. Dawson PH (1976) Quadrupole Mass Spectrometry and Its Applications. Elsevier, New York
107. Dawson PH (1986) Quadrupole Mass Analyzers: Performance, Design and Some Recent Applications. Mass Spectrom Rev 5:1–37. doi:10.1002/mas.1280050102
108. Douglas DJ (2009) Linear Quadrupoles in Mass Spectrometry. Mass Spectrom Rev 28:937–960. doi:10.1002/mas.20249
109. Blaum K, Geppert C, Müller P, Nörtershäuser W, Otten EW, Schmitt A, Trautmann N, Wendt K, Bushaw BA (1998) Properties and Performance of a Quadrupole Mass Filter Used for Resonance Ionization Mass Spectrometry. Int J Mass Spectrom 181:67–87. doi:10.1016/S1387-3806(98)14174-x
110. Amad MH, Houk RS (1998) High-Resolution Mass Spectrometry with a Multiple Pass Quadrupole Mass Analyzer. Anal Chem 70:4885–4889. doi:10.1021/ac980505w
111. Liyu Y, Amad MH, Winnik WM, Schoen AE, Schweingruber H, Mylchreest I, Rudewicz PJ (2002) Investigation of an Enhanced Resolution Triple Quadrupole Mass Spectrometer for High-Throughput Liquid Chromatography/Tandem Mass Spectrometry Assays. Rapid Commun Mass Spectrom 16:2060–2066. doi:10.1002/rcm.824
112. Denison DR (1971) Operating Parameters of a Quadrupole in a Grounded Cylindrical Housing. J Vac Sci Technol 8:266–269
113. Dawson PH, Whetten NR (1969) Nonlinear Resonances in Quadrupole Mass Spectrometers Due to Imperfect Fields. II. Quadrupole Mass Filter and the Monopole Mass Spectrometer. Int J Mass Spectrom Ion Phys 3:1–12. doi:10.1016/0020-7381(69)80054-9
114. Brubaker WM (1967) Comparison of Quadrupole Mass Spectrometers with Round and Hyperbolic Rods. J Vac Sci Technol 4:326
115. Gibson JR, Taylor S (2000) Prediction of Quadrupole Mass Filter Performance for Hyperbolic and Circular Cross Section Electrodes. Rapid Commun Mass Spectrom 14:1669–1673. doi:10.1002/1097-0231(20000930)14:18<1669::AID-RCM80>3.0.CO;2-%23

116. Chen W, Collings BA, Douglas DJ (2000) High-Resolution Mass Spectrometry with a Quadrupole Operated in the Fourth Stability Region. Anal Chem 72:540–545. doi:10.1021/ac990815u
117. Douglas DJ, Frank AJ, Mao D (2005) Linear Ion Traps in Mass Spectrometry. Mass Spectrom Rev 24:1–29. doi:10.1002/mas.20004
118. Giles K, Pringle SD, Worthington KR, Little D, Wildgoose JL, Bateman RH (2004) Applications of a Traveling Wave-Based Radio-Frequency-Only Stacked Ring Ion Guide. Rapid Commun Mass Spectrom 18:2401–2414. doi:10.1002/rcm.1641
119. Huang Y, Guan S, Kim HS, Marshall AG (1996) Ion Transport Through a Strong Magnetic Field Gradient by Radio Frequency-Only Octupole Ion Guides. Int J Mass Spectrom Ion Proc 152:121–133. doi:10.1016/0168-1176(95)04334-9
120. Douglas DJ, French JB (1992) Collisional Focusing Effects in Radiofrequency Quadrupoles. J Am Soc Mass Spectrom 3:398–408. doi:10.1016/1044-0305(92)87067-9
121. Tolmachev AV, Udseth HR, Smith RD (2000) Radial Stratification of Ions as a Function of Mass to Charge Ratio in Collisional Cooling Radio Frequency Multipoles Used as Ion Guides or Ion Traps. Rapid Commun Mass Spectrom 14:1907–1913. doi:10.1002/1097-0231(20001030)14:20<1907::AID-RCM111>3.0.CO;2-M
122. Collings BA, Campbell JM, Mao D, Douglas DJ (2001) A Combined Linear Ion Trap Time-of-Flight System with Improved Performance and $MS^n$ Capabilities. Rapid Commun Mass Spectrom 15:1777–1795. doi:10.1002/rcm.440
123. Douglas DJ (1998) Applications of Collision Dynamics in Quadrupole Mass Spectrometry. J Am Soc Mass Spectrom 9:101–113. doi:10.1016/S1044-0305(97)00246-8
124. Thomson BA (1998) 1997 McBryde Medal Award Lecture Radio Frequency Quadrupole Ion Guides in Modern Mass Spectrometry. Can J Chem 76:499–505. doi:10.1139/v98-073
125. Lock CM, Dyer E (1999) Characterization of High Pressure Quadrupole Collision Cells Possessing Direct Current Axial Fields. Rapid Commun Mass Spectrom 13:432–448. doi:10.1002/(SICI)1097-0231(19990315)13:5<432::AID-RCM504>3.0.CO;2-I
126. Lock CM, Dyer E (1999) Simulation of Ion Trajectories Through a High Pressure Radio Frequency Only Quadrupole Collision Cell by SIMION 6.0. Rapid Commun Mass Spectrom 13:422–431. doi:10.1002/(SICI)1097-0231(19990315)13:5<422::AID-RCM503>3.0.CO;2-M
127. Adlhart C, Hinderling C, Baumann H, Chen P (2000) Mechanistic Studies of Olefin Metathesis by Ruthenium Carbene Complexes Using Electrospray Ionization Tandem Mass Spectrometry. J Am Chem Soc 122:8204–8214. doi:10.1021/ja9938231
128. Mao D, Douglas DJ (2003) H/D Exchange of Gas Phase Bradykinin Ions in a Linear Quadrupole Ion Trap. J Am Soc Mass Spectrom 14:85–94. doi:10.1016/S1044-0305(02)00818-8
129. Hager JW (2002) A New Linear Ion Trap Mass Spectrometer. Rapid Commun Mass Spectrom 16:512–526. doi:10.1002/rcm.607
130. Schwartz JC, Senko MW, Syka JEP (2002) A Two-Dimensional Quadrupole Ion Trap Mass Spectrometer. J Am Soc Mass Spectrom 13:659–669. doi:10.1016/S1044-0305(02)00384-7
131. Hofstadler SA, Sannes-Lowery KA, Griffey RH (2000) Enhanced Gas-Phase Hydrogen-Deuterium Exchange of Oligonucleotide and Protein Ions Stored in an External Multipole Ion Reservoir. J Mass Spectrom 35:62–70. doi:10.1002/(SICI)1096-9888(200001)35:1<62::AID-JMS913>3.0.CO;2-9
132. Collings BA, Scott WR, Londry FA (2003) Resonant Excitation in a Low-Pressure Linear Ion Trap. J Am Soc Mass Spectrom 14:622–634. doi:10.1016/S1044-0305(03)00202-2
133. Aebersold R, Mann M (2003) Mass Spectrometry-Based Proteomics. Nature 422:198–207. doi:10.1038/nature01511
134. Hopfgartner G, Husser C, Zell M (2003) Rapid Screening and Characterization of Drug Metabolites Using a New Quadrupole-Linear Ion Trap Mass Spectrometer. J Mass Spectrom 38:138–150. doi:10.1002/jms.420

135. Hager JW (2004) Recent Trends in Mass Spectrometer Development. Anal Bioanal Chem 378:845–850. doi:10.1007/s00216-003-2287-1
136. Koizumi H, Whitten WB, Reilly PTA (2008) Trapping of Intact, Singly-Charged, Bovine Serum Albumin Ions Injected from the Atmosphere with a 10-cm Diameter, Frequency-Adjusted Linear Quadrupole Ion Trap. J Am Soc Mass Spectrom 19:1942–1947. doi:10.1016/j.jasms.2008.08.007
137. Welling M, Schuessler HA, Thompson RI, Walther H (1998) Ion/Molecule Reactions, Mass Spectrometry and Optical Spectroscopy in a Linear Ion Trap. Int J Mass Spectrom Ion Proc 172:95–114. doi:10.1016/S0168-1176(97)00251-6
138. Londry FA, Hager JW (2003) Mass Selective Axial Ion Ejection from a Linear Quadrupole Ion Trap. J Am Soc Mass Spectrom 14:1130–1147. doi:10.1016/S1044-0305(03)00446-X
139. March RE, Todd JFJ (2005) Quadrupole Ion Trap Mass Spectrometry. Wiley, Hoboken
140. Blake TA, Ouyang Z, Wiseman JM, Takats Z, Guymon AJ, Kothari S, Cooks RG (2004) Preparative Linear Ion Trap Mass Spectrometer for Separation and Collection of Purified Proteins and Peptides in Arrays Using Ion Soft Landing. Anal Chem 76:6293–6305. doi:10.1021/ac048981b
141. Ramanathan R (ed) (2009) Mass Spectrometry in Drug Metabolism and Pharmacokinetics. Wiley, Hoboken
142. Dahl DA, Delmore JE, Appelhans AD (1990) SIMION PC/PS2 Electrostatic Lens Design Program. Rev Sci Instrum 61:607–609. doi:10.1063/1.1141932
143. Dahl DA (2000) SIMION for the Personal Computer in Reflection. Int J Mass Spectrom 200:3–25. doi:10.1016/S1387-3806(00)00305-5
144. Magparangalan DP, Garrett TJ, Drexler DM, Yost RA (2010) Analysis of Large Peptides by MALDI Using a Linear Quadrupole Ion Trap with Mass Range Extension. Anal Chem 82:930–934. doi:10.1021/ac9021488
145. March RE, Hughes RJ (1989) Quadrupole Storage Mass Spectrometry. Wiley, Chichester
146. March RE (1998) Quadrupole Ion Trap Mass Spectrometry: Theory, Simulation, Recent Developments and Applications. Rapid Commun Mass Spectrom 12:1543–1554. doi:10.1002/(SICI)1097-0231(19981030)12:20<1543::AID-RCM343>3.0.CO;2-T
147. March RE (2000) Quadrupole Ion Trap Mass Spectrometry. A View at the Turn of the Century. Int J Mass Spectrom 200:285–312. doi:10.1016/S1387-3806(00)00345-6
148. Stafford GC Jr (2002) Ion Trap Mass Spectrometry: A Personal Perspective. J Am Soc Mass Spectrom 13:589–596. doi:10.1016/S1044-0305(02)00385-9
149. March RE (2009) Quadrupole Ion Traps. Mass Spectrom Rev 28:961–989. doi:10.1002/mas.20250
150. March RE, Todd JFJ (eds) (1995) Practical Aspects of Ion Trap Mass Spectrometry Vol. 1 – Fundamentals of Ion Trap Mass Spectrometry. CRC Press, Boca Raton
151. March RE, Todd JFJ (eds) (1995) Practical Aspects of Ion Trap Mass Spectrometry Vol. 2 – Ion Trap Instrumentation. CRC Press, Boca Raton
152. March RE, Todd JFJ (eds) (1995) Practical Aspects of Ion Trap Mass Spectrometry Vol. 3 – Chemical, Environmental, and Biomedical Applications. CRC Press, Boca Raton
153. Yoshinari K (2000) Theoretical and Numerical Analysis of the Behavior of Ions Injected into a Quadrupole Ion Trap Mass Spectrometer. Rapid Commun Mass Spectrom 14:215–223. doi:10.1002/(SICI)1097-0231(20000229)14:4<215::AID-RCM867>3.0.CO;2-T
154. Alheit R, Kleinadam S, Vedel F, Vedel M, Werth G (1996) Higher Order Non-Linear Resonances in a Paul Trap. Int J Mass Spectrom Ion Proc 154:155–169. doi:10.1016/0168-1176(96)04380-7
155. Stafford GC Jr, Kelley PE, Syka JEP, Reynolds WE, Todd JFJ (1984) Recent Improvements in and Analytical Applications of Advanced Ion Trap Technology. Int J Mass Spectrom Ion Proc 60:85–98. doi:10.1016/0168-1176(84)80077-4
156. Wu HF, Brodbelt JS (1992) Effects of Collisional Cooling on Ion Detection in a Quadrupole Ion Trap Mass Spectrometer. Int J Mass Spectrom Ion Proc 115:67–81. doi:10.1016/0168-1176(92)85032-U

157. Plass WR, Li H, Cooks RG (2003) Theory, Simulation and Measurement of Chemical Mass Shifts in RF Quadrupole Ion Traps. Int J Mass Spectrom 228:237–267. doi:10.1016/S1387-3806(03)00216-1
158. Wuerker RF, Shelton H, Langmuir RV (1959) Electrodynamic Containment of Charged Particles. J Appl Phys 30:342–349. doi:10.1063/1.1735165
159. Ehlers M, Schmidt S, Lee BJ, Grotemeyer J (2000) Design and Set-Up of an External Ion Source Coupled to a Quadrupole-Ion-Trap Reflectron-Time-of-Flight Hybrid Instrument. Eur J Mass Spectrom 6:377–385. doi:10.1255/ejms.356
160. Forbes MW, Sharifi M, Croley T, Lausevic Z, March RE (1999) Simulation of Ion Trajectories in a Quadrupole Ion Trap: A Comparison of Three Simulation Programs. J Mass Spectrom 34:1219–1239. doi:10.1002/(SICI)1096-9888(199912)34:12<1219::AID-JMS897>3.0.CO;2-L
161. Coon JJ, Steele HA, Laipis P, Harrison WW (2002) Laser Desorption-Atmospheric Pressure Chemical Ionization: A Novel Ion Source for the Direct Coupling of Polyacrylamide Gel Electrophoresis to Mass Spectrometry. J Mass Spectrom 37:1163–1167. doi:10.1002/jms.385
162. Nappi M, Weil C, Cleven CD, Horn LA, Wollnik H, Cooks RG (1997) Visual Representations of Simulated Three-Dimensional Ion Trajectories in an Ion Trap Mass Spectrometer. Int J Mass Spectrom Ion Proc 161:77–85. doi:10.1016/S0168-1176(96)04416-3
163. Dawson PH, Hedman JW, Whetten NR (1969) Mass Spectrometer. Rev Sci Instrum 40:1444–1450. doi:10.1063/1.1683822
164. Dawson PH, Whetten NR (1970) A Miniature Mass Spectrometer. Anal Chem 42:103A–108A. doi:10.1021/ac60294a799
165. Griffiths IW, Heesterman PJL (1990) Quadrupole Ion Store (QUISTOR) Mass Spectrometry. Int J Mass Spectrom Ion Proc 99:79–98. doi:10.1016/0168-1176(90)85022-T
166. Griffiths IW (1990) Recent Advances in Ion-Trap Technology. Rapid Commun Mass Spectrom 4:69–73. doi:10.1002/rcm.1290040302
167. Kelley PE, Stafford GC Jr, Syka JEP, Reynolds WE, Louris JN, Todd JFJ (1986) New Advances in the Operation of the Ion Trap Mass Spectrometer. Adv Mass Spectrom 10B:869–870
168. Splendore M, Lausevic M, Lausevic Z, March RE (1997) Resonant Excitation and/or Ejection of Ions Subjected to DC and RF Fields in a Commercial Quadrupole Ion Trap. Rapid Commun Mass Spectrom 11:228–233. doi:10.1002/(SICI)1097-0231(19970131)11:2<228::AID-RCM735>3.0.CO;2-C
169. Creaser CS, Stygall JW (1999) A Comparison of Overtone and Fundamental Resonances for Mass Range Extension by Resonance Ejection in a Quadrupole Ion Trap Mass Spectrometer. Int J Mass Spectrom 190(191):145–151. doi:10.1016/S1387-3806(99)00022-6
170. Williams JD, Cox KA, Cooks RG, McLuckey SA, Hart KJ, Goeringer DE (1994) Resonance Ejection Ion Trap Mass Spectrometry and Nonlinear Field Contributions: The Effect of Scan Direction on Mass Resolution. Anal Chem 66:725–729. doi:10.1021/ac00077a023
171. Ding L, Sudakov M, Brancia FL, Giles R, Kumashiro S (2004) A Digital Ion Trap Mass Spectrometer Coupled with Atmospheric Pressure Ion Sources. J Mass Spectrom 39:471–484. doi:10.1002/jms.637
172. Cooks RG, Amy JW, Bier M, Schwartz JC, Schey K (1989) New Mass Spectrometers. Adv Mass Spectrom 11A:33–52
173. Kaiser RE Jr, Louris JN, Amy JW, Cooks RG (1989) Extending the Mass Range of the Quadrupole Ion Trap Using Axial Modulation. Rapid Commun Mass Spectrom 3:225–229. doi:10.1002/rcm.1290030706
174. Weber-Grabau M, Kelley P, Bradshaw S, Hoekman D, Evans S, Bishop P (1989) Recent Advances in Ion-Trap Technology. Adv Mass Spectrom 11A:152–153
175. Siethoff C, Wagner-Redeker W, Schäfer M, Linscheid M (1999) HPLC-MS with an Ion Trap Mass Spectrometer. Chimia 53:484–491

176. Eades DM, Johnson JV, Yost RA (1993) Nonlinear Resonance Effects During Ion Storage in a Quadrupole Ion Trap. J Am Soc Mass Spectrom 4:917–929. doi:10.1016/1044-0305(93)80017-S
177. Makarov AA (1996) Resonance Ejection from the Paul Trap: A Theoretical Treatment Incorporating a Weak Octapole Field. Anal Chem 68:4257–4263. doi:10.1021/ac960653r
178. Doroshenko VM, Cotter RJ (1997) Losses of Ions During Forward and Reverse Scans in a Quadrupole Ion Trap Mass Spectrometer and How to Reduce Them. J Am Soc Mass Spectrom 8:1141–1146. doi:10.1016/S1044-0305(97)00162-1
179. von Busch F, Paul W (1961) Nonlinear Resonances in Electric Mass-Filters as a Consequence of Field Irregularities. Z Phys 164:588–594. doi:10.1007/BF01378433
180. Dawson PH, Whetten NR (1969) Nonlinear Resonances in Quadrupole Mass Spectrometers Due to Imperfect Fields. I. Quadrupole Ion Trap. Int J Mass Spectrom Ion Phys 2:45–59. doi:10.1016/0020-7381(69)80005-7
181. Wang Y, Franzen J (1994) The Non-Linear Ion Trap. Part 3. Multipole Components in Three Types of Practical Ion Trap. Int J Mass Spectrom Ion Proc 132:155–172. doi:10.1016/0168-1176(93)03913-7
182. Franzen J (1994) The Non-Linear Ion Trap. Part 5. Nature of Non-Linear Resonances and Resonant Ion Ejection. Int J Mass Spectrom Ion Proc 130:15–40. doi:10.1016/0168-1176(93)03907-4
183. Snyder DT, Pulliam CJ, Ouyang Z, Cooks RG (2015) Miniature and Fieldable Mass Spectrometers: Recent Advances. Anal Chem 88:2–29. doi:10.1021/acs.analchem.5b03070
184. Pulliam CJ, Bain RM, Wiley JS, Ouyang Z, Cooks RG (2015) Mass Spectrometry in the Home and Garden. J Am Soc Mass Spectrom 26:224–230. doi:10.1007/s13361-014-1056-z
185. Ouyang Z, Wu G, Song Y, Li H, Plass WR, Cooks RG (2004) Rectilinear Ion Trap: Concepts, Calculations, and Analytical Performance of a New Mass Analyzer. Anal Chem 76:4595–4605. doi:10.1021/ac049420n
186. Peng WP, Goodwin MP, Nie Z, Volny M, Ouyang Z, Cooks RG (2008) Ion Soft Landing Using a Rectilinear Ion Trap Mass Spectrometer. Anal Chem 80:6640–6649. doi:10.1021/ac800929w
187. Berton A, Traldi P, Ding L, Brancia FL (2008) Mapping the Stability Diagram of a Digital Ion Trap (DIT) Mass Spectrometer Varying the Duty Cycle of the Trapping Rectangular Waveform. J Am Soc Mass Spectrom 19:620–625. doi:10.1016/j.jasms.2007.12.012
188. Ding L, Kumashiro S (2006) Ion Motion in the Rectangular Wave Quadrupole Field and Digital Operation Mode of a Quadrupole Ion Trap Mass Spectrometer. Rapid Commun Mass Spectrom 20:3–8. doi:10.1002/rcm.2253
189. Li X, Jiang G, Luo C, Xu F, Wang Y, Ding L, Ding C (2009) Ion Trap Array Mass Analyzer: Structure and Performance. Anal Chem 81:4840–4846. doi:10.1021/ac900478e
190. Brodbelt JS, Louris JN, Cooks RG (1987) Chemical Ionization in an Ion Trap Mass Spectrometer. Anal Chem 59:1278–1285. doi:10.1021/ac00136a007
191. Doroshenko VM, Cotter RJ (1997) Injection of Externally Generated Ions into an Increasing Trapping Field of a Quadrupole Ion Trap Mass Spectrometer. J Mass Spectrom 31:602–615. doi:10.1002/(SICI)1096-9888(199706)32:6<602::AID-JMS513>3.0.CO;2-G
192. Van Berkel GJ, Glish GL, McLuckey SA (1990) Electrospray Ionization Combined with Ion Trap Mass Spectrometry. Anal Chem 62:1284–1295. doi:10.1021/ac00212a016
193. Wang Y, Schubert M, Ingendoh A, Franzen J (2000) Analysis of Non-Covalent Protein Complexes Up to 290 KDa Using Electrospray Ionization and Ion Trap Mass Spectrometry. Rapid Commun Mass Spectrom 14:12–17. doi:10.1002/(SICI)1097-0231(20000115)14:1<12::AID-RCM825>3.0.CO;2-7
194. Lawrence EO, Livingston MS (1932) The Production of High-Speed Light Ions Without the Use of High Voltages. Phys Rev 40:19–35. doi:10.1103/PhysRev.40.19
195. Comisarow MB, Marshall AG (1996) The Early Development of Fourier Transform Ion Cyclotron Resonance (FT-ICR) Spectroscopy. J Mass Spectrom 31:581–585. doi:10.1002/(SICI)1096-9888(199606)31:6<581::AID-JMS369>3.0.CO;2-1

196. Smith LG (1951) New Magnetic Period Mass Spectrometer. Rev Sci Instrum 22:115–116. doi:10.1063/1.1745849
197. Sommer H, Thomas HA, Hipple JA (1951) Measurement of E/M by Cyclotron Resonance. Phys Rev 82:697–702. doi:10.1103/PhysRev.82.697
198. Baldeschwieler JD (1968) Ion Cyclotron Resonance Spectroscopy. Science 159:263–273. doi:10.1126/science.159.3812.263
199. Assamoto B (ed) (1991) Analytical Applications of Fourier Transform Ion Cyclotron Resonance Mass Spectrometry. Weinheim, VCH
200. Comisarow MB, Marshall AG (1974) Fourier Transform Ion Cyclotron Resonance Spectroscopy. Chem Phys Lett 25:282–283. doi:10.1016/0009-2614(74)89137-2
201. Comisarow MB, Marshall AG (1974) Frequency-Sweep Fourier Transform Ion Cyclotron Resonance Spectroscopy. Chem Phys Lett 26:489–490. doi:10.1016/0009-2614(74)80397-0
202. Wanczek K-P (1989) ICR Spectrometry – A Review of New Developments in Theory, Instrumentation and Applications. I. 1983–1986. Int J Mass Spectrom Ion Proc 95:1–38. doi:10.1016/0168-1176(89)83044-7
203. Marshall AG, Grosshans PB (1991) Fourier Transform Ion Cyclotron Resonance Mass Spectrometry: The Teenage Years. Anal Chem 63:215A–229A. doi:10.1021/ac00004a001
204. Amster IJ (1996) Fourier Transform Mass Spectrometry. J Mass Spectrom 31:1325–1337. doi:10.1002/(SICI)1096-9888(199612)31:12<1325::AID-JMS453>3.0.CO;2-W
205. Dienes T, Salvador JP, Schürch S, Scott JR, Yao J, Cui S, Wilkins CL (1996) Fourier Transform Mass Spectrometry-Advancing Years (1992-Mid 1996). Mass Spectrom Rev 15:163–211. doi:10.1002/(SICI)1098-2787(1996)15:3<163::AID-MAS2>3.0.CO;2-G
206. Marshall AG (2000) Milestones in Fourier Transform Ion Cyclotron Resonance Mass Spectrometry Technique Development. Int J Mass Spectrom 200:331–356. doi:10.1016/S1387-3806(00)00324-9
207. Smith RD (2000) Evolution of ESI-Mass Spectrometry and Fourier Transform Ion Cyclotron Resonance for Proteomics and Other Biological Applications. Int J Mass Spectrom 200:509–544. doi:10.1016/S1387-3806(00)00352-3
208. Marshall AG, Hendrickson CL, Shi SDH (2002) Scaling MS Plateaus with High-Resolution FT-ICR-MS. Anal Chem 74:252A–259A. doi:10.1021/ac022010j
209. Schaub TM, Hendrickson CL, Horning S, Quinn JP, Senko MW, Marshall AG (2008) High-Performance Mass Spectrometry: Fourier Transform Ion Cyclotron Resonance at 14.5 Tesla. Anal Chem 80:3985–3990. doi:10.1021/ac800386h
210. Boldin IA, Nikolaev EN (2011) Fourier Transform Ion Cyclotron Resonance Cell with Dynamic Harmonization of the Electric Field in the Whole Volume by Shaping of the Excitation and Detection Electrode Assembly. Rapid Commun Mass Spectrom 25:122–126. doi:10.1002/rcm.4838
211. Nikolaev EN (2015) Some Notes About FT ICR Mass Spectrometry. Int J Mass Spectrom 377:421–431. doi:10.1016/j.ijms.2014.07.051
212. Marshall AG, Chen T (2015) 40 Years of Fourier Transform Ion Cyclotron Resonance Mass Spectrometry. Int J Mass Spectrom 377:410–420. doi:10.1016/j.ijms.2014.06.034
213. Hendrickson CL, Quinn JP, Kaiser NK, Smith DF, Blakney GT, Chen T, Marshall AG, Weisbrod CR, Beu SC (2015) 21 Tesla Fourier Transform Ion Cyclotron Resonance Mass Spectrometer: A National Resource for Ultrahigh Resolution Mass Analysis. J Am Soc Mass Spectrom 26:1626–1632. doi:10.1007/s13361-015-1182-2
214. He F, Hendrickson CL, Marshall AG (2001) Baseline Mass Resolution of Peptide Isobars: A Record for Molecular Mass Resolution. Anal Chem 73:647–650. doi:10.1021/ac000973h
215. Bossio RE, Marshall AG (2002) Baseline Resolution of Isobaric Phosphorylated and Sulfated Peptides and Nucleotides by Electrospray Ionization FT-ICR-MS: Another Step Toward MS-Based Proteomics. Anal Chem 74:1674–1679. doi:10.1021/ac0108461
216. Nikolaev EN, Jertz R, Grigoryev A, Baykut G (2012) Fine Structure in Isotopic Peak Distributions Measured Using a Dynamically Harmonized Fourier Transform Ion Cyclotron Resonance Cell at 7 T. Anal Chem 84:2275–2283. doi:10.1021/ac202804f

217. Popov IA, Nagornov K, Vladimirov GN, Kostyukevich YI, Nikolaev EN (2014) Twelve Million Resolving Power on 4.7 T Fourier Transform Ion Cyclotron Resonance Instrument with Dynamically Harmonized Cell-Observation of Fine Structure in Peptide Mass Spectra. J Am Soc Mass Spectrom 25:790–799. doi:10.1007/s13361-014-0846-7
218. White FM, Marto JA, Marshall AG (1996) An External Source 7 T Fourier Transform Ion Cyclotron Resonance Mass Spectrometer with Electrostatic Ion Guide. Rapid Commun Mass Spectrom 10:1845–1849. doi:10.1002/(SICI)1097-0231(199611)10:14<1845::AID-RCM749>3.0.CO;2-%23
219. Marshall AG, Hendrickson CL (2002) Fourier Transform Ion Cyclotron Resonance Detection: Principles and Experimental Configurations. Int J Mass Spectrom 215:59–75. doi:10.1016/S1387-3806(01)00588-7
220. Marshall AG, Hendrickson CL, Jackson GS (1998) Fourier Transform Ion Cyclotron Resonance Mass Spectrometry: A Primer. Mass Spectrom Rev 17:1–35. doi:10.1002/(SICI)1098-2787(1998)17:1<1::AID-MAS1>3.0.CO;2-K
221. Shi SDH, Drader JJ, Freitas MA, Hendrickson CL, Marshall AG (2000) Comparison and Interconversion of the Two Most Common Frequency-to-Mass Calibration Functions for Fourier Transform Ion Cyclotron Resonance Mass Spectrometry. Int J Mass Spectrom 195 (196):591–598. doi:10.1016/S1387-3806(99)00226-2
222. Nikolaev EN, Gorshkov MV (1985) Dynamics of Ion Motion in an Elongated Cylindrical Cell of an ICR Spectrometer and the Shape of the Signal Registered. Int J Mass Spectrom Ion Proc 64:115–125. doi:10.1016/0168-1176(85)85003-5
223. Pan Y, Ridge DP, Wronka J, Rockwood AL (1987) Resolution Improvement by Using Harmonic Detection in an Ion Cyclotron Resonance Mass Spectrometer. Rapid Commun Mass Spectrom 1:120–121. doi:10.1002/rcm.1290010709
224. Nikolaev EN, Boldin IA, Jertz R, Baykut G (2011) Initial Experimental Characterization of a New Ultra-High Resolution FTICR Cell with Dynamic Harmonization. J Am Soc Mass Spectrom 22:1125–1133. doi:10.1007/s13361-011-0125-9
225. Derome AE (1987) Modern NMR Techniques for Chemistry Research. Pergamon Press, Oxford
226. Guan S, Marshall AG (1996) Stored Waveform Inverse Fourier Transform (SWIFT) Ion Excitation in Trapped-Ion Mass Spectrometry: Theory and Applications. Int J Mass Spectrom Ion Proc 157(158):5–37. doi:10.1016/S0168-1176(96)04461-8
227. Schweikhard L, Ziegler J, Bopp H, Luetzenkirchen K (1995) The Trapping Condition and a New Instability of the Ion Motion in the Ion Cyclotron Resonance Trap. Int J Mass Spectrom Ion Proc 141:77–90. doi:10.1016/0168-1176(94)04092-L
228. Comisarow MB, Marshall AG (1976) Theory of Fourier Transform Ion Cyclotron Resonance Mass Spectroscopy. I. Fundamental Equations and Low-Pressure Line Shape. J Chem Phys 64:110–119. doi:10.1063/1.431959
229. Comisarow MB (1978) Signal Modeling for Ion Cyclotron Resonance. J Chem Phys 69:4097–4104. doi:10.1063/1.437143
230. Hughey CA, Rodgers RP, Marshall AG (2002) Resolution of 11,000 Compositionally Distinct Components in a Single Electrospray Ionization FT-ICR Mass Spectrum of Crude Oil. Anal Chem 74:4145–4149. doi:10.1021/ac020146b
231. Huang Y, Li G-Z, Guan S, Marshall AG (1997) A Combined Linear Ion Trap for Mass Spectrometry. J Am Soc Mass Spectrom 8:962–969. doi:10.1016/S1044-0305(97)82945-5
232. Guan S, Marshall AG (1995) Ion Traps for Fourier Transform Ion Cyclotron Resonance Mass Spectrometry: Principles and Design of Geometric and Electric Configurations. Int J Mass Spectrom Ion Proc 146(147):261–296. doi:10.1016/0168-1176(95)04190-V
233. Caravatti P, Allemann M (1991) The Infinity Cell: A New Trapped-Ion Cell with Radiofrequency Covered Trapping Electrodes for FT-ICR-MS. Org Mass Spectrom 26:514–518. doi:10.1002/oms.1210260527
234. Kostyukevich YI, Vladimirov GN, Nikolaev EN (2012) Dynamically Harmonized FT-ICR Cell with Specially Shaped Electrodes for Compensation of Inhomogeneity of the Magnetic

Field. Computer Simulations of the Electric Field and Ion Motion Dynamics. J Am Soc Mass Spectrom 23:2198–2207. doi:10.1007/s13361-012-0480-1
235. Nicolardi S, Switzar L, Deelder AM, Palmblad M, van der Burgt YEM (2015) Top-Down MALDI-In-Source Decay-FTICR Mass Spectrometry of Isotopically Resolved Proteins. Anal Chem 87:3429–3437. doi:10.1021/ac504708y
236. Solouki T, Emmet MR, Guan S, Marshall AG (1997) Detection, Number, and Sequence Location of Sulfur-Containing Amino Acids and Disulfide Bridges in Peptides by Ultrahigh-Resolution MALDI FTICR Mass Spectrometry. Anal Chem 69:1163–1168. doi:10.1021/ac960885q
237. Wu Z, Hendrickson CL, Rodgers RP, Marshall AG (2002) Composition of Explosives by Electrospray Ionization Fourier Transform Ion Cyclotron Resonance Mass Spectrometry. Anal Chem 74:1879–1883. doi:10.1021/ac011071z
238. Senko MW, Hendrickson CL, Emmett MR, Shi SDH, Marshall AG (1997) External Accumulation of Ions for Enhanced Electrospray Ionization Fourier Transform Ion Cyclotron Resonance Mass Spectrometry. J Am Soc Mass Spectrom 8:970–976. doi:10.1016/S1044-0305(97)00126-8
239. Wang Y, Shi SDH, Hendrickson CL, Marshall AG (2000) Mass-Selective Ion Accumulation and Fragmentation in a Linear Octopole Ion Trap External to a Fourier Transform Ion Cyclotron Resonance Mass Spectrometer. Int J Mass Spectrom 198:113–120. doi:10.1016/S1387-3806(00)00177-9
240. Makarov A (2000) Electrostatic Axially Harmonic Orbital Trapping: A High-Performance Technique of Mass Analysis. Anal Chem 72:1156–1162. doi:10.1021/ac991131p
241. Scigelova M, Makarov A (2006) Orbitrap Mass Analyzer – Overview and Applications in Proteomics. Pract Proteomics 6:16–21. doi:10.1002/pmic.200600528
242. Makarov A, Denisov E, Lange O, Horning S (2006) Dynamic Range of Mass Accuracy in LTQ Orbitrap Hybrid Mass Spectrometer. J Am Soc Mass Spectrom 17:977–982. doi:10.1016/j.jasms.2006.03.006
243. Makarov A, Denisov E, Kholomeev A, Balschun W, Lange O, Strupat K, Horning S (2006) Performance Evaluation of a Hybrid Linear Ion Trap/Orbitrap Mass Spectrometer. Anal Chem 78:2113–2120. doi:10.1021/ac0518811
244. Macek B, Waanders LF, Olsen JV, Mann M (2006) Top-Down Protein Sequencing and $MS^3$ on a Hybrid Linear Quadrupole Ion Trap-Orbitrap Mass Spectrometer. Mol Cell Proteomics 5:949–958. doi:10.1074/mcp.T500042-MCP200
245. Perry RH, Cooks RG, Noll RJ (2008) Orbitrap Mass Spectrometry: Instrumentation, Ion Motion and Applications. Mass Spectrom Rev 27:661–699. doi:10.1002/mas.20186
246. Kingdon KH (1923) A Method for Neutralizing the Electron Space Charge by Positive Ionization at Very Low Pressures. Phys Rev 21:408–418. doi:10.1103/PhysRev.21.408
247. Knight RD (1981) Storage of Ions from Laser-Produced Plasmas. Appl Phys Lett 38:221–223. doi:10.1063/1.92315
248. Oksman P (1995) A Fourier Transform Time-of-Flight Mass Spectrometer. A SIMION Calculation Approach. Int J Mass Spectrom Ion Proc 141:67–76. doi:10.1016/0168-1176(94)04086-M
249. Hardman M, Makarov AA (2003) Interfacing the Orbitrap Mass Analyzer to an Electrospray Ion Source. Anal Chem 75:1699–1705. doi:10.1021/ac0258047
250. Olsen JV, de Godoy LMF, Li G, Macek B, Mortensen P, Pesch R, Makarov A, Lange O, Horning S, Mann M (2005) Parts Per Million Mass Accuracy on an Orbitrap Mass Spectrometer Via Lock Mass Injection into a C-Trap. Mol Cell Proteomics 4:2010–2021. doi:10.1074/mcp.T500030-MCP200
251. Perry RH, Hu Q, Salazar GA, Cooks RG, Noll RJ (2009) Rephasing Ion Packets in the Orbitrap Mass Analyzer to Improve Resolution and Peak Shape. J Am Soc Mass Spectrom 20:1397–1404. doi:10.1016/j.jasms.2009.02.011
252. Makarov A, Denisov E (2009) Dynamics of Ions of Intact Proteins in the Orbitrap Mass Analyzer. J Am Soc Mass Spectrom 20:1486–1495. doi:10.1016/j.jasms.2009.03.024

253. Makarov A, Denisov E, Lange O (2009) Performance Evaluation of a High-Field Orbitrap Mass Analyzer. J Am Soc Mass Spectrom 20:1391–1396. doi:10.1016/j.jasms.2009.01.005
254. Lebedev AT, Damoc E, Makarov AA, Samgina TY (2014) Discrimination of Leucine and Isoleucine in Peptides Sequencing with Orbitrap Fusion Mass Spectrometer. Anal Chem 86:7017–7022. doi:10.1021/ac501200h
255. Senko MW, Remes PM, Canterbury JD, Mathur R, Song Q, Eliuk SM, Mullen C, Earley L, Hardman M, Blethrow JD, Bui H, Specht A, Lange O, Denisov E, Makarov A, Horning S, Zabrouskov V (2013) Novel Parallelized Quadrupole/Linear Ion Trap/Orbitrap Tribrid Mass Spectrometer Improving Proteome Coverage and Peptide Identification Rates. Anal Chem 85:11710–11714. doi:10.1021/ac403115c
256. Amy JW, Baitinger WE, Cooks RG (1990) Building Mass Spectrometers and a Philosophy of Research. J Am Soc Mass Spectrom 1:119–128. doi:10.1016/1044-0305(90)85047-P
257. Futrell JH (2000) Development of Tandem Mass Spectrometry. One Perspective. Int J Mass Spectrom 200:495–508. doi:10.1016/S1387-3806(00)00353-5
258. McLuckey SA, Glish GL, Cooks RG (1981) Kinetic Energy Effects in Mass Spectrometry/Mass Spectrometry Using a Sector/Quadrupole Tandem Instrument. Int J Mass Spectrom Ion Phys 39:219–230. doi:10.1016/0020-7381(81)80034-4
259. Glish GL, McLuckey SA, Ridley TY, Cooks RG (1982) A New "Hybrid" Sector/Quadrupole Mass Spectrometer for Mass Spectrometry/Mass Spectrometry. Int J Mass Spectrom Ion Phys 41:157–177. doi:10.1016/0020-7381(82)85032-8
260. Bradley CD, Curtis JM, Derrick PJ, Wright B (1992) Tandem Mass Spectrometry of Peptides Using a Magnetic Sector/Quadrupole Hybrid-the Case for Higher Collision Energy and Higher Radio-Frequency Power. Anal Chem 64:2628–2635. doi:10.1021/ac00045a028
261. Schoen AE, Amy JW, Ciupek JD, Cooks RG, Dobberstein P, Jung G (1985) A Hybrid BEQQ Mass Spectrometer. Int J Mass Spectrom Ion Proc 65:125–140. doi:10.1016/0168-1176(85)85059-X
262. Ciupek JD, Amy JW, Cooks RG, Schoen AE (1985) Performance of a Hybrid Mass Spectrometer. Int J Mass Spectrom Ion Proc 65:141–157. doi:10.1016/0168-1176(85)85060-6
263. Louris JN, Wright LG, Cooks RG, Schoen AE (1985) New Scan Modes Accessed with a Hybrid Mass Spectrometer. Anal Chem 57:2918–2924. doi:10.1021/ac00291a039
264. Loo JA, Münster H (1999) Magnetic Sector-Ion Trap Mass Spectrometry with Electrospray Ionization for High Sensitivity Peptide Sequencing. Rapid Commun Mass Spectrom 13:54–60. doi:10.1002/(SICI)1097-0231(19990115)13:1<54::AID-RCM450>3.0.CO;2-Y
265. Strobel FH, Solouki T, White MA, Russell DH (1991) Detection of Femtomole and Sub-Femtomole Levels of Peptides by Tandem Magnetic Sector/Reflectron Time-of-Flight Mass Spectrometry and Matrix-Assisted Laser Desorption Ionization. J Am Soc Mass Spectrom 2:91–94. doi:10.1016/1044-0305(91)80066-G
266. Bateman RH, Green MR, Scott G, Clayton E (1995) A Combined Magnetic Sector-Time-of-Flight Mass Spectrometer for Structural Determination Studies by Tandem Mass Spectrometry. Rapid Commun Mass Spectrom 9:1227–1233. doi:10.1002/rcm.1290091302
267. Aicher KP, Müller M, Wilhelm U, Grotemeyer J (1995) Design and Setup of an Ion Trap-Reflectron-Time-of-Flight Mass Spectrometer. Eur Mass Spectrom 1:331–340. doi:10.1255/ejms.117
268. Wilhelm U, Aicher KP, Grotemeyer J (1996) Ion Storage Combined with Reflectron Time-of-Flight Mass Spectrometry: Ion Cloud Motions As a Result of Jet-Cooled Molecules. Int J Mass Spectrom Ion Proc 152:111–120. doi:10.1016/0168-1176(95)04339-X
269. Morris HR, Paxton T, Dell A, Langhorne J, Berg M, Bordoli RS, Hoyes J, Bateman RH (1996) High Sensitivity Collisionally-Activated Decomposition Tandem Mass Spectrometry on a Novel Quadrupole/Orthogonal-Acceleration Time-of-Flight Mass Spectrometer. Rapid Commun Mass Spectrom 10:889–896. doi:10.1002/(SICI)1097-0231(19960610)10:8<889::AID-RCM615>3.0.CO;2-F

270. Shevchenko A, Chernushevich IV, Ens W, Standing KG, Thompson B, Wilm M, Mann M (1997) Rapid 'De Novo' Peptide Sequencing by a Combination of Nanoelectrospray, Isotopic Labeling and a Quadrupole/Time-of-Flight Mass Spectrometer. Rapid Commun Mass Spectrom 11:1015–1024. doi:10.1002/(SICI)1097-0231(19970615)11:9<1015::AID-RCM958>3.0.CO;2-H
271. Hopfgartner G, Chernushevich IV, Covey T, Plomley JB, Bonner R (1999) Exact Mass Measurement of Product Ions for the Structural Elucidation of Drug Metabolites with a Tandem Quadrupole Orthogonal-Acceleration Time-of-Flight Mass Spectrometer. J Am Soc Mass Spectrom 10:1305–1314. doi:10.1016/S1044-0305(99)00097-5
272. Borsdorf H, Eiceman GA (2006) Ion Mobility Spectrometry: Principles and Applications. Appl Spectrosc Rev 41:323–375. doi:10.1080/05704920600663469
273. Eiceman GA, Karpas Z, Hill HH Jr (2014) Ion Mobility Spectrometry. CRC Press, Boca Raton
274. Collins DC, Lee ML (2002) Developments in Ion Mobility Spectrometry-Mass Spectrometry. Anal Bioanal Chem 372:66–73. doi:10.1007/s00216-001-1195-5
275. Mukhopadhyay R (2008) IMS/MS: Its Time Has Come. Anal Chem 80:7918–7920. doi:10.1021/ac8018608
276. Bohrer BC, Merenbloom SI, Koeniger SL, Hilderbrand AE, Clemmer DE (2008) Biomolecule Analysis by Ion Mobility Spectrometry. Annu Rev Anal Chem 1:293–327. doi:10.1146/annurev.anchem.1.031207.113001
277. Karasek FW (1970) Drift-Mass Spectrometer. Res Developm 21:25–27
278. Karasek FW (1970) Plasma Chromatograph. Res Developm 21:34–37
279. Karasek FW, Cohen MJ, Carroll DI (1971) Trace Studies of Alcohols in the Plasma Chromatograph–Mass Spectrometer. J Chromatogr Sci 9:390–392. doi:10.1093/chromsci/9.7.390
280. Kanu AB, Dwivedi P, Tam M, Matz L, Hill HH Jr (2008) Ion Mobility-Mass Spectrometry. J Mass Spectrom 43:1–22. doi:10.1002/jms.1383
281. Pringle SD, Giles K, Wildgoose JL, Williams JP, Slade SE, Thalassinos K, Bateman RH, Bowers MT, Scrivens JH (2007) An Investigation of the Mobility Separation of Some Peptide and Protein Ions Using a New Hybrid Quadrupole/Travelling Wave IMS/Oa-ToF Instrument. Int J Mass Spectrom 261:1–12. doi:10.1016/j.ijms.2006.07.021
282. Guevremont R (2004) High-Field Asymmetric Waveform Ion Mobility Spectrometry: A New Tool for Mass Spectrometry. J Chromatogr A 1058:3–19. doi:10.1016/S0021-9673(04)01478-5
283. Kolakowski BM, Mester Z (2007) Review of Applications of High-Field Asymmetric Waveform Ion Mobility Spectrometry (FAIMS) and Differential Mobility Spectrometry (DMS). Analyst 132:842–864. doi:10.1039/B706039D
284. Harvey SR, Macphee CE, Barran PE (2011) Ion Mobility Mass Spectrometry for Peptide Analysis. Methods 54:454–461. doi:10.1016/j.ymeth.2011.05.004
285. Platzner IT, Habfast K, Walder AJ, Goetz A, Platzner IT (eds) (1997) Modern Isotope Ratio Mass Spectrometry. Wiley, Chichester
286. Stanton HE, Chupka WA, Inghram MG (1956) Electron Multipliers in Mass Spectrometry; Effect of Molecular Structure. Rev Sci Instrum 27:109. doi:10.1063/1.1715477
287. Weaver PJ, Laures AMF, Wolff JC (2007) Investigation of the Advanced Functionalities of a Hybrid Quadrupole Orthogonal Acceleration Time-of-Flight Mass Spectrometer. Rapid Commun Mass Spectrom 21:2415–2421. doi:10.1002/rcm.3052
288. Colombo M, Sirtori FR, Rizzo V (2004) A Fully Automated Method for Accurate Mass Determination Using High-Performance Liquid Chromatography with a Quadrupole/Orthogonal Acceleration Time-of-Flight Mass Spectrometer. Rapid Commun Mass Spectrom 18:511–517. doi:10.1002/rcm.1368
289. Allen JS (1947) An Improved Electron-Multiplier Particle Counter. Rev Sci Instrum 18:739–749. doi:10.1063/1.1740838

290. Wang GH, Aberth W, Falick AM (1986) Evidence Concerning the Identity of Secondary Particles in Post-Acceleration Detectors. Int J Mass Spectrom Ion Proc 69:233–237. doi:10.1016/0168-1176(86)87037-9
291. Busch KL (2000) The Electron Multiplier. Spectroscopy 15:28–33
292. Schröder E (1991) Massenspektrometrie – Begriffe und Definitionen. Springer, Heidelberg
293. Boerboom AJH (1991) Array Detection of Mass Spectra, a Comparison with Conventional Detection Methods. Org Mass Spectrom 26:929–935. doi:10.1002/oms.1210261103
294. Kurz EA (1979) Channel Electron Multipliers. Am Laboratory 11:67–82
295. Wiza JL (1979) Microchannel Plate Detectors. Nucl Instrum Methods 162:587–601. doi:10.1016/0029-554X(79)90734-1
296. Laprade BN, Labich RJ (1994) Microchannel Plate-Based Detectors in Mass Spectrometry. Spectroscopy 9:26–30
297. Alexandrov ML, Gall LN, Krasnov NV, Lokshin LR, Chuprikov AV (1990) Discrimination Effects in Inorganic Ion-Cluster Detection by Secondary-Electron Multiplier in Mass Spectrometry Experiments. Rapid Commun Mass Spectrom 4:9–12. doi:10.1002/rcm.1290040104
298. Geno PW, Macfarlane RD (1989) Secondary Electron Emission Induced by Impact of Low-Velocity Molecular Ions on a Microchannel Plate. Int J Mass Spectrom Ion Proc 92:195–210. doi:10.1016/0168-1176(89)83028-9
299. Hedin H, Håkansson K, Sundqvist BUR (1987) On the Detection of Large Organic Ions by Secondary Electron Production. Int J Mass Spectrom Ion Proc 75:275–289. doi:10.1016/0168-1176(87)83041-0
300. Hill JA, Biller JE, Martin SA, Biemann K, Yoshidome K, Sato K (1989) Design Considerations, Calibration and Applications of an Array Detector for a Four-Sector Tandem Mass Spectrometer. Int J Mass Spectrom Ion Proc 92:211–230. doi:10.1016/0168-1176(89)83029-0
301. Birkinshaw K (1997) Fundamentals of Focal Plane Detectors. J Mass Spectrom 32:795–806. doi:10.1002/(SICI)1096-9888(199708)32:8<795::AID-JMS540>3.0.CO;2-U
302. Cottrell JS, Evans S (1987) The Application of a Multichannel Electro-Optical Detection System to the Analysis of Large Molecules by FAB Mass Spectrometry. Rapid Commun Mass Spectrom 1:1–2. doi:10.1002/rcm.1290010103
303. Cottrell JS, Evans S (1987) Characteristics of a Multichannel Electrooptical Detection System and Its Application to the Analysis of Large Molecules by Fast Atom Bombardment Mass Spectrometry. Anal Chem 59:1990–1995. doi:10.1021/ac00142a021
304. Birkinshaw K, Langstaff DP (1996) The Ideal Detector. Rapid Commun Mass Spectrom 10:1675–1677. doi:10.1002/(SICI)1097-0231(199610)10:13<1675::AID-RCM712>3.0.CO;2-S
305. Hucknall DJ (1991) Vacuum Technology and Applications. Butterworth-Heinemann, Oxford
306. Pupp W, Hartmann HK (1991) Vakuum-Technik – Grundlagen und Anwendungen. Fachbuchverlag Leipzig, Leipzig
307. Wutz M, Adam H, Walcher W (1992) Theory and Practice of Vacuum Technology. Vieweg, Braunschweig/Wiesbaden
308. Lafferty JM (ed) (1998) Foundations of Vacuum Science and Technology. Wiley, New York
309. Umrath W (ed) (2001) Leybold Vacuum Products and Reference Book. Leybold Vacuum GmbH, Köln
310. Busch KL (2000) Vacuum in Mass Spectroscopy. Nothing Can Surprise You. Spectroscopy 15:22–25
311. Busch KL (2001) High-Vacuum Pumps in Mass Spectrometers. Spectroscopy 16:14–18